

INFLUENCE OF BLOCK CAVE MINING ON PIT SLOPE
DEFORMATION MECHANISMS

by

Haitham Magdi Ahmed

B.Sc., King Abdul Aziz University, 2002

A THESIS SUBMITTED IN PARTIAL FULFILLMENT OF
THE REQUIREMENTS FOR THE DEGREE OF

Master of Applied Science

(Mining Engineering)

in

THE FACULTY OF GRADUATE STUDIES

THE UNIVERSITY OF BRITISH COLUMBIA

(Vancouver)

April 2009

© Haitham Magdi Ahmed, 2009

ABSTRACT

Several mining operations are considering the switch from surface to underground in order to mine deeper resources. When making this switch block cave mining is often considered to minimize costs. The primary objective of this study is to investigate the mechanics of rock slope movements and failure in response to the block caving process. Different potential failure modes are investigated as a function of the orientation of the jointing pattern. The impact of two different caving locations on slope stability will be investigated: one where the cave is located under the toe of the slope, and another where the cave propagates upwards behind the crest of the slope. It is found that the position of the cave plays an equally major role in how the slope behaves and displaces. The potential of the toppling failure mechanism, flexural toppling of slender blocks or flexural block toppling of rocks with cross-joints, is characterized by inward movements of the rock mass toward the cave beneath the toe. However, huge vertical displacements on the upper part of the slope are distinguished as an influence of the cave behind the crest. Moreover, a consistent horizontal and vertical slope displacement toward the cave beneath the toe associated with sliding movements gives evidence that the cave zone influences the overall slope to move toward the toe.

TABLE OF CONTENTS

| | |
|--------------------------------------------------------|----|
| ABSTRACT | ii |
| LIST OF TABLES | v |
| LIST OF FIGURES | vi |
| ACKNOWLEDGEMENTS | x |
| DEDICATION | xi |
| 1 INTRODUCTION | 1 |
| 1.1 Overview and problem statement | 1 |
| 1.2 Thesis objectives..... | 4 |
| 1.3 Thesis contents..... | 5 |
| 2 LITERATURE REVIEW..... | 6 |
| 2.1 Block caving | 6 |
| 2.2 Block cave mining operation | 7 |
| 2.2.1 Transition from open pit mines..... | 8 |
| 2.2.2 Effects on natural slopes | 13 |
| 2.3 Subsidence..... | 16 |
| 2.3.1 Characterization of cave-induced subsidence..... | 18 |
| 2.4 Rock slope failure modes..... | 20 |
| 2.4.1 Planar failure | 20 |
| 2.4.2 Toppling failure..... | 22 |
| 2.4.3 Bi-planar & buckling failure | 24 |
| 2.5 Numerical modeling | 25 |
| 3 METHODOLOGY..... | 28 |
| 3.1 UDEC formulation..... | 28 |
| 3.2 Model setup | 30 |
| 3.3 Modeling assumptions | 35 |
| 3.3 Block caving simulation techniques | 38 |
| 3.4 Sensitivity to initial stress ratio | 43 |
| 4 DISTINCT-ELEMENT MODELING RESULTS..... | 48 |
| 4.1 Sliding-type model results..... | 50 |
| 4.2 Toppling-type model results..... | 63 |

| | |
|---------------------------------------------------------------------------------------------------------|-----|
| 4.3 Buckling- and bi-Planar- type model results..... | 77 |
| 5 DISCUSSION ON SURFACE SUBSIDENCE | 81 |
| 6 CONCLUSION | 88 |
| 6.1 Recommendations..... | 91 |
| 7 REFERENCES..... | 93 |
| 8 APPENDICES..... | 95 |
| Appendix 1 – sample of - UDEC input file (.dat) - sliding-type with cross joints, right-positioned cave | 95 |
| Appendix 2 – sample of volume tracker(.xlsx) - sliding-type with cross joints, left-positioned cave. | 100 |

LIST OF TABLES

| | |
|----------------------------------------------------------------------------------------------------------------------------|----|
| Table 2.1: Numerical Studies of surface subsidence. From Vyazmensky et al. (2007) | 26 |
| Table 3.1: Generic/conceptual models with different configurations of discontinuities (joints)..... | 33 |
| Table 3.2: Discontinuities and rock mass properties assigned for all simulations..... | 37 |
| Table 3.3: The different variables examined in the study..... | 38 |
| Table 3.4: Advantages and disadvantages of the two different block caving modeling techniques, (DBD) and (DBC)..... | 43 |
| Table 6.1: Ranking of the magnitude and the extent of deformations along the surface and slope face. | 90 |
| Table 6.2: Ranking of potential failure mechanism resulting from block caving..... | 91 |

LIST OF FIGURES

| | |
|-------------------------------------------------------------------------------------------------------------------------------------------------------------------------------------------------------------------------------------------------------------------------------------------|----|
| Figure 1.1: Satellite radar interferometry image of pit wall movements at Palabora subsequent to the northwest wall failure. The northwest wall failure is outlined by the thin blue line. From AMEC (2005) accessed April, 05, 2009. | 2 |
| Figure 1.2: Apache Leap at sundown, view looking east from Superior, Arizona. The proposed Resolution block cave operation is located below the Leap further to the east of the cliff edge. www.city-data.com/picfilesc/picc28065.php accessed April, 05, 2009..... | 3 |
| Figure 2.1: Right: Aerial photo of Palabora open pit. Photo courtesy of A. Moss. Left: 3D model of the pit and the caving geometry. From Brummer et al. (2006). | 9 |
| Figure 2.2: The geology of Palabora and pit slope angles. From Moss et al.(2006)..... | 10 |
| Figure 2.4: Reserve and Geological Resource of Chuqicamata ore. From Olavarría et al.(2006)..... | 11 |
| Figure 2.5: The geotechnical challenges associated with the block caving transition. From Olavarría et al. (2006)..... | 12 |
| Figure 2.6: E-W view of Apache leap. From Resolution copper mining -Sustainable development report (2006). | 13 |
| Figure 2.7: Resolution copper mining site plane – town of superior. From www.aznews.us/mine accessed April, 05, 2009. | 14 |
| Figure 2.9: Expected block caving operation and associate surface subsidence. From Resolution copper mining -Sustainable development report (2006). | 15 |
| Figure 2.10: General conceptual explanation and description of subsidence. From www.wvgs.wvnet.edu accessed April, 05, 2009..... | 16 |
| Figure 2.12: Cave propagation mechanism toward surface and surface subsidence initiation. From Van | 19 |
| Figure 2.13: General cross-section geometry and released surface exhibiting plane failure. From Hoek & Bray (2001). | 20 |
| Figure 2.14: Simple diagram presents: (a) Block toppling of columns of rocks, (b) flexural toppling of slabs of rocks, and (c) block-flexural toppling of long columns through accumulated motions along numerous cross-joints. From Hoek & Bray (2001). | 22 |
| Figure 3.1: Calculation cycle for the distinct element method employed by UDEC (Itasca, 2004) | 29 |
| Figure 3.2: Two different caving positions and six different generic configurations of structural discontinuities: case 1 to case 6. (Slope height is 800 meters). | 31 |
| Figure 3.3: Cave propagation mechanism toward surface and surface subsidence initiation. From Van As et al. (2003) | 35 |
| Figure 3.4: Model geometry and cave initiation using “Direct Block Deletion, DBD” technique. Left: Cave positioned behind the crest. Right: Cave positioned underneath the toe..... | 39 |

| | |
|-----------------------------------------------------------------------------------------------------------------------------------------------------------------------------------------------------------------------------------------------------------------------------------------------|----|
| Figure 3.5: vertical displacement contour of the Sliding-type with cross-joints where cave positioned beneath the toe using “Displacement Boundary condition” technique. (Slope height is 800 meters and displacements in meters) | 40 |
| Figure 3.6: vertical displacement contour of the toppling-type with cross-joints where cave positioned behind the crest using “Displacement Boundary condition” technique. (Slope height is 800 meters and displacements in meters) | 41 |
| Figure 3.7: Horizontal displacement contour simulated by “DBD” technique; (Slope height is 800 meters and displacements in meters). Left: Cave positioned behind the crest. Right: Cave positioned underneath the toe. | 42 |
| Figure 3.8: Plasticity indicator simulated by “DBD” technique (slope height is 800 meters). Left: Cave positioned behind the crest. Right: Cave positioned underneath the toe. | 42 |
| Figure 3.9: Plasticity indicator as a result of initial stress ratio $K=2$ in the toppling-type with cross-joints, with the cave positioned under the toe of the slope model. (Green: plastic yielding, Red: at yielding edge, slope height is 800 meters..... | 44 |
| Figure 3.10: Plasticity indicator as a result of initial stress ratio $K=2$ in the toppling-type with cross-joints, with the cave positioned under the toe of the slope model. (Green: plastic yielding, Red: at yielding edge, slope height is 800 meters. | 44 |
| Figure 3.11: Plasticity indicator of the “Sliding-type with cross-joints”, with the cave positioned underneath the toe of the slope. (Green: plastic yielding, Red: at yielding edge, slope height is 800 meters. (Left: $K=1$, Right: $K=0.33$) | 45 |
| Figure 3.12: Horizontal stress contour of the “Sliding-type with cross-joints”, with the cave positioned underneath the toe of the slope. (Slope height is 800 meters, stress units in Pascal, $K=0.33$) | 46 |
| Figure 3.13: Horizontal stress contour of the “Sliding-type with cross-joints”, with the cave positioned underneath the toe of the slope. (Slope height is 800 meters, stress units in pascal, $K=1$) | 46 |
| Figure 3.14: History of vertical deformation of the monitoring points along the slope face. “Sliding-type with cross-joints”, with the cave positioned underneath the toe of the slope, $K=0.33$. (Horizontal axis: UDEC time step, Vertical axis: Deformations in meters)..... | 47 |
| Figure 3.15: History of vertical deformation of the monitoring points along the slope face. “Sliding-type with cross-joints”, with the cave positioned underneath the toe of the slope, $K=1$. (Horizontal axis: UDEC time step, Vertical axis: Deformations in meters)..... | 47 |
| Figure 4.1: General geometry of the block cave simulations, showing cave located under the slope crest or positioned under the slope toe..... | 49 |
| Figure 4.2: General geometry of the block cave simulations, showing the simulated monitoring on, the upper surface, slope face, and bottom of pits. (200m apart between every two adjacent points, slope height is 800 m) | 50 |
| Figure 4.3: Vertical rock slope displacements for A: the model of pure-sliding-type (cave behind the crest); and B: the model of sliding-type with cross-joints (cave behind the crest). | 53 |
| Figure 4.4: Vertical rock slope displacements for A: the model of pure-sliding-type (cave underneath the toe); and B: the model of sliding-type with cross-joints and (cave underneath the toe). | 54 |

| | |
|--------------------------------------------------------------------------------------------------------------------------------------------------------------------------------------------------------------------------------------------------------|----|
| Figure 4.5: Horizontal rock slope displacements for A: the model of pure-sliding-type (cave behind the crest); and B: the model of sliding-type with cross-joints (cave behind the crest). | 55 |
| Figure 4.6: Horizontal rock slope displacements for A: the model of pure-sliding-type (cave underneath the toe); and B: the model of sliding-type with cross-joints (cave underneath the toe). | 56 |
| Figure 4.7: Horizontal and vertical components of displacements for the sliding-type rock slope cases. | 57 |
| Figure 4.8: Horizontal and vertical components of displacements for the sliding-type with cross-joints models. | 58 |
| Figure 4.9: Displacements for the sliding-type with cross-joints models magnified 20 times for Left: cave behind the crest ; and Right: Cave beneath the toe (Slope height is 800 meters)..... | 58 |
| Figure 4.10: Modeled magnitudes and directions of slope deformations (sliding type)..... | 59 |
| Figure 4.11: The direction of principal stress after caving starts. (Slope height is 800 meters)..... | 60 |
| Figure 4.12: The contours distribution of the horizontal and vertical stress around the cave zone. Relaxation zone (dotted white) and confinement zone (black). (Slope height is 800m)..... | 61 |
| Figure 4.13: Plasticity induced by cave behind the crest models Left: Sliding-type with cross-joints. Right: Pure sliding-type model. (Slope height is 800 meters) | 62 |
| Figure 4.14: Plasticity induced by the cave beneath the toe models Left: Pure sliding-type model. Right: Sliding-type with cross-joints. (Slope height is 800 meters) | 63 |
| Figure 4.15: Vertical displacements of rock slope A: the model of pure-toppling-type (cave behind the crest) B: The model of toppling-type with cross-joints (cave behind the crest). | 65 |
| Figure 4.16: The Vertical displacements of rock slope A: the model of pure-toppling-type (cave underneath the toe) B: The model of toppling-type with cross-joints (cave underneath the toe)..... | 66 |
| Figure 4.18: The Horizontal displacements of rock slope A: the model of pure-toppling-type (cave underneath the toe). B: The model of toppling-type with cross-joints (cave underneath the toe)..... | 68 |
| Figure 4.19: The contours distribution of the vertical rock slope displacements (cave behind the crest). Left: toppling – type model. Right: toppling-type with cross joints. (Slope height is 800 meters, units in meters) | 69 |
| Figure 4.20: The contours distribution of the vertical rock slope displacements (cave beneath the toe). Left: toppling – type model. Right: toppling-type with cross joints (Slope height is 800 meters, units in meters) | 69 |
| Figure 4.21: Horizontal and vertical components of displacements of rock slope (Generated by UDEC in Toppling type cases) | 70 |
| Figure 4.22: Horizontal and vertical components of displacements of rock slope (Generated by UDEC in Toppling type cases) | 71 |
| Figure 4.23: Displacements for the toppling-type with cross-joints models magnified 20 times for Left: cave behind the crest ; and Right: Cave beneath the toe (Slope height is 800 meters)..... | 71 |
| Figure 4.24: Magnitudes and Directions of Slope Deformations (Toppling Type Case) | 72 |

| | |
|----------------------------------------------------------------------------------------------------------------------------------------------------------------------------------------------------------------------------------------------------------------------|----|
| Figure 4.25: The contours of the vertical stress state induced by the cave behind the crest (Pure-toppling-type model). (Slope height is 800 meters, stress units in Pascal)..... | 73 |
| Figure 4.26: Left: the major principal stress is parallel to the slope face. Right: The vertical stress state induced by right cave (Pure-toppling-type model). (Slope height is 800 meters, stress units in Pascal) . | 74 |
| Figure 4.27: Plasticity induced by cave behind the crest models: Left: Toppling-type with cross-joints. Right: Pure-Toppling-type model..... | 75 |
| Figure 4.28: Plasticity induced by Right cave models; Left: Toppling-type with cross-joints. Right: Pure-Toppling-type model. | 76 |
| Figure 4.29: Self-stabilizing of rock blocks and potential catastrophic rock mass failure. (Magnified deformation - 10 times, Slope height – 800 meters) | 76 |
| Figure 4.30: Simulated A: horizontal, and B: vertical deformations in for the Bi-planar and Buckling-type models. (Slope height is 800 meters, Deformation units in meters) | 77 |
| Figure 4.31: Displacement contour induced by the cave beneath the toe “buckling-type model”. A: Horizontal displacements. B: Vertical displacement. . (Slope height is 800 meters)..... | 78 |
| Figure 4.32: Displacement contour induced by the cave behind the toe “buckling-type model”. Left: Horizontal displacements. (Slope height is 800 m) | 79 |
| Figure 4.33: Plasticity induced by cave behind the crest models in “Buckling-type model”. (Slope is 800 meters) | 80 |
| Figure 4.34: Plasticity induced by right cave in “Buckling-type model”. (Slope is 800 meters)..... | 80 |
| Figure 5.1: The general scheme of the contour line of the vertical displacement for both the pure-sliding-type and sliding-type with cross cuts; Left: cave underneath the toe. Right: Cave behind the crest. (Slope height is 800 meters)..... | 81 |
| Figure 5.2: The induced surface and rock slope subsidence (vertical deformations) at selected monitoring points (Sliding Type simulations)..... | 82 |
| Figure 5.3: Subsidence zones for pure-sliding-type simulation induced by the left cave. | 83 |
| Figure 5.4: Subsidence zones for sliding-type with cross joints simulation induced by the cave beneath the toe. | 84 |
| Figure 5.5: The induced surface and rock slope subsidence (vertical deformations) at selected monitoring points (Toppling Type simulations) | 85 |
| Figure 5.6: Subsidence zones for pure-toppling-type simulation induced by the cave behind the crest | 86 |
| Figure 5.7: Subsidence zones for toppling-type with cross-joints simulation induced by the cave behind the crest..... | 87 |

ACKNOWLEDGEMENTS

I am very grateful to all colleagues, fellows, and friends who helped me complete this thesis.

I owe particular thanks and appreciation to Dr. Erik Eberhardt , who guided, supervised, and helped me throughout my research. His time and effort is absolutely appreciated. His professional attitude helped me develop my skills.

A special thanks to Dr. W. Scott Dunbar, for enlarging my vision, providing practical answers to my questions, and supporting me. His practical experience helped me understand the bigger picture.

Haitham M. A. Eissa

To my parents

To my lovely wife, Ghadeer

To my university, King Abdul Aziz

1 INTRODUCTION

1.1 Overview and problem statement

With increasing worldwide demand of mineral resources, mass mining has gained acceptance within the international mining community. In particular, the “Block Cave Mining Method” has gained strong attraction in recent years because low cost and high mining productivity can be achieved. Many countries have applied block caving, either directly as an underground mass mining operation or through a transition to underground mining from a large open pit operation, e.g. Northparkes (Australia), Palabora (South Africa), Questa Mine (New Mexico), Henderson Mine (Colorado), Freeport (Indonesia), and Resolution copper mine (USA). This trend is also seen in Canada where at least two operations are switching to block caving: the Diavik diamond mine (Lac de Gras, NWT) and the New Afton project (west of Kamloops, British Columbia). Super pits like Chuquibambilla (Antofagasta, Chile) and Bingham Canyon (Utah, USA) are also planning to start this transition from open pit mining to block caving.

Several mining companies have decided to go deeper than usual, using underground mining methods, to economically and efficiently extract deeper ore bodies. Some mining operations are considering switching from surface mining such as open pit operations to underground mining to extend the life of such projects. The transition from open pit mining to underground block caving has globally gained acceptance in the mining sector. A good example is the Palabora copper project in South Africa, which started its move underground in 2001. Other projects, such as the Resolution copper project currently under development in Arizona, USA, is turning to block caving as their start-up mining method in order to mine deep resources cost-effectively. Economically, block caving is considered one of the most cost effective mining methods due to low labor intensity compared to the amount of deposit extracted when dealing with low grade ore.

Despite these economic benefits, the interactions that develop between the block cave and surface environment are extremely complex. In the case of Palabora, the block cave operations triggered a massive 800 m high rock slope failure in the open pit. Monitoring of the displacements and consequently the northwest wall failure indicated that undermining of the slope through block caving was responsible for the pit slope failure. The Palabora mining company has successfully switched from surface to underground mining, with operations producing between 30,000 and 35,000 tpd. Although this move can extend the mine life economically, it is a challenging task to take into account safety and environmental consequences related to the potential for catastrophic failures as well as discontinuous

surface subsidence that may adversely affect the integrity of strain-sensitive surface structures. At Palabora, Brummer et al. (2006) showed that the failure mechanism of the northwest wall was controlled by the cave zone, in which the north wall progressively moved into the pit as the ore was caved and removed from the production level. Figure 1.1 shows a satellite radar interferometry image (DInSAR) outlining the location of the pit wall failure (thin blue line) and subsequent movements of the north wall at Palabora.

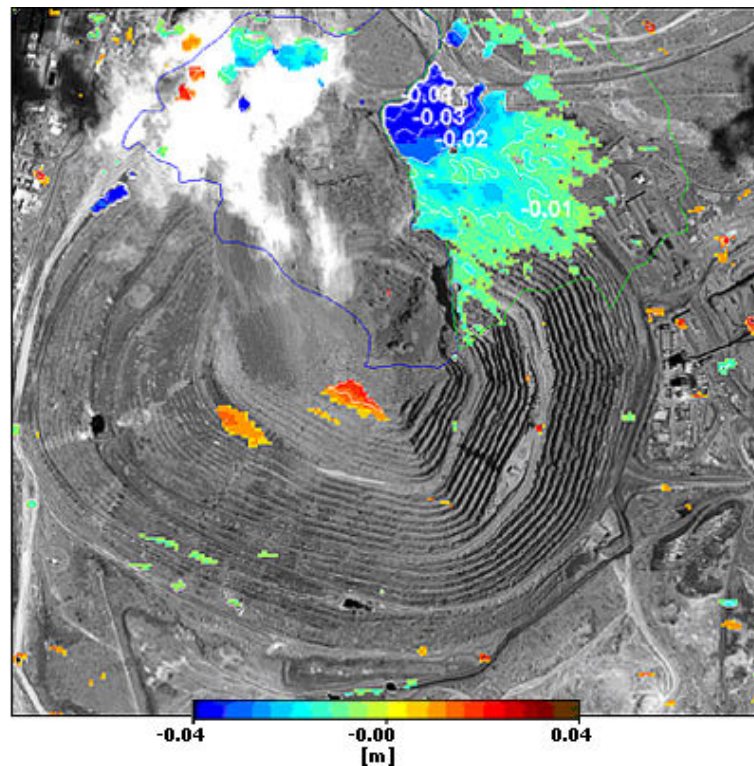


Figure 1.1: Satellite radar interferometry image of pit wall movements at Palabora subsequent to the northwest wall failure. The northwest wall failure is outlined by the thin blue line. From AMEC (2005) accessed April, 05, 2009.

The Resolution copper project, located in Arizona, USA, is another example in which the environmental consequences due to block caving are considered to be highly sensitive. As the ore is extracted, surface subsidence is expected due to movement of rock above the orebody. This could affect Apache Leap, a natural rock formation near the mine site. Therefore close monitoring of mining-induced subsidence near Apache leap will be required gather ground movement information to make sure mining activities have no adverse impact on Apache leap. The Resolution copper sustainable development report (2006) specifies that if a threat is identified, the mining practices will be modified to ensure Apache Leap is protected. Because the mine plans are still under development, state-of-the-art numerical modeling approaches, such as the finite element and distinct-element methods; provide an important means to

investigate the potential impact of different mining plans on the surface environment. It should be stressed that as shown in Figure 1.2, the importance to not negatively affect the historic national park and native nation community will be a major challenge in the planning of the Resolution copper mine.



Figure 1.2: Apache Leap at sundown, view looking east from Superior, Arizona. The proposed Resolution block cave operation is located below the Leap further to the east of the cliff edge. www.city-data.com/picfilesc/picc28065.php accessed April, 05, 2009.

The interaction between the rock mass behavior and the block caving operation is difficult if not impossible to investigate using deterministic approaches alone. Empirical relationships have been established by compiling data from numerous similar mining operations and employing those collective experiences for such analysis, especially in conventional open stoping mining operations. However, a fundamental understanding of the complexity of rock mass response in block caving remains limited (Eberhardt et al., 2007). Laubscher et al., (1981) provide relationships that correlate the mining rock mass rating (MRMR), and mining geometry to the break angle. However, it does not account for dominant geological structure if structurally controlled failure is expected. Therefore, state-of-the-art numerical modeling techniques that can explicitly include the effects of geological structures, complex geometries and variable rock mass properties provide one of the few options available to deal with the complex interactions involved.

Safety and environmental concerns continue to be major focus point for these large-scale mega projects nowadays. Experiences at Palabora and plans for the Resolution copper mine obviously raise alarms as to our understanding of the complexities involved and our ability to evaluate and predict subsidence and ground deformations in response to block cave mining. It is clear to the mining

community that an improved understanding of the interaction between the rock mass behavior and the block caving operation more accurate and precise prediction of subsidence and rock slope movements, which in turn will allow better decisions to be made where open pit mining operations are considering switching to block caving operations.

1.2 Thesis objectives

The purpose of this research is to investigate the mechanics of rock slope movements and failure in response to the block caving process. Numerical modeling is used to simulate ore extraction from the undercut level, and the reaction of a cut slope through rock mass interactions are studied in terms of deformations, stress changes, and plastic yielding. A generic geometry based on that commonly encountered for a deep open pit or high natural rock slope is used, for which twelve different scenarios are modeled involving varying discontinuity network configurations and caving positions relative to the foot and crest of the slope. The modeling is performed using the distinct element code UDEC (Itasca, 2004).

The following points are the main themes of this study:

- The primary goal of the research is to investigate the mechanics of slope deformations and slope failure mechanism, if failure occurs, due to block caving. Different potential failure modes are investigated as a function of the orientation of the jointing pattern. Accordingly, conclusion are provided for practitioners who are responsible for overlying pit movements with respect to further understanding the interaction between the rock mass behavior and deformation kinematics.
- The impact of two different caving locations on slope stability will be investigated: one where the cave is located under the toe of the slope, and another where the cave propagates upwards behind the crest of the slope. Although cases involving open pits transitioning to underground operations almost always involve caving below the toe of the slope, several block cave projects like Resolution involve scenarios where the block cave will be developed behind the crest of a natural slope or neighboring open pit slope.
- Investigation of the limitations of numerical modeling will be undertaken with respect to the sensitivity of each selected variable and how it contributes to the surface subsidence and slope deformations modeled (for the different scenarios). Recommendations are provided with respect to parameter sensitivity.

1.3 Thesis contents

This thesis is divided into five main chapters including this introductory overview, problem statement and the thesis objectives. A literature review, chapter 2, is conducted based on research findings published in the public domain. It covers several topics related to rock mechanics that are pertinent to this study. Block caving techniques and mining case studies are discussed. Three different examples are presented and discussed in terms of issues and considerations arising from planning and mine development perspectives: Palabora copper mine, Resolution copper mine, and Chuquicamata copper mine. Subsidence deformations and rock slope failure mechanisms are also discussed. The final part of the literature review presents the numerical modeling techniques used by different authors related to rock mass modeling. The methodology, chapter 3, follows the literature review and explains the main approach used in this research thesis. It describes in detail the modeling assumptions and provides a systematic accounting of the modeling setup and techniques used. Chapter 4 is the discussion and interpretation of the results and is followed by the final conclusions and summaries of the results in chapter 5. Recommendations for future work are also provided in chapter 5.

2 LITERATURE REVIEW

A literature review is provided here covering several different topics, approaches, and case studies related to mass mining methods especially block caving. Types of block caving systems associated with the nature of their ore bodies, the financial and environmental advantages and merits of using this mining method, and the way block caving works are presented. Case studies from actual mining operations, that have either switched over from a different mining method to block caving or initially began operations with block caving as the primary method, are discussed. Tangible impact of block caving on these examples are also touched on and discussed in section 2.2.

Subsidence in particular is defined and explained in detail since block caving has a major impact on surface subsidence. How subsidence occurs and progresses from the active block caving zone to the surface is comprehensively explained. The importance of addressing the relationship between block caving and subsidence is emphasized in a sense of predicting the impact of subsidence over the surface environment. This leads to the discussion of factors and geological parameters which may affect the magnitude and extent of subsidence.

Of these, geological structure plays a major role in rock slope failure, where the mode of failure (e.g. planar, toppling, bi-planar, and buckling failure) depends on the orientation of the discontinuities with respect to the rock slope. Different types of slope failure mechanisms and conditions of potential failure are discussed in section 2.4.

Numerical modeling is a powerful tool in analyzing many engineering problems. The state-of-the-art numerical tools frequently used in rock mechanics is discussed in section 2.5. The advantages and disadvantages of different numerical approaches such as continuum, discontinuum, and hybrid techniques are also explained. Specifically, the discrete element code UDEC, is selected among others based on its suitability to the research objectives outlined. Specifically, a list of numerical studies of mine-induced surface subsidence is tabulated.

2.1 Block caving

Block caving is a general term that refers to mass mining where the extraction of typically low grade ore in weak rock depends on the action of gravity. Starting by undercutting the ore at the mining production level, the subsequently unsupported weak rock and ore starts to cave by gravity body forces. As this operation progresses and ore is extracted from the mining level, the ore above the cave

that forms continues to break and cave under gravity. Typically, a porphyry-type deposit with well-disseminated mineralization with large lateral and vertical extent of ore body is suitable for block caving. The rock mass strength is usually preferred to be weak and heavily fractured, although moderately strong rock may be caveable to if the total mass is adequately fractured so as to allow for the ore body to break into small pieces and to pass through the drawpoints. Julin (1992) suggests that the minimum horizontal dimension of the ore body is generally 90 m (300 ft).

There are three major systems of block caving presented by Julin (1992) based on the production equipment used: grizzly or gravity, slusher, and rubber-tired system. The grizzly system is the best alternative for ore that breaks very finely and flows directly to the transfer raisers after being sized at the grizzly. It requires closely spaced drawpoints. It is a labor intensive system that requires minimal equipment. Another method, best suited for medium-coarse pieces of falling rocks, is the slusher system that uses scrapers at the main production level. It uses electrical slushers and requires highly trained mechanical expertise to handle this equipment. The last system is the rubber-tired system, which is preferred since it provides greater productivity and efficiency. It uses load-haul-dump (LHD) vehicles at the main level, which requires well-trained operators, but is less labor intensive. Block caving is one of the safest and most cost-effective mining methods aimed at low grade ore bodies. The technique on the whole involves three essential phases to develop the undercut level, drawbell, and production level. The first phase involves constructing a set of parallel tunnels along an upper undercut level and then drilling and blasting holes into the tunnel roofs. The resulting broken rock is then removed which initiates the caving process above the undercut through the loss of stability of the roof. Phase two involves the development of the drawbells. Tunnels are constructed below the broken rock mass in the undercut level. Vertical holes are then drilled up from these tunnels and blasted to form drawbells into which the broken caved rock mass can pass through. The last phase is to blast the connection between the drawbells and the undercut to allow the caving process to continue from the undercut to the drawbells. Loaders subsequently collect the falling rock and transport it to the underground crushers to be carried up through the production shafts.

2.2 Block cave mining operation

Using underground mining methods, several mining companies have decided to go deeper than usual to economically and efficiently exploit deeper ore bodies. In Canada, several mines have switched to block cave mining to mine deeper resources: Porcupine joint venture gold mine (Timmins, Ontario), Lac des Iles palladium mine (Thunder Bay, Ontario) and the QR gold mine (Quesnel, British Columbia), with

the New Afton copper mine (near Kamloops, British Columbia) also considering the switch to block cave mining.

Economically, block caving is considered one of the lowest cost mining methods due to its low labor requirements relative to the tonnage produced. The transition from open pit mining to underground block caving method has gained increasing attention as a number of large open pits approach their design depths. A good example of a mine that has already undergone this transition is the Palabora copper project in South Africa, which initially began operations as an open pit mine. With open pit operations coming to an end, Palabora made the transition to block cave mining in 2001. In terms of new mining projects currently under development, those where the ore body is deep are being planned to start as a block caving operation in order to cost-effectively mine the deep resources. The Resolution copper project in Arizona, USA is one such example. Other projects involve plans to switch to block caving from open pit mining, but only if careful study of the major challenges and issues that they may face during construction and operation show the projects to be feasible; e.g Chuquicamata, Chile.

2.2.1 Transition from open pit mines

Most cases where a block cave is developed under an open pit intend to continue mining the ore body at greater depths. The Palabora and Chuquicamata open pit mine are two examples presented in this section in which the mine life is either extended or planned to be extended using block cave mining methods. The transition from open pit to block caving is challenging and detailed study is required; on the other hand, huge economic benefits can be achieved if this transition is carried out properly.

Palabora

The Palabora mining company (PMC) has transformed from an 82,000 tpd open pit mining operation to a 30,000 tpd block caving operation. This move extended the life of the project, which otherwise would have closed in 2002. The Palabora copper orebody involves an elliptical vertical dipping volcanic pipe approximately 1400 m by 800 m in plane and 1800 m deep (Moss et al., 2006). The production level is located 400 m below the final pit bottom at a depth of 1200 meters as shown in Figure 2.1. This cutting edge design was technically and operationally challenging given the competency of the Palabora rock mass.

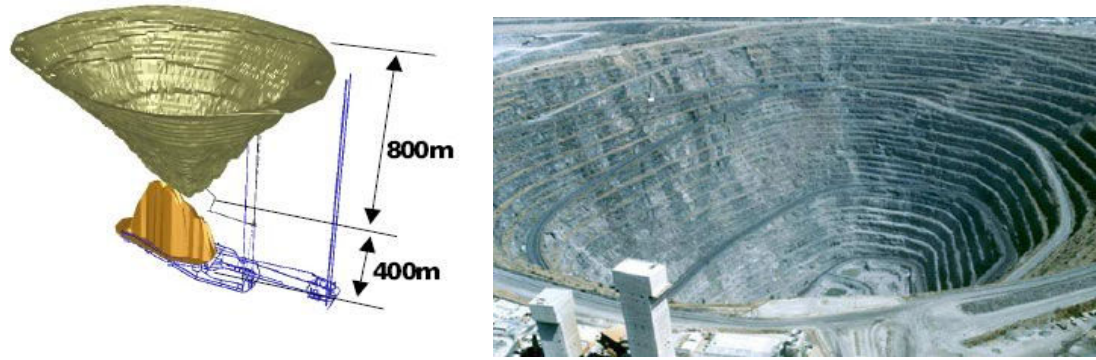


Figure 2.1: **Right:** Aerial photo of Palabora open pit. Photo courtesy of A. Moss. **Left:** 3D model of the pit and the caving geometry. From Brummer et al (2006).

The geology and economic deposit of Palabora is described in detail in Palabora Mining Company Limited (1976). The kidney-shaped igneous complex resulted from an alkaline intrusive cycle, which emplaced, in several successive stages, a suite of rocks ranging from ultramafic to peralkaline in character. The core consists of phlogopite serpentine with subsidiary amount of diopside, medium to extremely coarse grained in texture. The outer zone consists of medium to fine- grained phlogopite-diopside rock with minor amount of apatite. Moss (2006) discussed the rock mass characteristics of these rock types at Palabora. The intact rock strength ranges from 80 to 140 MPa for the most competent rocks being caved. Figure 2.2 shows the wall slope angles and the variation of geology in Palabora.

Du Plessis & Martin (1991) assessed the deformation behavior of the proposed steep high slopes at Palabora using the explicit finite difference code FLAC. Their results showed the potential for instability of the steep and high slopes, but they emphasized that it would be difficult to confirm that the models were predictive.

Later studies by Brummer et al. (2006) investigated the slope failure mechanism of the north wall that began in 2003 as shown in Figure 2.3. Three-dimensional distinct-element (3DEC) models were used to show that the instability of a portion of the north wall was due to wedges that formed and moved toward the caving zone. Both papers showed the need to establish comprehensive methods for evaluating the deformation for such high rock slopes.

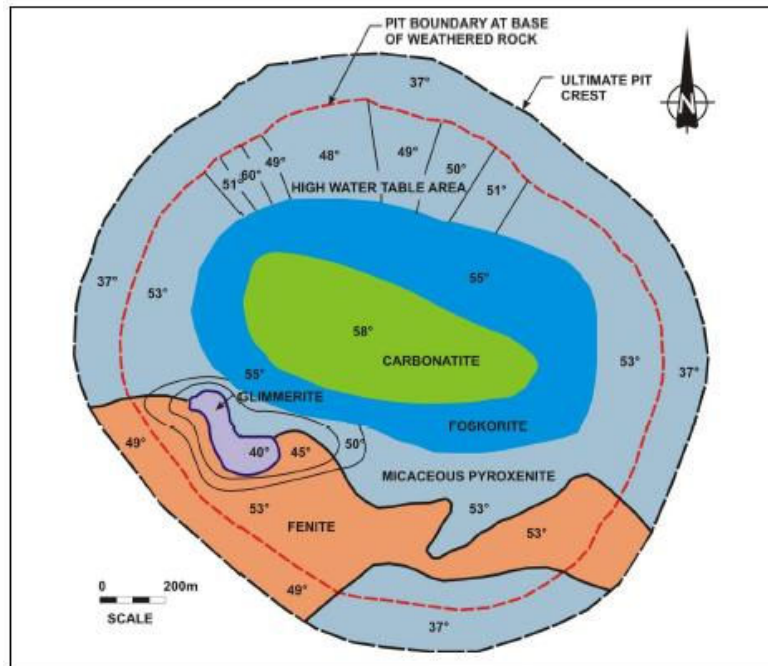


Figure 2.2: The geology of Palabora and pit slope angles. From Moss et al.(2006)

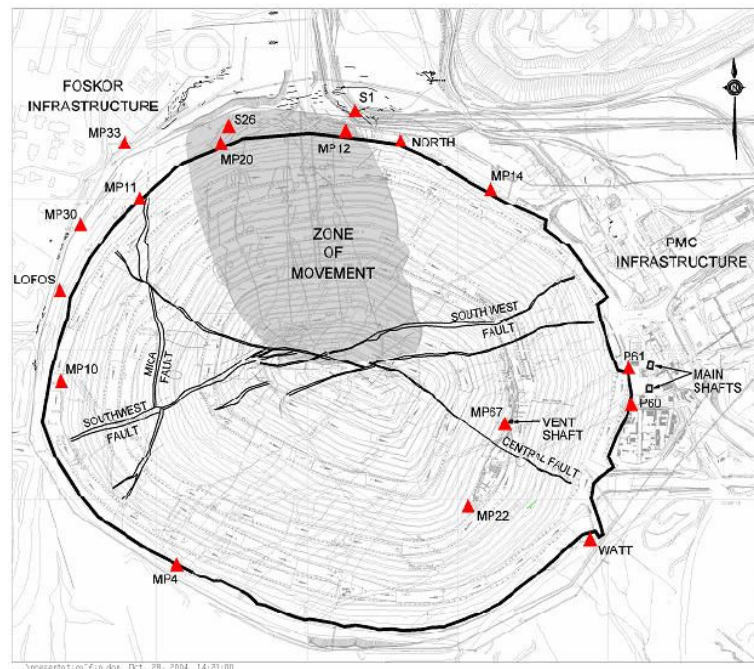


Figure 2.3: Pit plan showing the zone of movements and location of monitoring points. From Brummer et al (2006).

Chuqicamata

Another example of a large-scale deep copper mine, for which the feasibility of moving from open pit to underground mining is being explored, is Chuqicamata, Chile. Started in 1915, the mine has produced over 2.6 billion tons of copper ore with a grade of 1.53%. The pit has reached a depth of 850 m as shown in Figure 2.5. Current plans are to extract approximately 700 million tonnes from 2006 to 2014. At the end of this stage, the pit will move towards block cave mining, with the final pit having reached a depth of 1100 m as shown in Figures 2.4 and 2.5. Borehole data suggests a further 2.3 billion tonnes of ore at 0.81% grade can be further exploited. The block cave plan consists of three successive lifts of 250 m each to achieve the goal; nevertheless, focusing on the geotechnical issues, defining the appropriate surface and underground infrastructure, and executing the project deadline are major challenges that need to be dealt with (Olavarria et al., 2006).

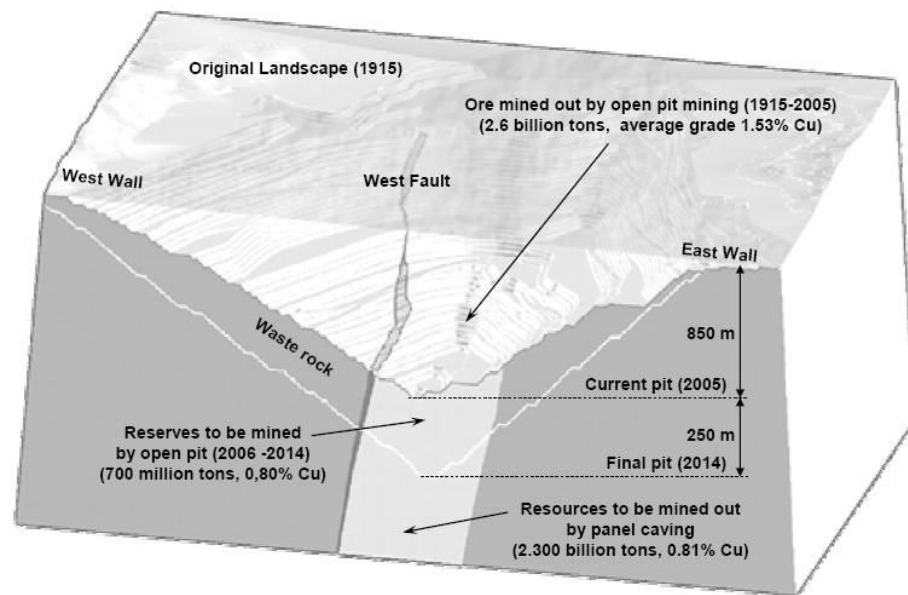


Figure 2.4: Reserve and Geological Resource of Chuqicamata ore. From Olavarría et al (2006)

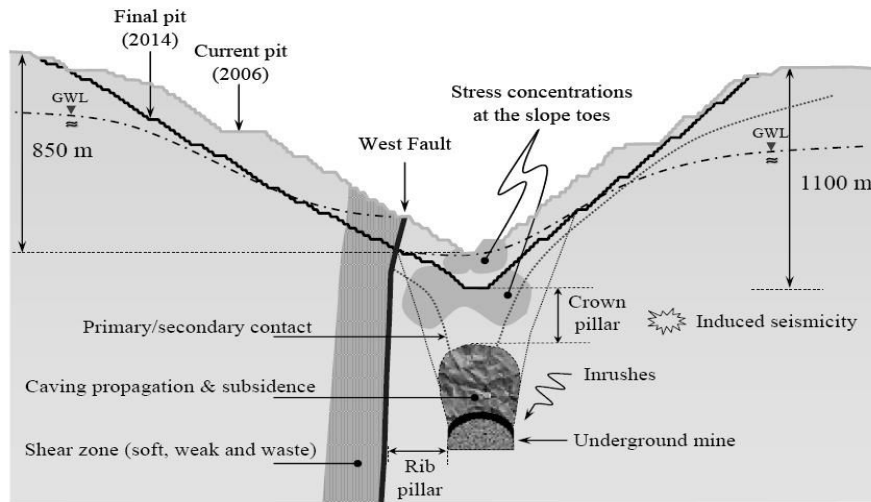


Figure 2.5: The geotechnical challenges associated with the block caving transition. From Olavarría et al (2006).

The transition from an open pit mine to block cave mining at Chuqicamata presents major challenges. Some of the geotechnical issues are (Olavarria et al, 2006):

- 1- The rate of the caving propagation is affected by the presence of the open pit which redistributes the stress between the stress concentration zone or the low confinement zone . Accordingly, the propagation will be either accelerating or arresting the process.
- 2- The stability of the large deep open pit slope is affected by the presence of the west fault and shear zones. Figure 2.5 illustrates the fact that the stability of the rib pillar is influenced by the west fault. If this rib pillar is too thin, it could fail and early dilution may occur; however, if too wide, high grade ore would be left behind.
- 3- Rock bursting potential is expected at the final pit condition in 2014. As a result of induced seismicity, when the pit reaches 1100 m, the undercut level of left 1 will be located at a depth of 1350 m.
- 4- A major environmental concern with the caving-pit slope interaction is subsidence. The zone of influence will defiantly extend over the pit perimeter and evolve with time. The rock mass quality and the presence of major geological structures are the essential parameters contributing to the surface subsidence and pit stability as shown in Figure 2.5.

Two other concerns are highlighted also by Olavarria et al (2006). These include the series of shafts and declines required to access the deep deposit. The ventilation shaft and material handling system is part of the design and construction phase. Besides the technical factors, the proposed planning and

scheduling is a major challenge to overcome since it is based on a simple determination of the present value (NPV) of the next feasibility open pit pushback. Careful and realistic planning is requisite.

2.2.2 Effects on natural slopes

In other cases, e.g. the Resolution copper mine project, concern with respect the impact of block caving on the surface environment is extended to natural slopes. In these cases, the cave may not necessarily be under the slope but may be advancing behind the crest of the slope and have a completely different influence on slope stability.

Apache Leap

The Resolution project is located in the historic Pioneer Mining District of Arizona. The ore body, which has been explored from 2001 to 2003, shows that copper resources exist at depths of 7000 ft below surface (about 2100 m). It was expected that 600,000 tons per year would be extracted for at least 40 years. However, it was necessary to insure that the impact of the mine on the nearby community and historic Apache Leap site would be minimal. Block cave mining has been selected as the method to mine this ore body.

Manske & Paul (2002) describe the geology, host rocks, structural setting, and alteration system of the porphyry deposit in detail. The deposit lies within the well-known Superior district as shown in Figure 2.8. The district lies on the eastern margin of the Basin and Range province in south eastern Arizona. Near surface, the general geology of the superior area consists of Tertiary volcanic units and Quaternary gravels. Near the mine, the geology is a complex structural collage of Mesozoic and older rocks. Figures 2.6 and 2.7 capture different views of Apache Leap.



Figure 2.6: E-W view of Apache leap. From Resolution copper mining -Sustainable development report (2006).



Figure 2.7: Resolution copper mining site plane – town of superior. From www.aznews.us/mine accessed April, 05, 2009.

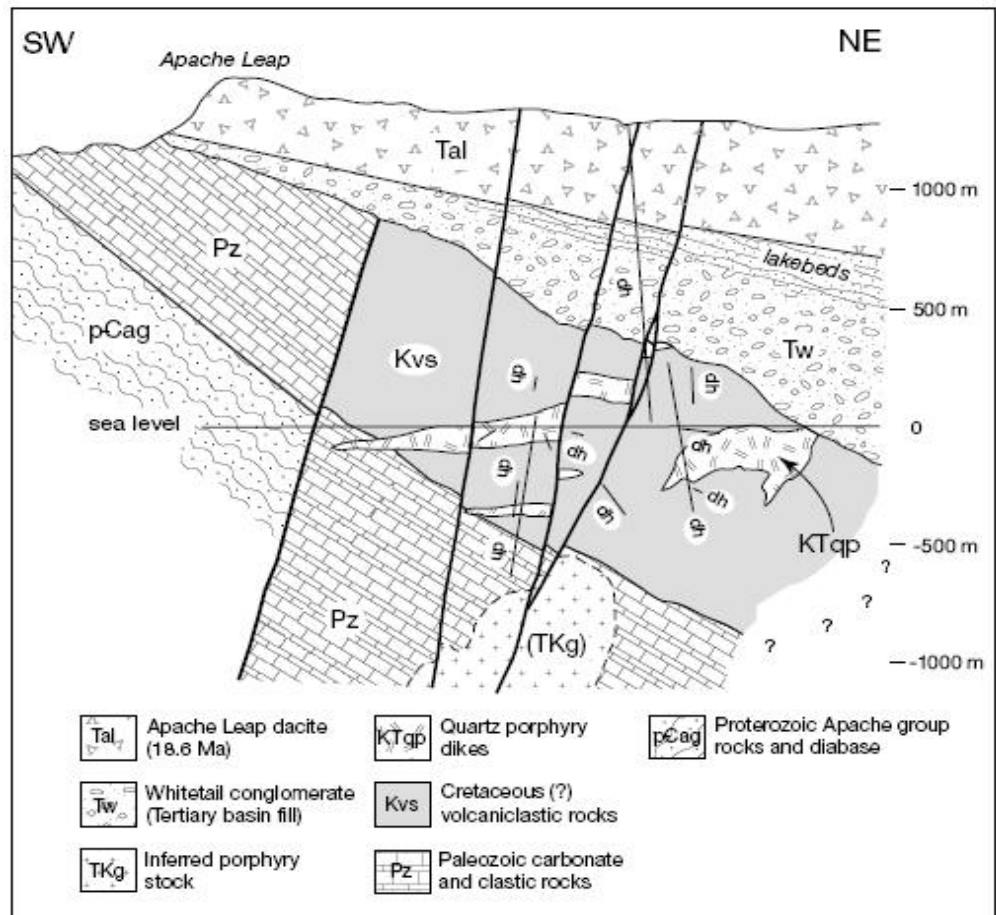


Figure 2.8: Resolution copper mine, Geology Cross-section. From Manske & Paul (2002).

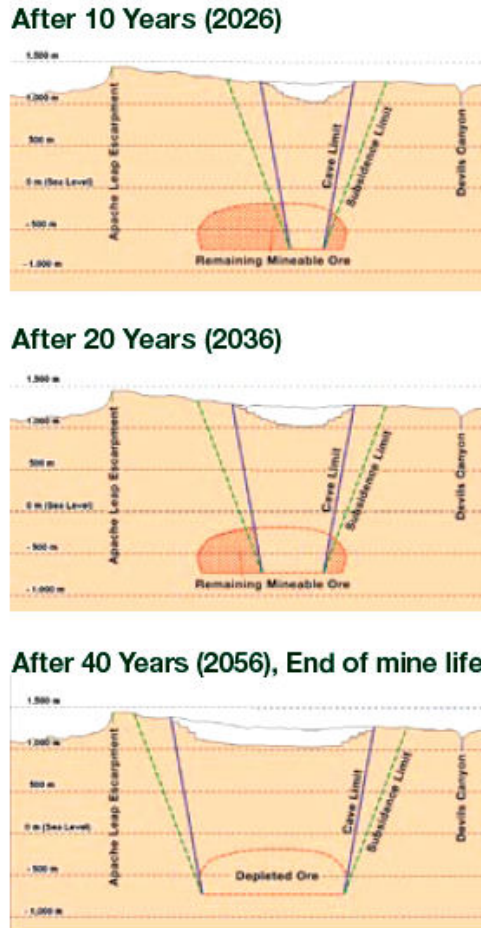


Figure 2.9: Expected block caving operation and associate surface subsidence. From Resolution copper mining -Sustainable development report (2006).

Figure 2.9 shows the Resolution copper project’s preliminary estimate of the final extent of surface subsidence. The Resolution report indicates that any potential mining-induced subsidence will be prevented beneath Apache leap. The report indicates that “If a threat is identified, we will change our mining practices to insure the leap is protected”, (Resolution copper mining -Sustainable development report, 2006).

Subsidence might also put mine infrastructure at risk in addition to the Apache leap issue. Three main shafts which will provide fresh air to the miners and accommodate material handling, are to be placed in the affected area. After 25 years of operation, the expected subsidence zone is projected to be more than 3000 ft (900 m) from the boundary of Apache leap. Moreover, mining is being started away from Apache Leap and monitoring systems will be employed to provide continuous monitoring data throughout mining to make sure the leap is not affected.

2.3 Subsidence

Subsidence due to underground mining is difficult to prevent, especially for those methods involving mass mining. It may vary from small areas directly over the footprint of the mine, to large areas that extend beyond. The consequences of subsidence should not be ignored due to its impact. Proper assessment must be conducted. Mining subsidence engineering has a long history, the major objective of which has been to predict ground movements, determine the effects of such movements on surface structures and renewable resources, and minimize damage due to subsidence. Thus, subsidence engineering not only involves the study of ground movement, and the geology that controls it, but also entails knowledge of surveying, mining and property law, mining methods and techniques, agricultural science, hydrology and hydrogeology, urban planning, and socioeconomics (SME, 1992).

Subsidence is simply created by the distress of the rock mass due to caving or mining of minerals underground. The stress field in the surrounding strata is disturbed and this stress change produces deformations and displacements of the strata affected. The associated displacements and strains may be immediate or delayed for many years. With time, the supporting structures deteriorate and the cavity enlarges. Instability in the rock mass induces the superjacent strata to move into the void. Progressively, these movements propagate to the surface creating a depression. Thus mine subsidence can be defined as the ground movements that occur due to the collapse of the overlying strata into mine voids. Figure 2.10 illustrates explanation and description of subsidence.

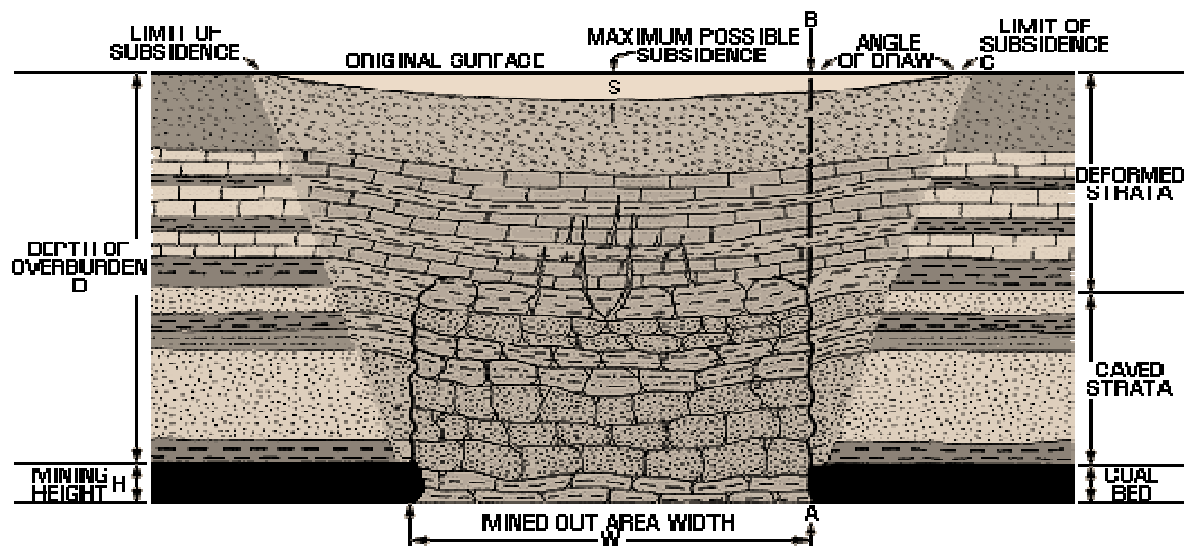


Figure 2.10: General conceptual explanation and description of subsidence. From www.wvgs.wvnet.edu accessed April, 05, 2009.

Subsidence implies the total phenomenon of surface deformation associated with mining. Surface subsidence generally entails both vertical and lateral movements. It manifests itself in cracks, pits, or troughs. Singh (1992) discussed the three major ways surface subsidence develops. Surface fractures, open cracks, stepped slips, or cave-in pits are all signs of tension or shear stresses in the ground surface. Pits or sinkholes are generally associated with a relatively small collapse into the mine void such as a shallow room and pillar mine opening. On the other hand, when the mine void is of large size due to for example, long wall mining, the collapsed strata falls down into the excavation. In other words, the broken material occupies a larger bulk volume than when unfragmented in situ, unless the material is transported or compacted by other means of cyclic wetting or drying. When the void is filled with broken rock, the debris contributes to some support to the superjacent beds. As these strata settle or sag, bed separation may occur since the lower strata subside more than the higher beds. Consequently, as various strata settle and subside, they sag rather than break and produce a trough (dish-shaped) depression on the surface. This type is bigger and wider than a sink-hole and termed a trough or sag subsidence.

As the subsidence progresses due to underground mining, the surface points move toward the subsidence center. Generally, the amount of vertical displacement experienced is greatest at the center, while the lateral displacements are minimal. These displacements are not uniform, and therefore, the changes in length per unit length, or strain, tends to stretch the surface near the edge of the trough (i.e., tensile strain) and push inward within the boundaries (i.e. compressive strain). Five deformation components combined produce subsidence: vertical and horizontal displacements, slope, and the derivation of vertical displacement with respect to the horizontal displacement, horizontal strain, and vertical curvature.

Several mining and geological parameters affect the magnitude and extent of subsidence. Rock mass, geological structure, in situ stresses, and mining method are the key factors influencing surface subsidence. The characteristics of the mine roof and floor rock are critical in the initiation of subsidence movements. Competent roof beds tend to support the overlying strata longer; and therefore, delay subsidence. Also, the nature of overburden may play a big role in surface subsidence. Strong massive beds above the mine level tend to support the overburden and defer the occurrence of subsidence. Moreover, the existence of faults, folds, and/or geological discontinuities may increase subsidence potential. Because of the ease of slippage along discontinuities due to the disturbance of the equilibrium of forces in the strata, settlement or up thrust may occur at the surface, which may

appear as a series of stepped fractures. On the other hand, high horizontal stress tend to restrain subsidence by forming a ground arch in the immediate mine roof (Lee & Abel, 1983).

Other factors may also control the surface subsidence: surface topography, ground water, degree of extraction, water level elevation and fluctuations, mined area, method of working, rate of face advance, back filling, degree of extraction, and structural characteristics. For example, the amount of subsidence experienced is a function of time. In longwall mines, the surface may start sagging almost immediately after the face passes below an area. However, in room and pillar operations, evidence of subsidence may not be observed until the mine is completed and the pillars deteriorate or punch into the floor.

2.3.1 Characterization of cave-induced subsidence

Several types of cave-induced subsidence deformations are discussed by Lupo (1996). The surface subsidence of narrow bedded deposited such as coal seams overlain by stratified sedimentary rocks is called "Trough subsidence. It increases as mining progresses as a form of continuous subsidence. On the other hand, the discontinuous subsidence is related to cave mining. The zone of impact is characterized by subsurface caving, plug caving, and chimneying. Lupo (1996) also conducted a review of several cave mining and summaries the features of subsidence deformation zones related to mass mining as shown in Figure 2.11. It should be noted that subsidence is a dynamic process. The more extraction of ore from the production level, the more change and extended the subsidence deformation is on surface. Therefore it is difficult to predict the subsidence accurately given the complex behavior of the dynamic evolution of subsidence with respect to mass mining.

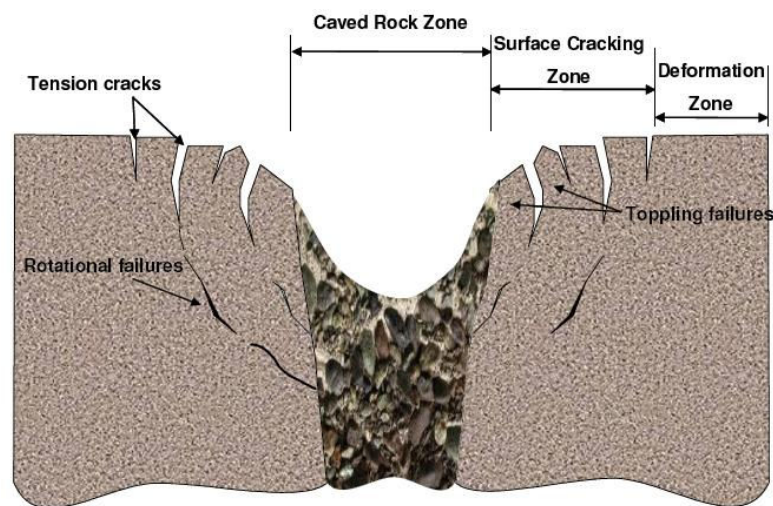


Figure 2.11: Subsidence deformation zones. From Lupo (1996).

Surface disturbance and subsidence was defined by Van As et al. (2003) to establish the framework of zone of progressive deformation results attributed to block caving modeling. The terminology used is proposed and defined below in Figure 2.12. Here, the 'Subsidence zone' encompasses all caving induced deformations on the surface. The 'Caving rock zone' (i.e. zone of active movement) is comprised of the failed caved rock which is moving downwards as it is drawn from below. The 'Breakthrough zone' (i.e. crater) is where the cave breaches the surface and the failed material moves vertically down into the cave muck pile. The 'Fracture zone' encompasses all of the obvious surface deformations. Lastly, the 'Continuous subsidence zone' is the area that exhibits elastic deformation or continuous non-elastic strains (movements about 2 mm or greater).

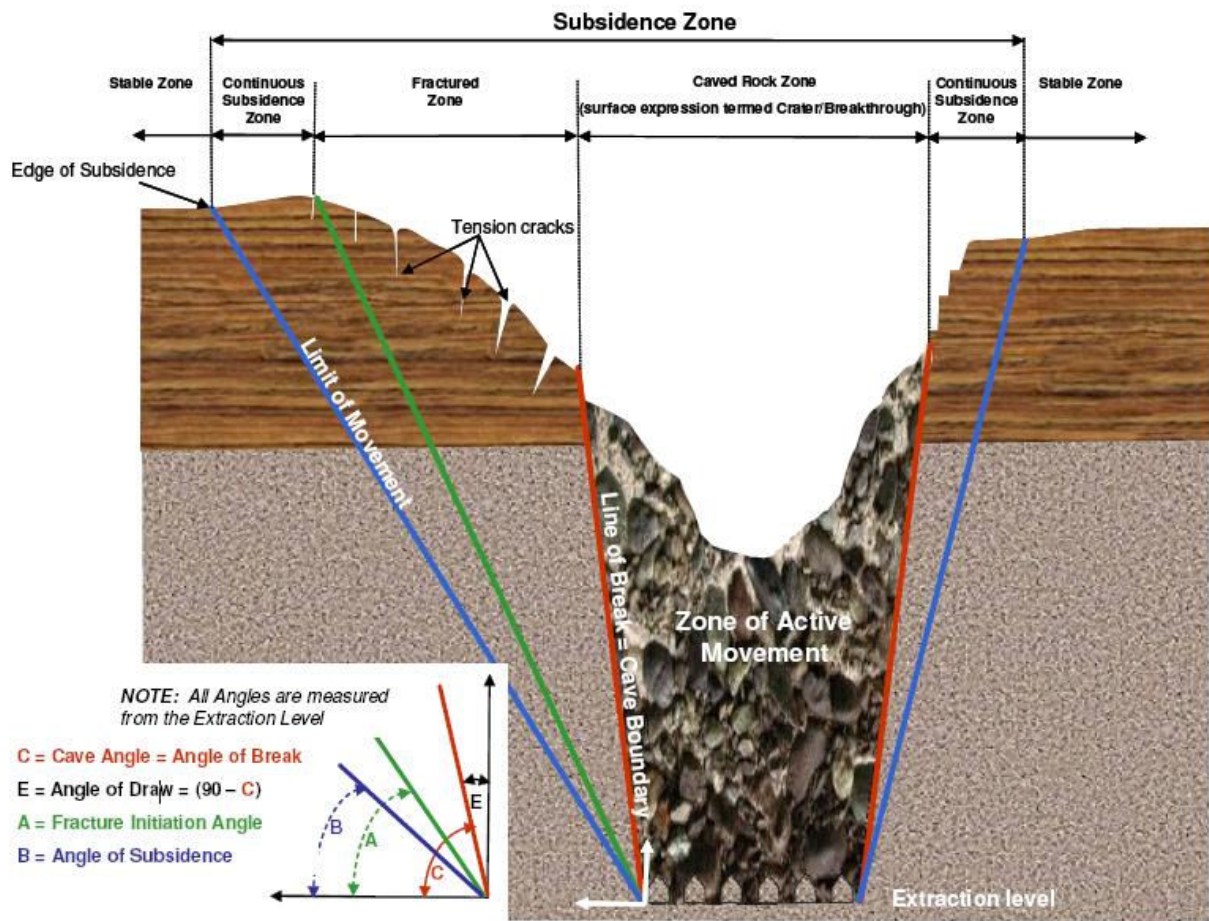


Figure 2.12: Cave propagation mechanism toward surface and surface subsidence initiation. From Van As et al (2003).

2.4 Rock slope failure modes

A brief introduction to some of the most common rock slope failure modes is presented in this section. Some particular issues and points are highlighted within the scope of each to explain some of the observed phenomena. Planar, toppling, bi-planar, and buckling failure modes are discussed below.

2.4.1 Planar failure

Planar failures involve translational sliding along a planar or undulating rupture surface. This failure mode is relatively rare compared to translational wedge failures, as usually it is a combination of intersecting discontinuities that promote failure as opposed to a single persistent discontinuity (as in the case of planar failure; Figure 2.13). Nevertheless, rock engineering practitioners and researchers would not ignore this considerably simple case of slope failure due to the fact that there are many valuable lessons to be learned from the mechanics of this failure mode. In particular, the sensitivity of the slope changes in shear and ground water condition are demonstrated by this two dimensional case study, in contrast with the actual complex three-dimensional rock slope kinematics, where changes are less obvious. Figure 2.13 shows the geometry of the planar failure mode.

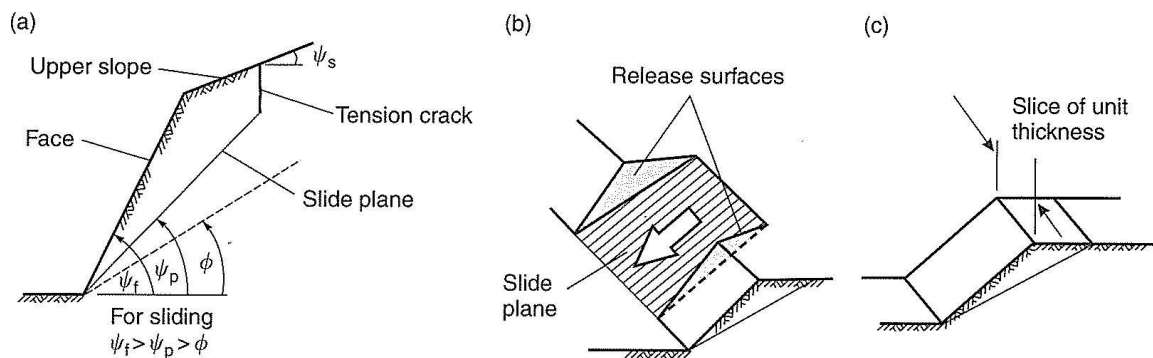


Figure 2.13: General cross-section geometry and released surface exhibiting plane failure. From Hoek & Bray (2001).

Ideally, based on Wyllie and Mah (2004), the general conditions for planar failure to occur are as follows:

- The sliding plane must daylight in the slope face.
 $\Psi_p < \Psi_f$
- The angle of friction of the sliding plane must be less than the dip of this plane.
 $\phi < \Psi_p$.
- Failure can take place on a sliding plane passing through the convex of a slope.
- The upper end of the sliding plane must terminate in a tension crack or intersect the upper slope surface.

where Ψ_p , Ψ_f and ϕ are the dip of the sliding plane, slope face angle, and the friction angle of the sliding surface respectively.

It is also important to highlight the significant control of the ground water pore pressure as well as the slope geometry on the analysis of planar failures, since the kinematics of planar failure accounts only for the geometry of the slope and structural discontinuities. Hoek & Bray (1981) presented an equation to calculate the factor of safety (FS) based on several assumptions made.

$$FS = \frac{\text{Resisting force}}{\text{Driving force}}$$

$$FS = \frac{cA + (W \cos \Psi_p - U - V \sin \Psi_p) \tan \phi}{W \sin \Psi_p + V \cos \Psi_p}$$

where c and A are the cohesion and the area of the sliding plane respectively. U , and V are the water forces acting on the sliding plane and tension crack correspondingly, and W is the weight of the sliding block.

Many case studies discuss the influence of a tension crack on the stability state. In the upper surface of some examined excavated slopes, the tension cracks can be clearly and frequently observed. Some of them are visible for several years but have no adverse influence on the stability of the slopes (Hoek & Bray, 1981). Barton (1971) found through a very detailed model study on the failure of slopes in jointed rocks, that the tension cracks were generated as a consequence of small shear movements within the rock mass. Therefore, their cumulative effect was a significant displacement on the slope surface; the tension cracks are caused by shear movements, which are sufficient to create separation of vertical

joints behind the slope crest. The study suggests that when the tension cracks become more visible on the surface of the slope, they are an indicator of instability within the rock mass (Hoek & Bray, 1981).

2.4.2 Toppling failure

Different from translational planar sliding, toppling involves the forward rotation of the rock mass about the central base. Commonly, there are two unique-kinds of toppling: block and flexural toppling. In both cases, toppling requires removal of fixed block at the face, e.g. rock slope, to allow columns or blocks of rocks to topple. That is due to the fact that the center of gravity of those blocks lies outside the base. Frequently in nature, the movement of the toe in artificial or natural rock slope plays a great role in developing toppling failure. Figure 2.14 presents simple diagrams of different types of toppling scenarios.

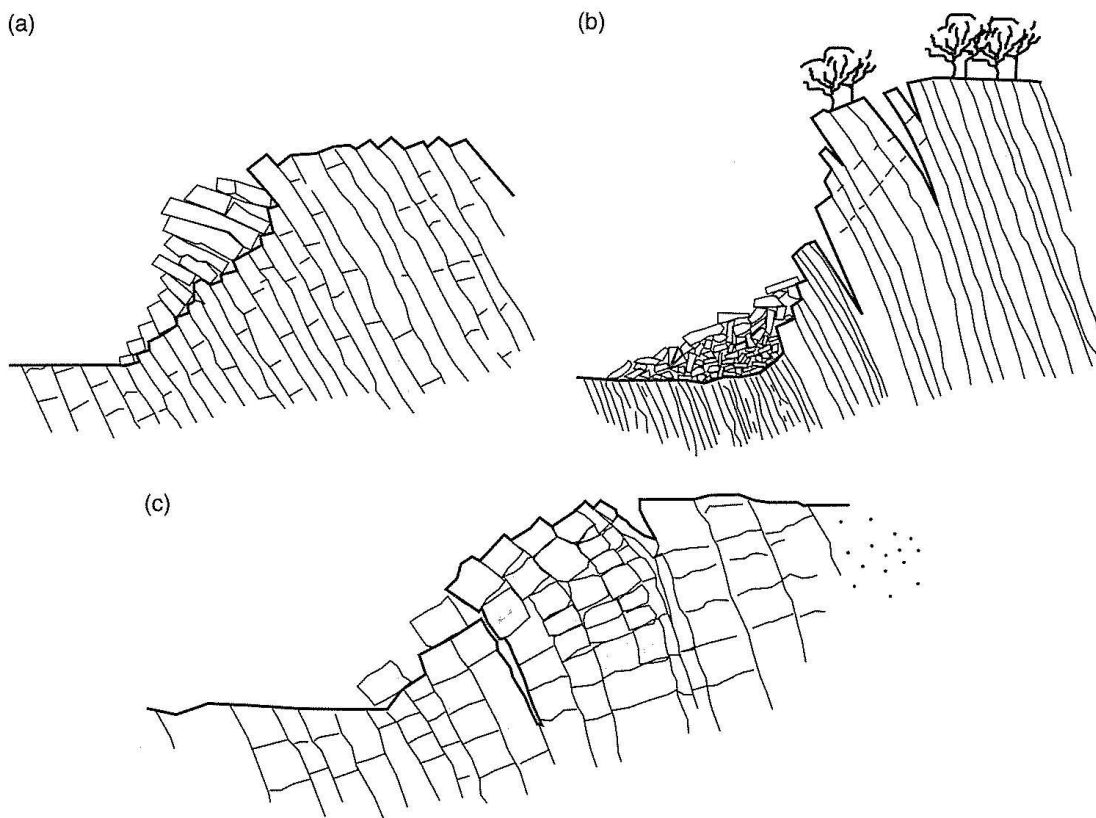


Figure 2.14: Simple diagram presents: **(a)** Block toppling of columns of rocks, **(b)** flexural toppling of slabs of rocks, and **(c)** block-flexural toppling of long columns through accumulated motions along numerous cross-joints. From Hoek & Bray (2001).

Several toppling mechanisms are described by Goodman & Bray (1976). The most common cases encountered in the field are block toppling and flexural toppling. Block toppling starts when the short columns, dipping steeply into the face at the toe, are pushed by the adjacent columns. The orthogonal cross-joints and the main joint set form the blocks. Sliding of the toe allows toppling to advance and to widen along the rock slope.

On the other hand, flexural toppling involves slender columns of rock, formed by a single well-defined joint set dip steeply into the face, breaking in flexure as they bend forward. Typically, erosion and excavation of the toe allow the toppling to develop by creating tension within the slender rock columns. Interlayer slip between the columns is important in controlling the degree to which the rock mass deforms toward the toe of the rock slope.

In addition, Hoek & Bray (1981) discussed other types of toppling. Block-flexural toppling is characterized by pseudo-continuous flexure along long columns that are divided by numerous cross joints. The large number of small movements in this category leads to fewer tension cracks than in flexural toppling, and fewer edge-to-face contact and voids than in block toppling. Likewise, secondary toppling may occur as a result of primary failure which could be controlled by sliding or physical breakdown of rock, particularly in horizontal bedded rock.

The failure of block toppling can be estimated by two different kinematic tests. The first examines the shape of the blocks. The second test assesses the relationship between the dip of the planes and the face angle. The following are criteria for potential toppling conditions.

- The dip of the base plane is smaller than the friction angle between the base (stable)

$$\psi_p < \phi_p$$

and

$$\frac{\Delta x}{y} < \tan \psi_p$$

- The condition for interlayer slip is :

$$\psi_d \geq (90 - \psi_f) + \phi_p$$

- The dip direction of the planes forming the sides of the blocks (α_d) is within about 10 degrees of the dip direction of the slope face (α_f).

$$|(\alpha_f - \alpha_d)| < 10^\circ$$

where y and Δx are the height and width of toppling blocks. Ψ_p , Ψ_d , Ψ_f , and ϕ_p are the dip of the plane, the dip of the planes forming the sides of the blocks, the dip of the slope face, and the friction angle of the sides of the blocks, respectively.

A study by Nichol et al. (2002) examined the typical toppling failure modes that are widespread in many mountainous areas. The study identified those modes that lead to either ductile or brittle failure behavior. The distinct-element code UDEC was employed in the theoretical part of their parametric study. Different parameters were examined: strength, discontinuity orientation, spacing, and persistence, and the condition at the toe of the slope. Two different scenarios of toppling mechanism are simulated, flexural toppling and block toppling defined by Goodman & Bray (1976).

Results given in Nichol et al (2002) show that flexural toppling involves predominantly ductile behavior and is self-stabilizing, at least for those cases that made up the study. The principal stress associated with the ductile behavior is different at the top and bottom of the slope. At the top of the slope the principal stress is parallel to the face while at the bottom principal stress is vertical. On the other hand, the high persistence of cross-joints in block toppling modes emphasizes that the block toppling is solely a brittle process. Variations in rock mass parameters can lead to extremely rapid (catastrophic) failure.

2.4.3 Bi-planar & buckling failure

A special case where the dip angle of the prominent discontinuity or set of discontinuities coincides with that of the natural or engineered rock slope is a dip slope. Since the inclination of both the cut slope and the failure controlling discontinuities are similar, “daylighting” of a sliding surface does not occur requiring shearing through the rock mass material at the toe of the slope, or toe-breakout, for failure to occur (Fisher & Eberhardt, 2007). Bi-planar, buckling, and ploughing are generally the three failure mechanisms characterized by the dip slope failure mode. Fisher & Eberhardt (2007) discussed the scenario of bi-planar failure mechanism where the adverse cross-cutting structure daylighting at the slope is the primary factor influencing mine slope failure. Therefore, three toe-breakout failure mechanisms, primarily related to slope specific geology, are encountered: failure at the toe along cross cutting joints, failure at the toe through shearing of the intact rock mass, or a combination of these two in which a step-path surface develops at the toe. The study emphasized the importance of realistically accounting for parameter uncertainty, e.g. rock mass and structural discontinuities. The distinct-element method used in the study discussed by Fisher & Eberhardt (2007), was able to reproduce the plastic yield (shear localization), toe breakout and internal shearing that develops in these failures. These results showed that the failure angle at which toe breakout occurs is related to the angle between the principal stress and the failure surface (θ):

$$\theta = 45 - \phi'/2$$

2.5 Numerical modeling

The recent advancement in computational power and user proficiency in state-of-the-art numerical modeling tools has enabled a greater potential in advanced understanding of rock mass characterization and complex rock slope deformations. Stead et al. (2005) discussed three different level of sophistication in the analysis of complex rock slopes and associated failure mechanisms. Each level of complexity has unique advantages and limitations. Kinematic and limit equilibrium assessments of rock slope stability is the first level. Because these are fairly simple to use, they have been used for simple and preliminary design or for non-critical slopes problems (Stead et al., 2005). On the other hand, the use of continuum/discontinuum numerical models has gained wide popularity in academic research and in engineering practice. In particular, numerical discontinuum techniques are being increasingly used in practice due to their ability to allow for block deformation and relative movements of blocks (rigid or flexible). They are especially adept at modeling complex behavior and mechanisms related to jointed rock masses. Moreover, dynamic and hydro-mechanical analysis can be coupled to discontinuity behavior. It must be recognized, however, that limitations restrict the degree of complexity that can be incorporated into the model given excessive run time constraints, in particular limited data on joint properties and unrealistic models of progressive failure mechanisms. Currently the most sophisticated analysis that can be undertaken involves using hybrid continuum-discontinuum approaches which allow fracture simulation. Because these models are computationally expensive, they are best suited for complex translation/rotation instabilities where failure requires internal yielding, brittle fracturing, and shearing in addition to strength degradation along release surfaces (Stead et al., 2005).

A study by Vyazmensky et al. (2007) investigating mechanisms governing subsidence development over block cave mines showed that reasonable simulation of surface subsidence can be achieved using equivalent continuum and mixed approaches. The study started by discussing the techniques used to predict surface subsidence associated with block caving mining. Laubscher (1981) proposed a design chart employing the MRMR (mining rock mass rating), the density of caved rock, and the height of caved rock and mining geometry to predict the cave angle. This empirical method does not take into account the effect of geological structure, which has a significant effect on the prediction. It is also important to highlight the fact that it is difficult to accurately calculate the density of caved rock. Another means to assess subsidence is through limit equilibrium techniques. However, solutions, like

that presented by Hoek (1974), require the failure mechanism to be assumed, for which the solution must be specifically derived, and provides estimates for the angle of break only.

Large strain continuum approaches and discontinuum approaches are two numerical analysis strategies that are being used in analyzing induced block caving subsidence. Vyazmensky et al. (2007) summarized the studies in which numerical modeling methods were used (Table 2.1).

Table 2.1: Numerical Studies of surface subsidence. From Vyazmensky et al. (2007)

| Author | Approach | Type of Analysis | comment |
|----------------------------|-------------------|-------------------------------------------------------|-----------------------------------------------------------------------------------------|
| Singt et al. (1993) | LSC (FLAC)* | Site specific : Rajpura Dariba and Kiruna mines | |
| Karzulovic et al. (1999) | LSC (FLAC) | Site specific : El Teninta mine conceptual | |
| Flores & Karzulovic (2004) | LSC (FLAC/FLAC3D) | | Provide general guidelines for surface subsidence associated with Block caving |
| Li & Brummer (2005) | D (3DEC)** | Site specific : Palabora mine | |
| Gilbride et al. (2005) | D (PFC3D) | Site specific : Questa mine | |

- * LSC : Large strain continuum approach ** D: Discontinuum approach

More recent approaches to subsidence analysis involve the use of hybrid finite/discrete element codes, such as ELFEN (Rockfield Technology Ltd., UK) as described by Vyazmensky et al (2007), that allow for the simulation of fracture initiation and propagation. This allows the caving process to be simulated as a brittle fracture driven continuum-discontinuum transition. In the work of Vyazmensky et al (2007) work, two constitutive fracture models are applied: a Rankine rotating crack model and a Mohr-Coulomb model with a Rankine cut-off. The detailed conceptual study presented by the authors demonstrates that our understanding of rock mass behavior in block caving can be significantly improved through the use of these improved modeling methodologies for subsidence prediction.

A study by Elmo et al. (2007) uses the same approach, presents the interaction between open pit and block cave mining in a jointed rock mass. Rock mass strength, the in-situ stress field, geological

structure (e.g. joints, bedding, faults, etc.) and the geometry of the excavation are the fundamental key factors affecting the stability of a surface crown pillar. A generic model is used and rock properties for the intact rock and rock fractures are undertaken in the simulated models. The models show that without the block caving, the open pit walls appear relatively stable. The study reflects the potential impact of block caving mining on existing open pit operations (Elmo et al., 2007).

Another study by Eberhardt et al (2004) emphasized the need to consider rock slope failure using the principal of fracture mechanics, considering damage, energy, fatigue, and time in the analysis. These considerations are similar to those required for the investigation and prediction of the impact of block caving on rock slope stability, the subject of this thesis. In particular, the controlling influence of different patterns of jointing on the deformations and failure mode that arises. As shown by numerous authors, the Universal Distinct Element Code (UDEC4.0, Itasca Ltd.) is a powerful tool for such studies (Stead et al. 2005), and is utilized in the study (and discussed further in Chapter 3, Methodology).

3 METHODOLOGY

The Universal Distinct Element Code (UDEC 4.0), a numerical tool favored for rock engineering projects, is employed in this thesis research to study the influence of block caving on the stability of several hypothetical jointed rock slopes with different jointing patterns. UDEC is a two-dimensional numerical code based on the distinct element theory for discontinuum modeling. Static and dynamic loading response of discontinuum media, represented as an assemblage of discrete blocks, can be successfully simulated by UDEC. Boundary condition between either rigid or deformable blocks, represents the discontinuum media. Linear or non-linear stress-strain constitutive relationships can be prescribed for a mesh of finite difference elements intended for deformable blocks. A linear or non-linear force-displacement relationship governs the relative behavior of the discontinuities. The Lagrangian calculation scheme is used to model large movements and deformations of the blocks.

This section will discuss the methodology of how the block caving process is simulated using UDEC. The Modeling setup section will present the geometry, rock mass properties, properties of discontinuities, and other modeling setup factors applicable to the research undertaken. Another section will highlight the assumptions used in this research to manage the uncertainties in the modeling of the simulated rock mass behavior. Based on the study by Van As et al. (2003), a recommended terminology for subsidence definition is also presented in this methodology section to emphasize and encompass the terminology used in following results section.

3.1 UDEC formulation

The UDEC formulation works to carry out a series of calculations based on the application of a force-displacement law and Newton's second law of motion for all blocks and contacts in the model. The force-displacement law is used to find contacts for known and fixed displacements. This calculation is done at one time since the force depends on displacement. Thus, these fixed and known resultant forces are used to calculate the motion of the assembled blocks using Newton's second law. Figure 3.1 presents a schematic diagram of the calculation cycle for the distinct element method.

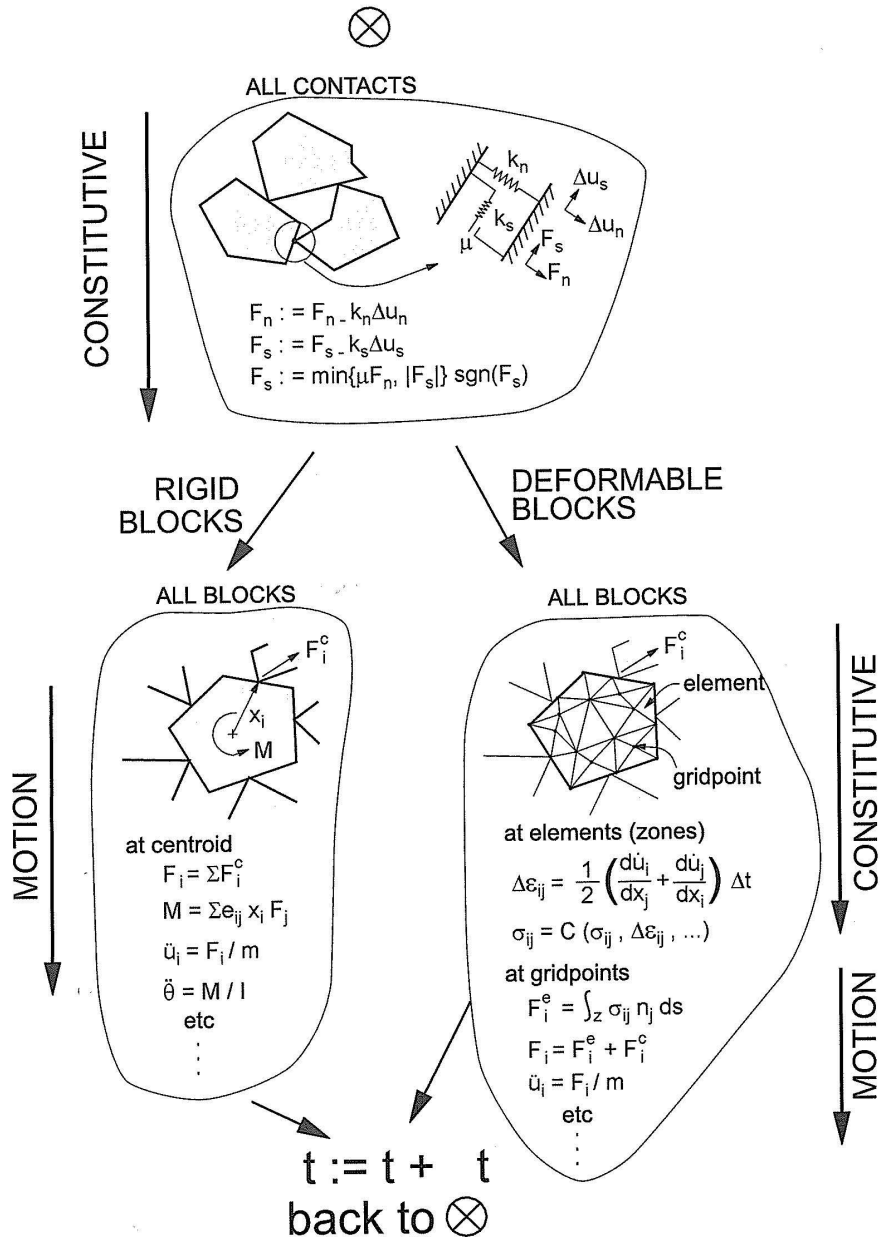


Figure 3.1: Calculation cycle for the distinct element method employed by UDEC (Itasca, 2004)

3.2 Model setup

Although, modeling for the purpose of subsidence prediction and slope stability would require site specific details of the topography, geology, and mine layout, this study uses a series of generic models to investigate the specific influence of several of these factors through a comparative analysis. The geometry of these conceptual models is based on the dimensions encountered for several actual large open pit slopes (e.g. Palabora in South Africa). Twelve different scenarios (generic cases) are assumed, for a 800-m high rock slope with model dimensions of 4000 m by 2200 m. These extended boundaries are required to represent both rock slope and block caving zones, while minimizing boundary effects. The different scenarios involve varying structural discontinuity configurations and block caving locations. Potential sliding, toppling, bi-planar, and buckling failure configurations are generated in UDEC to study the impact of discontinuity dip angles, orthogonal cross-joints, etc., as a function of cave propagation. The caving zones are set equal in height for all models, 1000 m below the upper surface of the mine. Typically two positions of the caving zone are tested for each joint network configuration, one where the cave advances beneath the toe of the slope towards the pit bottom, and one where the cave is positioned behind the crest of the slope. Caving is simulated in stages (of increasing cave height) to represent the continuous mining of the ore body (Fig. 3.2). As illustrated in Figure 3.2, the dimensions of the cave are (400 m in width and approximately 300 m in height), modeled in five lifts between 50-100 meters each, depending on the numerical stability of the solution. The model boundaries are extended from both sides to eliminate the effect of numerical errors and boundary effects, as well as to study the pattern of subsidence away from the rock slope.

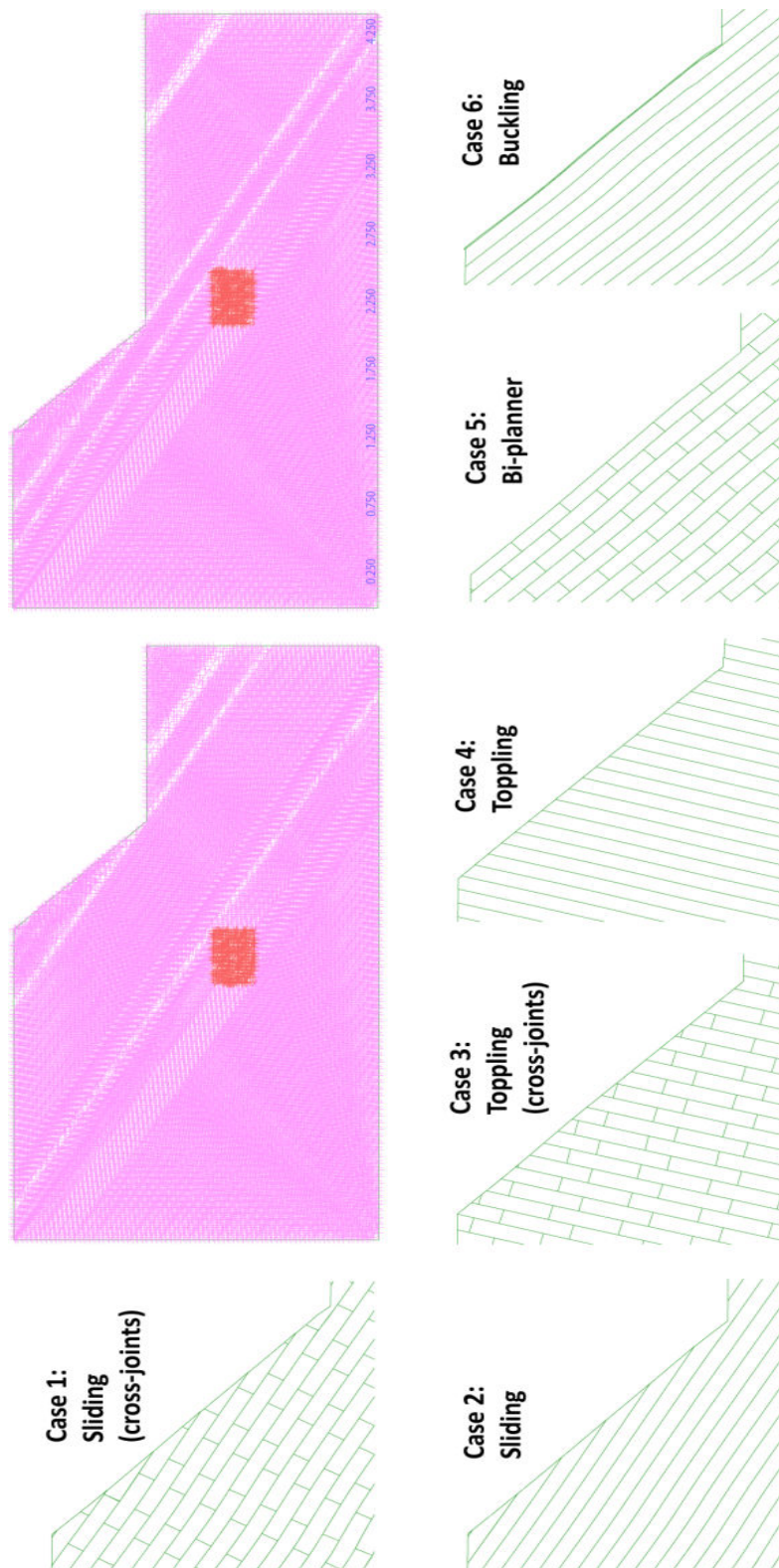


Figure 3.2: Two different caving positions and six different generic configurations of structural discontinuities: case 1 to case 6. (Slope height is 800 meters).

In this study, different jointing configurations are performed using six generic models as shown in Figure 3.2. Table 3.1 also describes the different potential kinematic failure patterns as discussed in this research.. They are examined and referred to as cases one to six:

- Case 1: Continuous main joint set dipping out of the face (i.e. daylighting), favoring translational sliding. An orthogonal non-persistent cross-cutting joint set is included to provide an additional degree of kinematic freedom and to allow the development of step-paths. This case is defined in this study as "Sliding-type with cross-joints".
- Case 2: Configuration similar to Case 1, but without cross-cutting joints. This case is referred to as "pure-sliding-type".
- Case 3: Continuous main joint set dips much steeper here, relative to Case 1, where together with the non-persistent cross-cutting joint set, promotes a toppling failure mode. This configuration is referred to as "Toppling-type with cross-joints".
- Case 4: Configuration similar to Case 3, but without orthogonal cross-joints, named "Pure-toppling-type".
- Case 5: Continuous jointing parallel to the slope face with cross-jointing, referred to as "Bi-planar type".
- Case 6: Continuous joint set parallel to slope face without cross-cutting joints, referred to as "Buckling type".

Table 3.1: Generic/conceptual models with different configurations of discontinuities (joints).

| | Description | Dip | Trace | Gap | Spacing |
|---------------|------------------------------------|-------------------------|---------------------|---------------------|---------------------|
| | | <i>Angle degree</i> | <i>Length m</i> | <i>Length m</i> | <i>Length m</i> |
| Case 1 | Sliding type with cross joints | 30 | 1200 | 0 | 50 |
| | | 120 | 50 | 50 | 200 |
| Case 2 | Pure-sliding-type | 30 | 1200 | 0 | 50 |
| | | NA | NA | NA | NA |
| Case 3 | Toppling type with cross joints | 75 | 1200 | 0 | 50 |
| | | 165 | 50 | 50 | 200 |
| Case 4 | Pure-toppling-type | 75 | 1200 | 0 | 50 |
| | | NA | NA | NA | NA |
| Case 5 | Bi-planar | 45 | 1200 | 0 | 50 |
| | | 135 | 50 | 50 | 200 |
| Case 6 | Buckling | 45 | 1200 | 0 | 50 |
| | | NA | NA | NA | NA |

Each model was initialized by establishing the geometry and assigning the rock mass and discontinuity properties. The initial loading condition (gravity) and in situ stresses were executed using an elastic constitutive model to avoid numerical defects related to plastic yielding during the initial consolidation of the model. The displacements from this step were reset to zero and the constitutive model changed to elasto-plastic for the subsequent simulations of block caving. Block caving was simulated successfully using a direct block deletion technique for each of the different scenarios modeled.

Modeling block caving is challenging in the sense of precisely initiating the dynamic process of block caving and to successfully simulate cave development through continuous drawn down of the extracted material through the draw points. As explained in detail by Van As et al. (2003), the increase in volume due to cave propagation is defined. As the material is extracted from the active cave zone, the volume of the detached primary blocks of the cave back is increased due to the voids between muck piles. The term “Bulking” or “swelling factor” is defined as the proportional increase in volume of in situ rock when it has caved or bulked. Figure 3.3 illustrates the cave propagation mechanism toward surface. It shows that the in situ volume becomes a caved volume on bulking. Consequently, to reserve the conservation of volume, a vertical distance from the cave back must swell to fill its own volume plus the

drawn volume. Therefore the caved height is simply a function of the in situ material drawn and the swell factor. The following is the mathematical definitions of those terminologies.

$$V_{swell} = V_{in\ situ} \times B$$

$$V_{caved} = V_{in\ situ} \times (1 + B)$$

$$S_f = 1 + B$$

$$H_c = H_d/B + H_d$$

where:

B : Bulking factor

S_f : Swelling factor

V_{caved} : Caved volume

V_{swell} : Swelled volume

$V_{in\ situ}$: In situ volume

H_c : Caved height

H_d : Height of the in situ material drawn

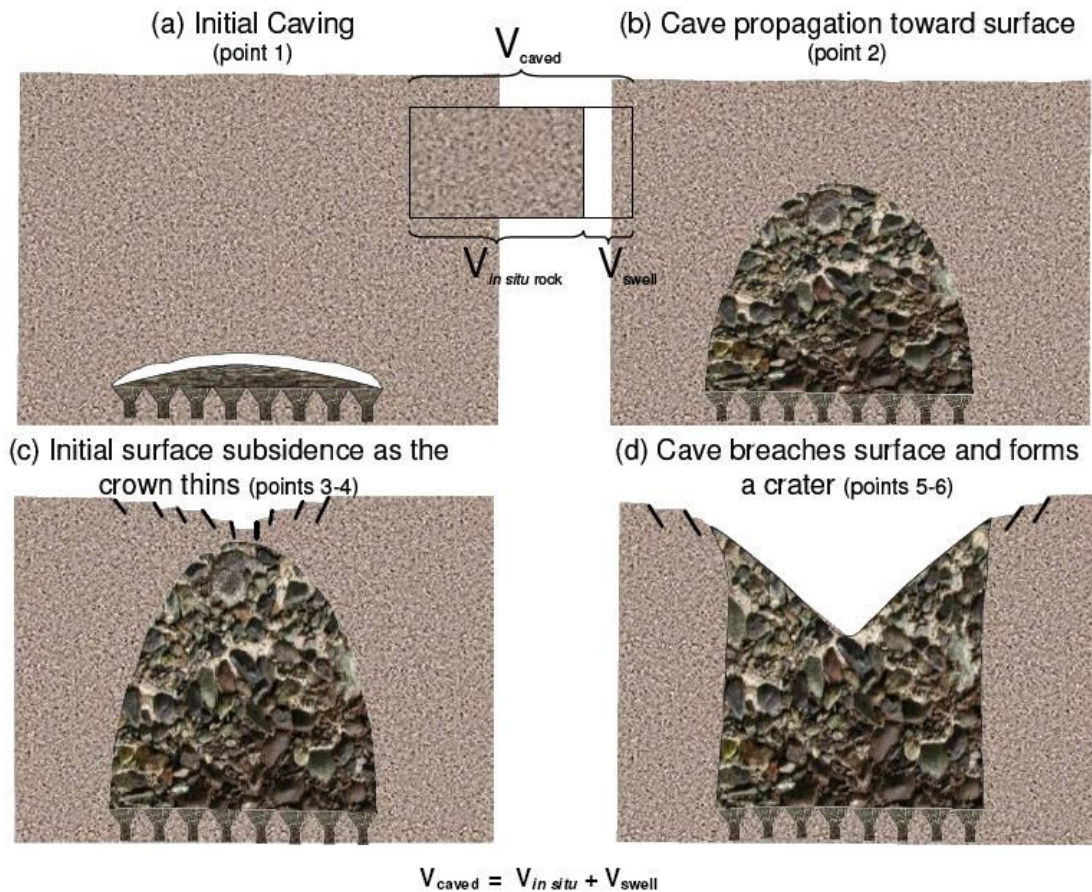


Figure 3.3: Cave propagation mechanism toward surface and surface subsidence initiation. From Van As et al. (2003)

3.3 Modeling assumptions

All simulations adopt a two-dimensional plane strain assumption; the influence of curvature in the third dimension is neglected, which if present can provide more lateral resistance. It is also assumed that the slope face is planar and continuous in the out-of-plane direction. In reality, the material from each side provides more resistance to potential failure.

Strength degradation and progressive failure of the rock mass through brittle fracturing is not modeled in UDEC; the assumption in this research study therefore is that the influence of block caving on rock slope deformation is purely a function of the different generic jointing patterns. This limitation in the software restricts the main emphasis of this research to the study of joint-controlling failure mechanisms. The ability to simulate fracture propagation would add a further degree of realism to the model as discussed in the literature review section.

Although part of this research is to examine the impact of block caving on open pit slopes which are elliptical in shape, plane strain is by default set for all models. It is the basic formulation intended for

long structures or excavations with constant cross section. The assigned loads are acting in the plane of the cross section. Discontinuities are treated the same way; they are considered as planer features oriented normal to the plane of analysis. It should be stressed that the out-of-plane stress exists and therefore flexible blocks may exhibit plastic yield and failure due to this stress, (σ_{zz}), if the out-of-plane stress turns out to have a major effect on stability.

A Coulomb slip failure criterion is assumed to adequately represent the physical response of the joints. It is intended for blocks in contact across an area (as opposed to a point). The model provides linear representation of joint stiffness and a yield limit. It is based on elastic stiffness, friction angle, cohesion, dilation angle, and tensile strength properties.

It is assumed that the normal stiffness, k_n , friction angle, and cohesion of the joints surrounded by the caving perimeter have stronger properties to avoid one block penetrating into another (this generates a numerical error message "Contact over lap too great"). Modeling recommendations provided in the UDEC manual (Itasca 2004) show that the normal, k_n , and shear stiffness, k_s , of the joints "should be kept smaller than ten times the equivalent stiffness of the stiffest neighborhood zone in blocks adjoining the joint":

$$k_n \text{ and } k_s \leq 10 \left[\left(K + \frac{4}{3G} \right) / \Delta Z_{min} \right]$$

Where K and G are the bulk and shear modulus, respectively, and ΔZ_{min} the element width. A Mohr-Coulomb plasticity model is assigned for deformable blocks. This material model is widely used to represent rock and soil behavior. The model assumes that yielding takes place when the material is subjected to shear loading and the shear strength is exceeded. The failure criteria in UDEC are based on only the two principal stresses, the major and the minor stresses. The Mohr-Coulomb model requires the elastic properties of the rock mass plus the extra plastic properties. All rock mass properties are set equal for each model simulation, as shown in Table 3.2. A selected value of Poisson's ratio of 0.25 and elastic modulus of 20 GPa were used. It should be stated that the Poisson's ratio plays a role in the Mohr-coulomb failure criteria since intact rock and the joints are pressure-sensitive. The bulk modulus, K , and the shear modulus, G , as defined in UDEC are interchangeable with both the Young's modulus, E , and Poisson's ratio, ν as follows:

$$K = \frac{E}{3} (1 - 2\nu)$$

$$G = E/2(1 + \nu)$$

$$E = 9KG/(3K + G)$$

$$\nu = (3K - 2G)/2(3K + G)$$

Table 3.2: Discontinuities and rock mass properties assigned for all simulations.

| Coulomb Slip Model | | | Mohr-Coulomb Plasticity Model | |
|---------------------------|-----|-----------------------|--------------------------------------|------|
| Discontinuities | | At the caving zone | Rock mass | |
| Normal Stiffness(GPa) | 5.0 | 10.0 | Density (Kg/m ³) | 2600 |
| Shear Stiffness (GPa) | 0.5 | 0.5 | Bulk Modulus (GPa) | 13.3 |
| Friction Angle | 35 | 40 | Shear Modulus(GPa) | 8.0 |
| Cohesion (MPa) | 0 | 0.1 | Friction Angle (Degree) | 40 |
| Dilation Angle | 0 | 0 | Cohesion (MPa) | 1.0 |
| Tensile strength (MPa) | 0 | 0 | Dilation Angle (Degree) | 10 |
| | | | Tensile Strength (MPa) | 0.5 |

As a result of the rock mass properties assigned to the deformable blocks, a static equilibrium of the initial model simulation is created, balancing the stresses and the initial stress conditions resulting from the boundary conditions. The vertical initial stress component is assumed to increase as a function of depth, which is generally accepted as a valid assumption. More problematic is the assumed ratio between the initial horizontal and vertical stress. Although this ratio can vary from 0.3 based on an elastic assumption to values greater than 2.0 where tectonic forces and other geological factors contribute to high horizontal stresses, the assumption of K=0.33 was adopted here, initialized directly through simple gravity loading. Although the influence of the horizontal to vertical stress ratio is a key parameter to which the model results may be sensitive to, the lower ratio was selected to minimize clamping effects around the simulated block cave, so that the caving process could develop freely. Boundary conditions are assumed to be fixed in both orthogonal global directions, horizontal (x-axis) and vertical (y-axis), with respect to boundary displacements (i.e. roller boundaries). They are extended far away from the slope and cave zones to ensure that they do not adversely affect the model results.

Since one focus of this study is to examine the influence of block caving on the rock slope and surface, the joint properties are chosen to be at the limit of stability prior to block caving. In the sliding-type model, the angle of friction is chosen to be 35°. Based on the criteria of Goodman & Bray (1976), the major joint set angle is calculated to be 30° dipping out of the 45° face, which is less than both the angle of friction and the face angle, making it unlikely to slide in the original condition. In addition, the same approach is applied for the toppling-type models. A joint dipping angle of 75° is calculated using the same kinematic criteria for toppling. All cross-cuts are chosen to be orthogonal to the major continuous joint set as shown in Figure 3.2. The joint set spacing is set at 50 meters for the continuous joints in all models. Cross-joints are 200 meters apart when present.

Different variables are tested in this study, based on the factors mentioned in the literature review that may have significant influence on subsidence, potential failure mechanism, and rock mass behavior. Table 3.3 lists these variables as well as the factors that are fixed between different model simulations.

Table 3.3: The different variables examined in the study

| | |
|------------------------------------|------------------|
| The dip of the ore body | Variable |
| The depth of mining (cave) | Fixed |
| The slope of the ground surface | Fixed |
| Prior surface mining | Open pit / slope |
| Major geological features (faults) | NA |
| Water pressure | NA |
| Location of the cave | Variable |

3.3 Block caving simulation techniques

This section will focus on the advantages and disadvantages of two different techniques of block cave modeling: direct block deletion (DBD) and displacement boundary condition (DBC). As mentioned in the methodology, DBD is a technique used to model the block caving process in which sequential block deletions are performed to simulate the mining process. The volume of deleted blocks between sequential model runs simulates the volume of ore extracted continuously in reality. Volume is measured in a sense of two-dimensional scheme. On the other hand, DBC specifies a specific deformation boundary condition applied to the bottom of the model. This applied deformation simulates the sagging of the rock mass above the cave as the ore is extracted from the cave zone.

Both the “Direct Block Deletion” and “Imposed Boundary Displacement” were tested to see which of the two modeling techniques would best simulate the physical behavior of block caving. The first approach, direct block deletion, presents better results in terms of capturing the “expected physical response of rock slope behavior. From the bottom of the caving area, the extraction of the ore body is simulated by deleting blocks moving into the undercut created as shown in Figure 3.4. Each sequence of block deletion is performed from the same area (the undercut) and allows the cave to propagate upward due to the effect of volume loss in that area. It should be stated that the deleted areas are considered to have 1 meter of out-of-plane thickness. The reason for this is to monitor the volume of ore extracted from the cave as a unit volume in the sense of three dimensions /m (volume – m^3/m). A series of mined lifts are modeled using this technique; however, some simulations encountered the numerical error of “overlap too great”. To overcome this error in many models, the effected blocks within the active cave zone were also deleted and, accordingly, their volume added to the total volume of extracted ore. This was not seen to affect the results significantly as their volume was much less than the total volume of each simulated caved zone.

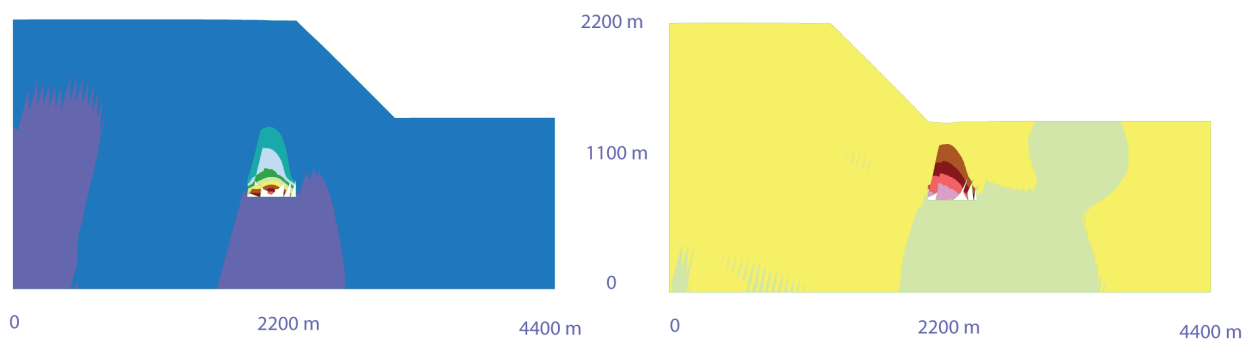


Figure 3.4: Model geometry and cave initiation using “Direct Block Deletion, DBD” technique. Left: Cave positioned behind the crest. Right: Cave positioned underneath the toe

The other method for simulating block caving, i.e. imposing a boundary displacement, was likewise examined to measure the accuracy of this technique compared to the direct block deletion technique. This was undertaken in UDEC by prescribe a boundary velocity for a fixed segment at the bottom of the model directly over where the undercut would be and then solving for a given number of times steps. The desired displacement, D , is the multiplication of the prescribed velocity, V , and the time increment, T , where the time increment is also the multiplication of the time step, Δt , and the number of steps, N . In practice, the velocity should be kept small and the number of steps should be high in order to minimize the dynamic shock to the system being simulated. Based on this study, each simulated model being tested with this technique showed approximately unique time step for different prescribed

velocities and number of cycles. The following equations are a brief summary as to how the desired deformation boundary condition was calculated.

$$D = V \times T$$

$$T = \Delta t \times N$$

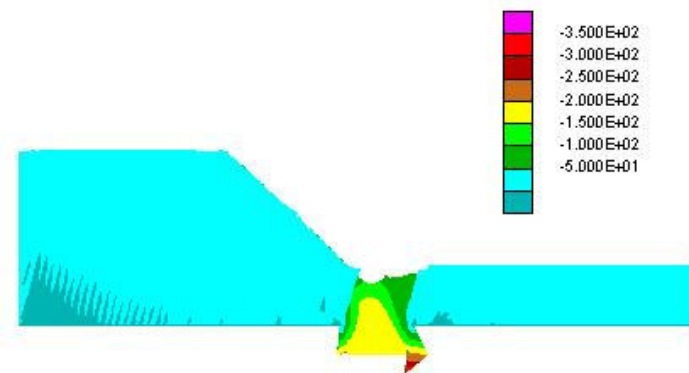


Figure 3.5: vertical displacement contour of the Sliding-type with cross-joints where cave positioned beneath the toe using “Displacement Boundary condition” technique. (Slope height is 800 meters and displacements in meters)

Only two cases out of the twelve generic models were tested and compared to decide which technique to apply to the full study. These were the Sliding-type with cross-joints, with the cave positioned under the crest of the slope, as shown in Figure 3.6, and the toppling-type with cross-joints, with the cave positioned under the toe of the slope, as shown in Figure 3.5. As discussed previously, the desired displacement (D), is equal to the prescribed velocity (V), applied for a time increment (T). It was found that time steps (ΔT) were $2.466 \text{ E-}3$ for the sliding-type model and $2.496 \text{ E-}3$ in the toppling-type model, resulting in calculated prescribed velocities of 1.6 m/s and 0.8 m/s , respectively for 100,000 time steps. As such, the comparative analysis was based on results from the DBD models for the same magnitudes of boundary displacements.

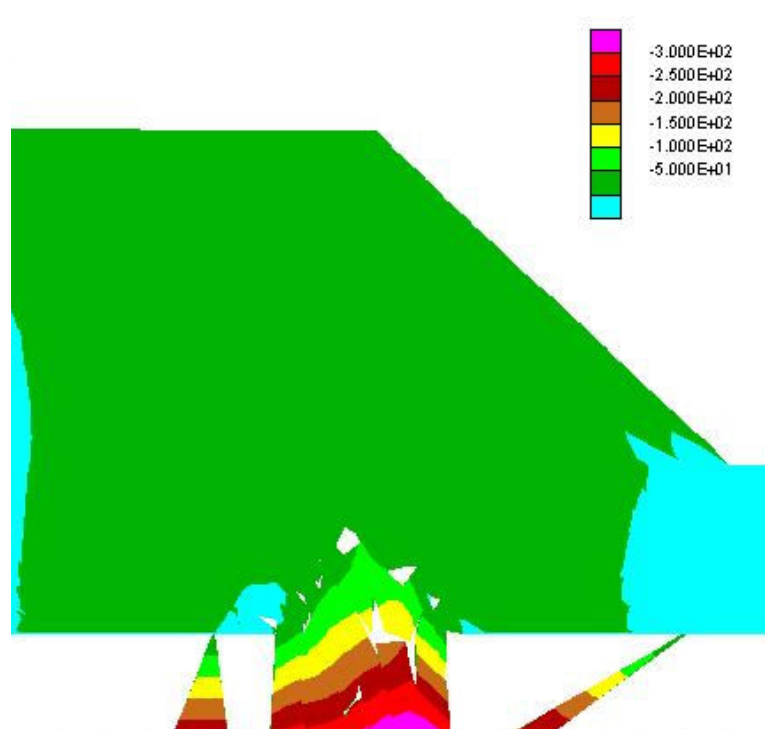


Figure 3.6: vertical displacement contour of the toppling-type with cross-joints where cave positioned behind the crest using “Displacement Boundary condition” technique. (Slope height is 800 meters and displacements in meters)

The results of these two models present some advantages and disadvantages of the DBC block cave modeling technique. In particular for this case study, model generation is easier to create utilizing DBC. There is no need to define the geometry of the cave, but only to prescribe the displacement boundary condition along the affected area. Although the calculation run time is more efficient using DBC, the boundary effect on the results is significant. Table 4.1 presents the most commonly identified pros and cons of employing the DBC and DBD techniques.

Rock slope deformations are predicted using the DBC techniques; however, a number of simulation results are unrealistic. The toppling-type case with cross joints presents impractical horizontal deformations of 70 meters at the crest in response to a cave developed below the toe of the slope as illustrated in Figure 3.7. The reason for this is that the strata above the cave undergo significant downward movement as a result of the displacement boundary condition, thus leaving an unreasonably large void around the toe which leads to the unrealistically high slope movements.

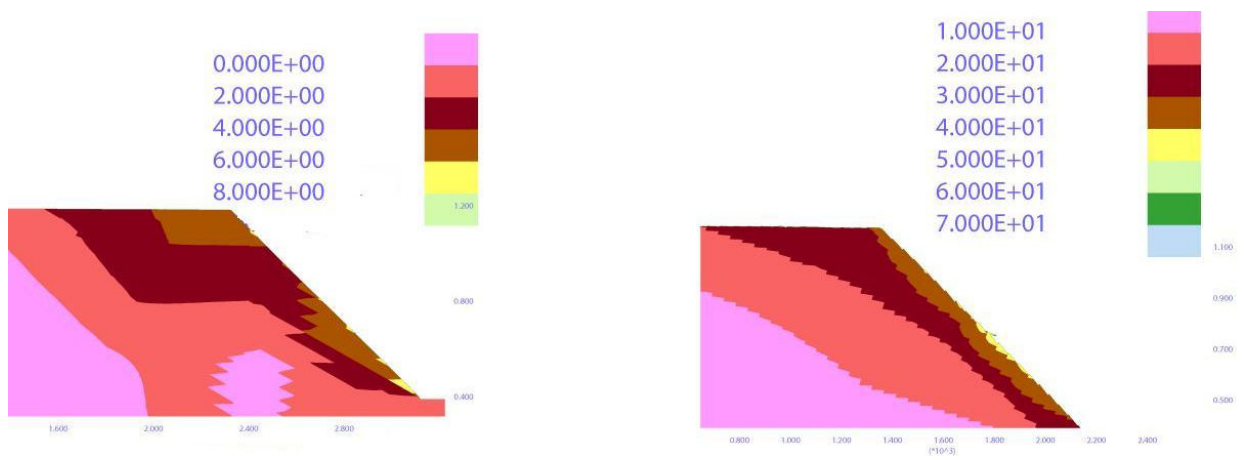


Figure 3.7: Horizontal displacement contour simulated by “DBD” technique; (Slope height is 800 meters and displacements in meters). **Left:** Cave positioned behind the crest. **Right:** Cave positioned underneath the toe.

The DBC simulates the relaxation of rock mass to some extent. Redistribution of stress is effectively simulated by DBC; however, the effect of the boundary condition to plastic yielding (as shown by the plasticity indicators as presented in Figure 3.8 affects the overall results of elasto-plastic behavior. Toppling movements of the rock slope suggest tension failure of the rock mass along the slope as shown in Figure 3.6 and 3.8. It should be stated that the direct block deletion technique presents more accurate results compared to the displacement boundary condition, since the extent of the boundary for this particular problem is only 400 m from the bottom of the slope. Therefore, the significant effect of the boundary cannot be avoided unless the lower boundary is extended below the actual level of the block cave.

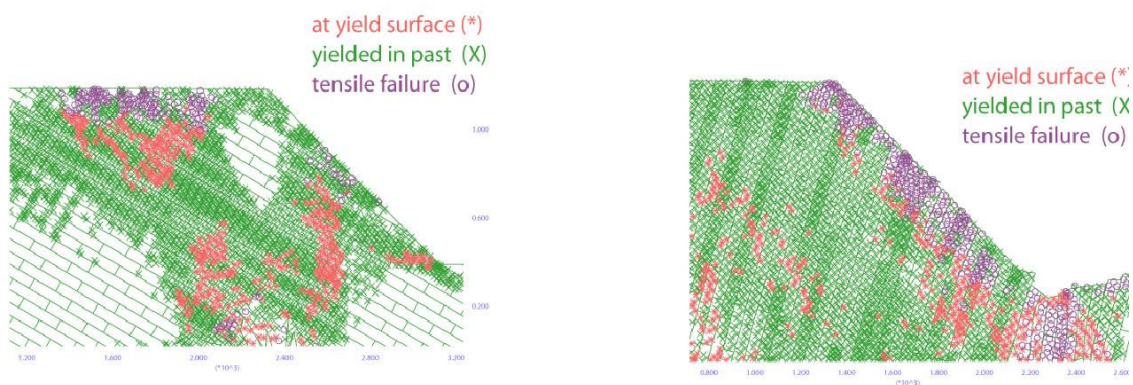


Figure 3.8: Plasticity indicator simulated by “DBD” technique (slope height is 800 meters). **Left:** Cave positioned behind the crest. **Right:** Cave positioned underneath the toe.

Table 3.4: Advantages and disadvantages of the two different block caving modeling techniques, (DBD) and (DBC).

| Modeling Technique | Advantages | Disadvantages |
|----------------------------------------------|-----------------------------------------------------------------------------------------------------------------------------------------------------------------------------------------------------------------------------------------------------------------------------|------------------------------------------------------------------------------------------------------------------------------------------------------------------------------------------------------------------------|
| Direct Block Deletion (DBD) | <ul style="list-style-type: none"> Better captures the physical mechanism of rock mass failure. Better predicts rock slope and surface deformations. Destressing of rock mass well-represents the gravity free fall of rock into the cave. | <ul style="list-style-type: none"> More complicated block cave model geometry generation. Longer numerical calculation time. Often “overlap error” encountered after sequential cuts. |
| Displacement Boundary Condition (DBC) | <ul style="list-style-type: none"> More efficient numerical calculation time. Simpler block cave model geometry. Smaller models. | <ul style="list-style-type: none"> Boundary effects significantly influence results. Prescribing values of velocities instead of actual velocity related to actual gravitational acceleration. |

3.4 Sensitivity to initial stress ratio

The sensitivity of the magnitude of the horizontal stresses within hard rock mass is examined. Four models are been simulated to capture hard rock mines in terms of how the ratio between the horizontal and vertical stress may affect block caving. From experience, the horizontal stress is generally greater than the vertical stress but both tend to be equal at greater depth. In Canadian shields the ratio of the maximum and minimum horizontal to the vertical stress are approximately 2:1 and 1:1 respectively.

Only three cases out of the twelve generic models were calibrated and tested at ratio $K=1$ and $K=2$. However, the toppling-type with cross-joints, with the cave positioned under the toe of the slope and the toppling-type with cross-joints, with the cave positioned behind the crest of the slope encounter relatively high horizontal stress forced the cylinder block to yield at the lower part of the slope before block caving starts. The reason for that is when the model is trying to achieve equilibrium, the large-scale rock slope forces and confines the rock mass near to the bottom of the pit in the horizontal

direction. Moreover, the excessive load performed by the model to maintain the ratio at $K=1$ and $K=2$ adds more stress in the same direction. On the other hand, the rock mass exposed to the surface has little confinement from the adjacent strata from the opposite direction, the vertical direction. Therefore, rock mass is yielded as shown in Figure 3.9 and 3.10.

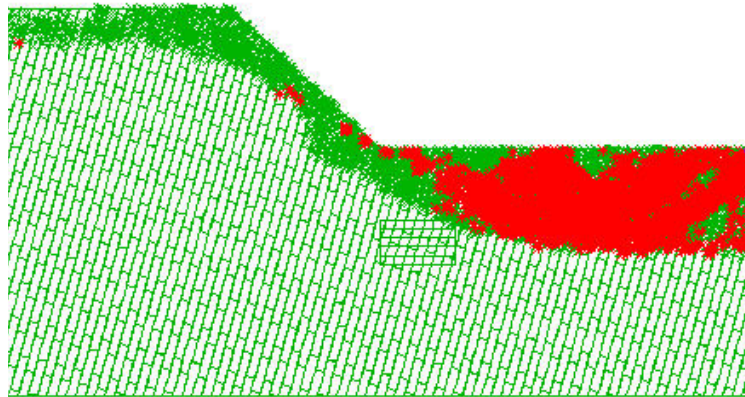


Figure 3.9: Plasticity indicator as a result of initial stress ratio $K=2$ in the toppling-type with cross-joints, with the cave positioned under the toe of the slope model. (Green: plastic yielding, Red: at yielding edge, slope height is 800 meters).

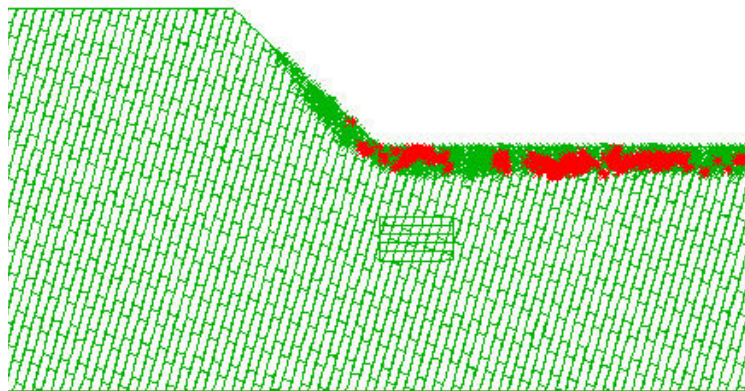


Figure 3.10: Plasticity indicator as a result of initial stress ratio $K=2$ in the toppling-type with cross-joints, with the cave positioned under the toe of the slope model. (Green: plastic yielding, Red: at yielding edge, slope height is 800 meters).

The sliding-type with cross-joints, with the cave positioned underneath the toe of the slope scenario is modeled utilizing the horizontal stress to vertical stress ratio approximately equal 1:1. Only three progressive lifts are modeled to capture the block caving process. To understand the sensitivity of the initial stress ratio on this model, another model is adopted where the initial stress ratio is 0.33:1 which

elastic consolidation due to simple gravity loading is modeled. Although, the initial stress ratio is a key factor in which results are sensitive to, It was shown that the sensitivity of structural jointing has a bigger influence on the model results. The 200m by 50 m cylinder blocks dipping at angle of 30 degree into the face attract most of horizontal stress on the long semi-horizontal direction. Since the position of the cave allows blocks to slide toward the cave, the plastic behavior was quite similar in both models as shown in figure 3.11. More discussion on plasticity indicator is in chapter 4 the results.

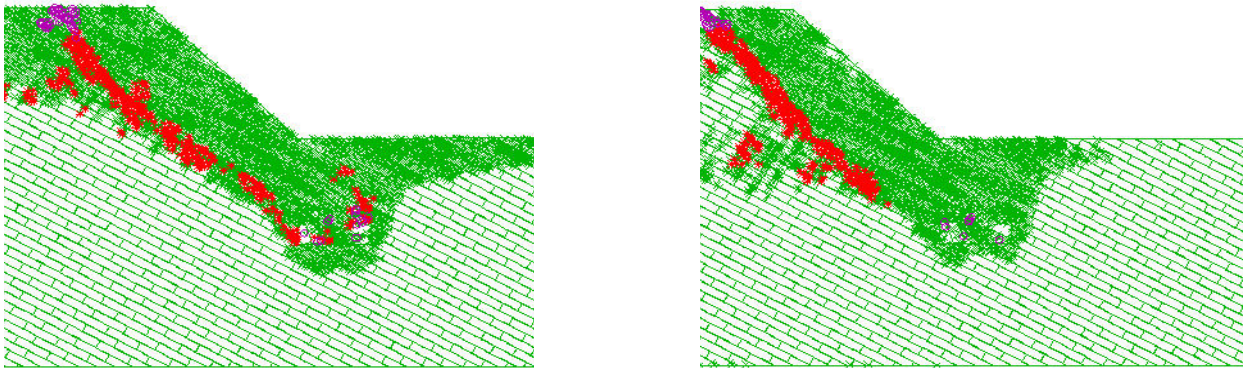


Figure 3.11: Plasticity indicator of the “Sliding-type with cross-joints”, with the cave positioned underneath the toe of the slope. (**Green:** plastic yielding, **Red:** at yielding edge, slope height is 800 meters. (**Left:** $K=1$, **Right:** $K=0.33$))

The induced horizontal stresses that result from cave excavation are shown in Figures 3.12 and 3.13. In both models where two different values of K ratio are assigned, an approximately 10 MPa is obtained as a result of the stress redistribution due to the excavation; however, as we move away from the cave zone, the stress redistribution is diminished and stress becomes back to its original form. On the same manner, the induced vertical stress component contributes to the redistribution scheme around the cave zone. Approximately similar values of vertical stresses are obtained from both numerical modeling simulations. Moreover, as a result of the destressing the rock mass, the vertical slope deformations are modeled and history of deformation are presented in Figures 3.14 and 3.15. The clamping of the rock mass at the toe prevent reduce its vertical movement as a result of both the horizontal stress and the bottom of the slope. Figure 3.15 shows that the toe was sensitive to the “K” ratio since its location relative to structural discontinuity influences its behavior.

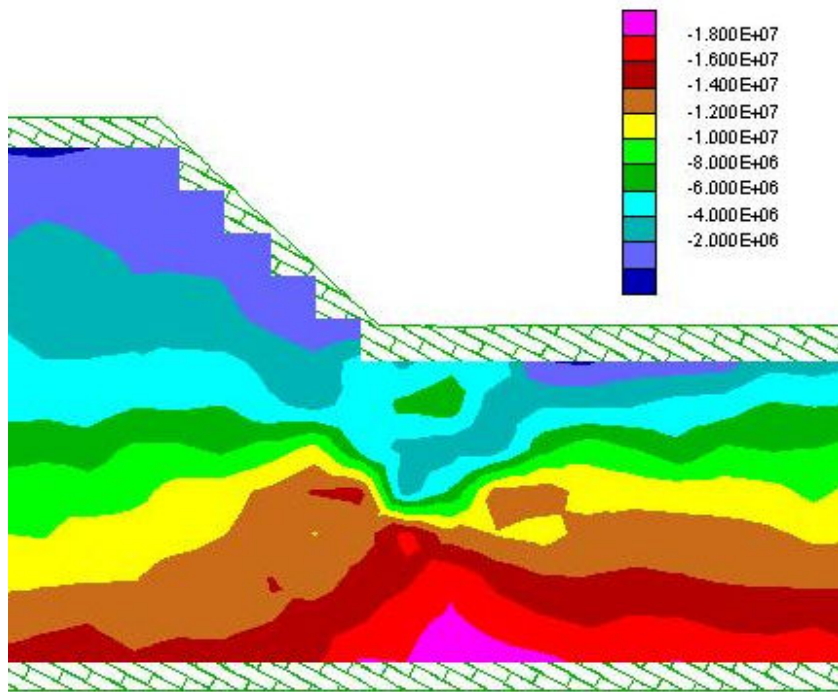


Figure 3.12: Horizontal stress contour of the “Sliding-type with cross-joints”, with the cave positioned underneath the toe of the slope. (Slope height is 800 meters, stress units in Pascal, $K=0.33$)

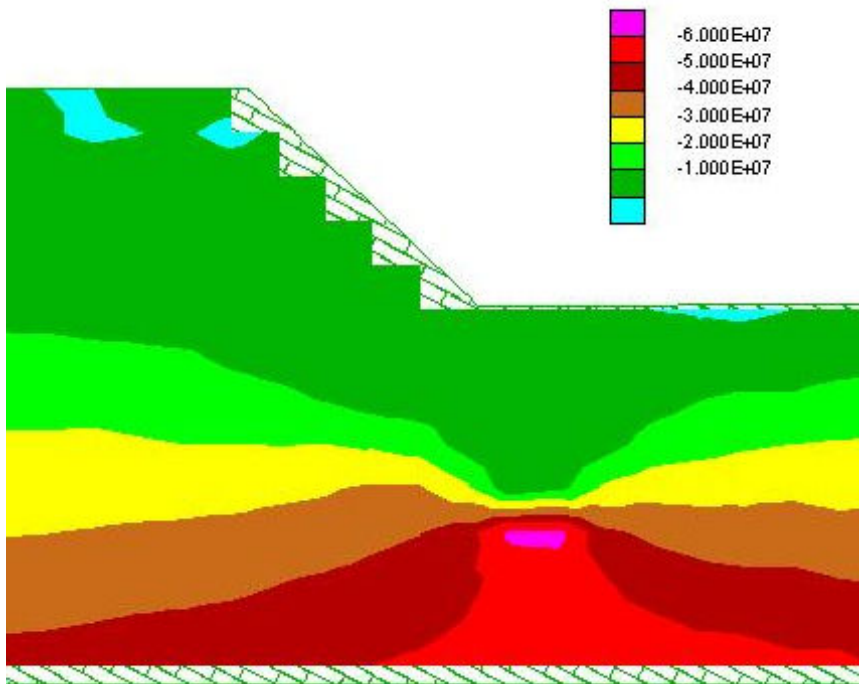


Figure 3.13: Horizontal stress contour of the “Sliding-type with cross-joints”, with the cave positioned underneath the toe of the slope. (Slope height is 800 meters, stress units in pascal, $K=1$)

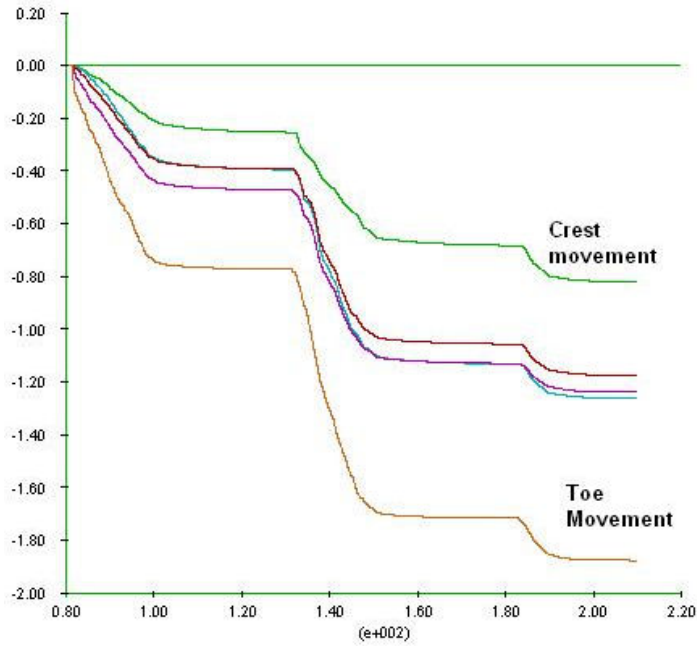


Figure 3.14: History of vertical deformation of the monitoring points along the slope face. “Sliding-type with cross-joints”, with the cave positioned underneath the toe of the slope, $K=0.33$. (Horizontal axis: UDEC time step, Vertical axis: Deformations in meters)

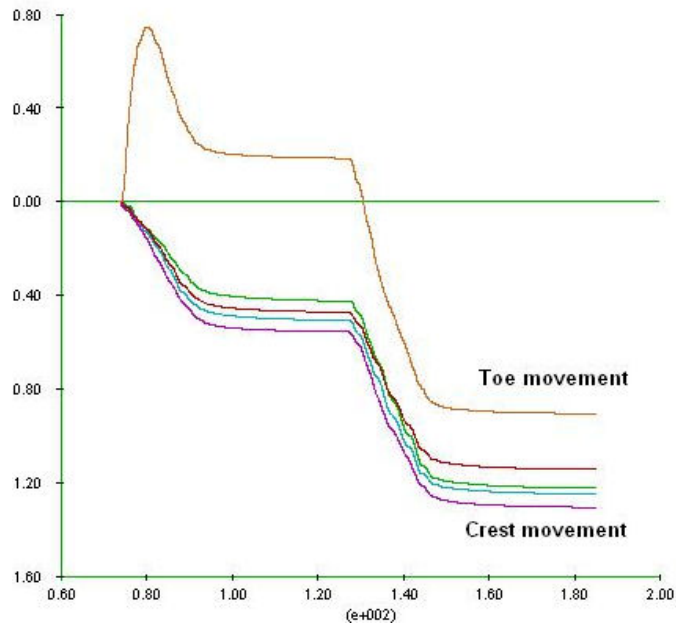


Figure 3.15: History of vertical deformation of the monitoring points along the slope face. “Sliding-type with cross-joints”, with the cave positioned underneath the toe of the slope, $K=1$. (Horizontal axis: UDEC time step, Vertical axis: Deformations in meters)

4 DISTINCT-ELEMENT MODELING RESULTS

The scope of this study is to investigate the potential effects of block cave mining on the stability of jointed rock slopes, particularly, with respect to different jointing patterns and cave location relative to the slope. There are several other parameters which may contribute to the phenomena of the slope failure, e.g. rock mass joint spacing, water table and associated pore pressure, rock slope height, rock mass characteristics, initial in situ stress, and mining methods.

As a point of interest, the study will focus on two main aspects:

1. Geological structure orientations that favor sliding, toppling, bucking, and bi-planar modes of failure.
2. The position of the cave relative to the crest and toe of the slope above.

As discussed in Table 3.1 in the methodology section, the terminology used in this thesis are briefly defined. Sliding-type and toppling-type refer to the configuration of jointing patterns which promote sliding and toppling mechanisms of rock slope deformation, respectively. Each of those categories has two different joint configurations, e.g. pure-sliding-type, pure-toppling-type, sliding-type with cross-joints, and toppling-type with cross-joints. Moreover, buckling-type and bi-planar-type refer to models which have continuous joints parallel to the slope, without and with cross joints respectively.

As also noted in the methodology section, the simulation process is standardized for all models and involves three phases: an initialization phase where the in situ stress state is applied under elastic conditions; a second phase where the model is changed to a Mohr-Coulomb elasto-plastic model; and a third phase where the model displacements are reset to zero and the caving process is simulated. Each phase is solved until a condition of static equilibrium is reached (unless failure of the slope occurs).

To capture the physical behavior of the dynamic mining process, each simulated stage in the caving process is also time stepped until equilibrium is reached. The goal is to extract the maximum amount of ore with the minimum effect on stability of the numerical model by extracting five lifts of 100m height, one at a time, from the bottom of the cave (i.e. undercut) upwards towards the surface. In some simulated models, a numerical error may occur reported as “contact overlap” due to excessive stresses between the interlocking edges of two or more blocks in contact.

The cave position and caving process simulated in UDEC is illustrated in Figure 4.1. The cave behind the crest reflects a scenario where the cave is being developed beside a natural rock slope or open pit. The cave beneath the toe is typical to numerous caves developed under an open pit operation as a means to continue mining the ore body to greater depths (e.g. Palabora, Chuqicamata). The first simulated undercut was named 'cut-1', with subsequent lifts being numbered sequentially up to the fifth simulated level named 'cut-5'. A summary of the simulated volumes extracted with each phase of the caving process is shown in Appendix 2 (Simulated volume extracted using UDEC).

In this chapter, the results will be discussed based on the theories of rock mechanics and rock slope engineering as well as interpretations of the simulations. The horizontal and vertical displacements will be discussed according to the results obtained through the simulations. The stress distribution and plasticity indicators for various simulations are included where they lend help in understanding how the rock mass behaves in response to the block caving. The stress analysis is explained and interpreted according to the stress/strain constitutive relationships applied in the simulations. These results are subsequently used to summarize and discuss. Eventually, the subsidence that develops in each model scenario is presented and summarized based on the assumptions listed in the methodology section and results is discussed in Chapter 5.

Each section of this chapter focuses on different kinematic models with respect to the orientation of the geological structures. These include discussions on the modeled rock slope deformations caused by block caving, together with the rock mass plastic yielding, redistributed stresses and slip along the joints and subsidence associate with them.

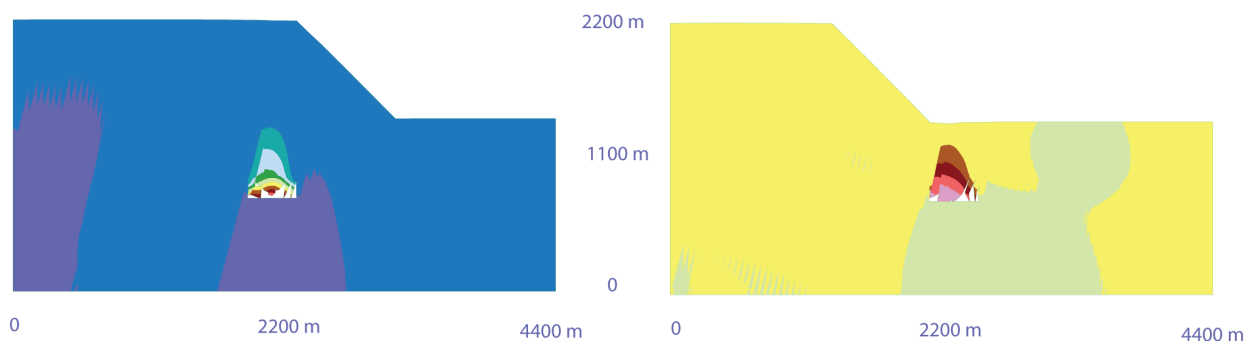


Figure 4.1: General geometry of the block cave simulations, showing cave located under the slope crest or positioned under the slope toe.

4.1 Sliding-type model results

During the numerical runs, monitoring points were used to track the time history" of selected variables, primarily the horizontal and vertical displacements along the surface and rock slope at every time step. Figure 4.2 shows the monitoring points on the rock slope. The vertical and horizontal displacements for the monitoring points on the slope face (between the crest and toe) for the different sliding-type models (with and without cross-joints) are shown Figures 4.3 to 4.6.

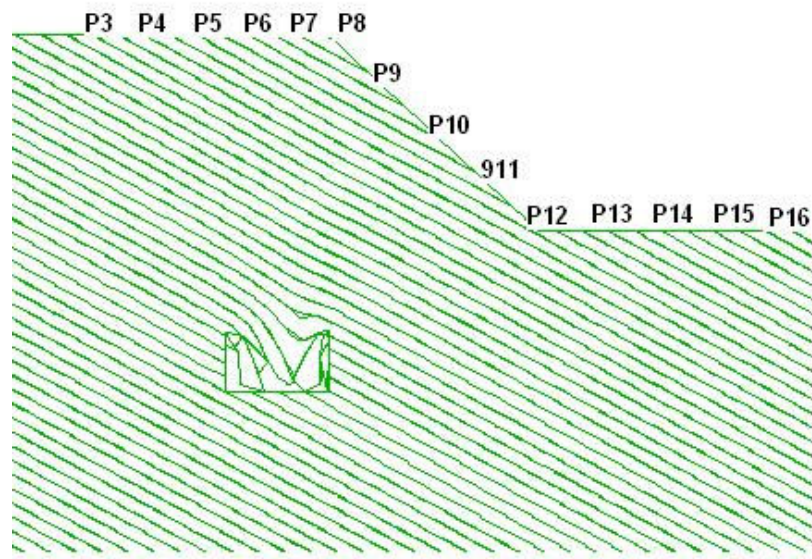


Figure 4.2: General geometry of the block cave simulations, showing the simulated monitoring on, the upper surface, slope face, and bottom of pits. (200m apart between every two adjacent points, slope height is 800 m)

Simulated horizontal and vertical displacements of the rock slope are functions of the volume of ore extracted as shown in Figures 4.3 to 4.6. They demonstrate that the more ore extracted, the higher the magnitudes of deformation are developed. Approximately, 150,000 to 160,000 (m^3/m) of ore is extracted from the sliding-type models following the fifth, and last, undercut. In these Figures, the vertical axis corresponds to the vertical displacements (Y-displacements) and the horizontal axis denotes the "extracted rock mass volume". Slight differences in the final volume loss between simulations with the cave behind the crest and underneath the toe are due to geometric differences in the shapes, orientations, and interlocking nature of the individual blocks located in the caving zone. The deleting procedure used to simulate the mining process works to remove those blocks whose centers of gravity fall within the undercut zone. The summation of the 2-D block areas of those extracted

constitute the volume reported. It should be stated that the final volume loss is achieved through five block deletion sequences (i.e. lifts). Each numerical run was solved until equilibrium conditions were attained (i.e. allowing the unbalanced force to self-stabilize).

The results show that the position of the cave has a significant impact on the vertical slope displacements. The cave behind the crest imposes higher value of vertical displacements than those cases where the cave is positioned beneath the toe. Differences develop as a result of the types of block movements promoted by the expanding cave and the interactions of the strain field with the geological structures. It was also observed that greater displacements develop when cross joints are included, due to the extra degrees of freedom they afford. As an example, the upper part of the slope encounters the highest vertical movements when the undercut level is located directly underneath it. Specifically, as shown in Figure 4.3, the displacements at the crest of the slope in the pure-sliding-type and sliding-type with cross joints exceeds 8 meters and 13 meters, respectively, in response to the approximately 160 m of vertical deformation that occurs at the undercut level (extracted volume = $160,000 \text{ m}^3 / \text{m}$).

Stress redistribution around the cave geometry influences the rock mass strata from the cave zone all the way to the slope (Figures 4.11 and 4.12). As such, the behaviors of the slope, and consequently the magnitude and direction of deformations, are highly dependent on the direction of discontinuities relative to the magnitude and directions of the de-stressed rock mass.

First, with respect to the cave position located behind the crest of the slope, the cave behind the crest imposes higher downward vertical deformations from the advancing cave zone up to the crest, with movement around the toe being less impacted (Figures 4.3 and 4.5). At the bottom of the pit, just right of the toe, the ground moves upwards in response to the rock mass displacing towards the cave, which in turn leads to slumping and the pushing of the adjacent blocks of the lower slope upwards. Figure 4.3 shows that point 12 (the toe) is moved slightly upward, less than a meter for both sliding-type models. This reverse slumping mechanism is reflected in the horizontal deformations shown in Figure 4.5. Here, the highest horizontal deformations are encountered at point 11 (one quarter from the bottom; Fig. 4.5), which develop through a combination of movements along the daylighting discontinuities and partly due to the redistribution of forces at the toe that leads to bulging and upward movements. The toe itself does not move as much as the points immediately above, since the discontinuity dipping out of the slope near this point is constrained (pinned) by the pit bottom. This is in contrast to the case with the cave beneath the toe where the destressing of the crown pillar beneath the toe affords extra

kinematic freedom that results in both the vertical and horizontal displacements being greatest at the toe.

When the cave position is beneath the toe, translational sliding along the joints leads to increased horizontal displacements, whereas the vertical displacements move directly downwards towards the cave. As shown in Figure 4.4, point 12 located at the toe moved vertically over 3 meters and 5 meters in both pure-sliding-type and sliding-type with cross joints, respectively. The well-defined continuous daylighting joint set in both sliding-type models enable the rock mass to slide into the cave and, consequently, the middle of the slope encounters relatively the same amount of vertical displacement. Figure 4.6 show that the slope encounters a range of from 3 to 5 meters of horizontal displacement. In contrast, the lower of the slope encounters higher horizontal deformations especially at the toe, where it moves horizontally up to 6 meters and 7 meters in both pure-sliding-type and sliding-type with cross joints, respectively.

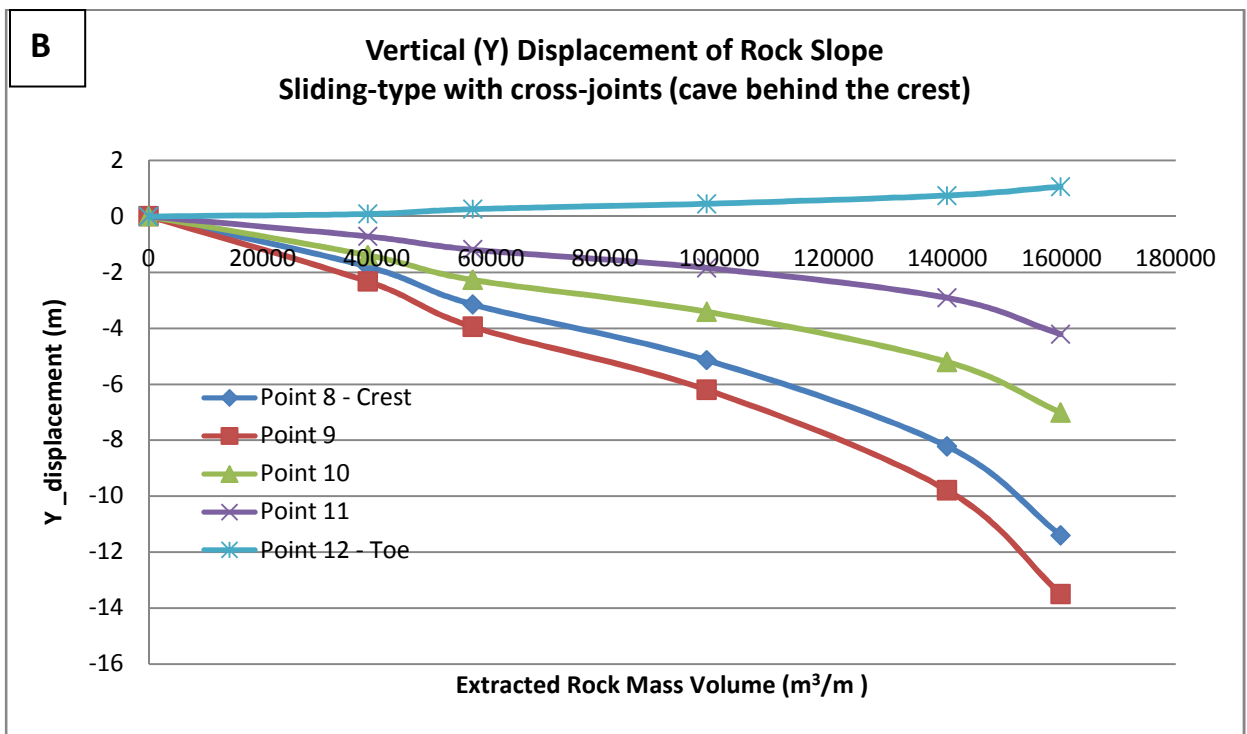
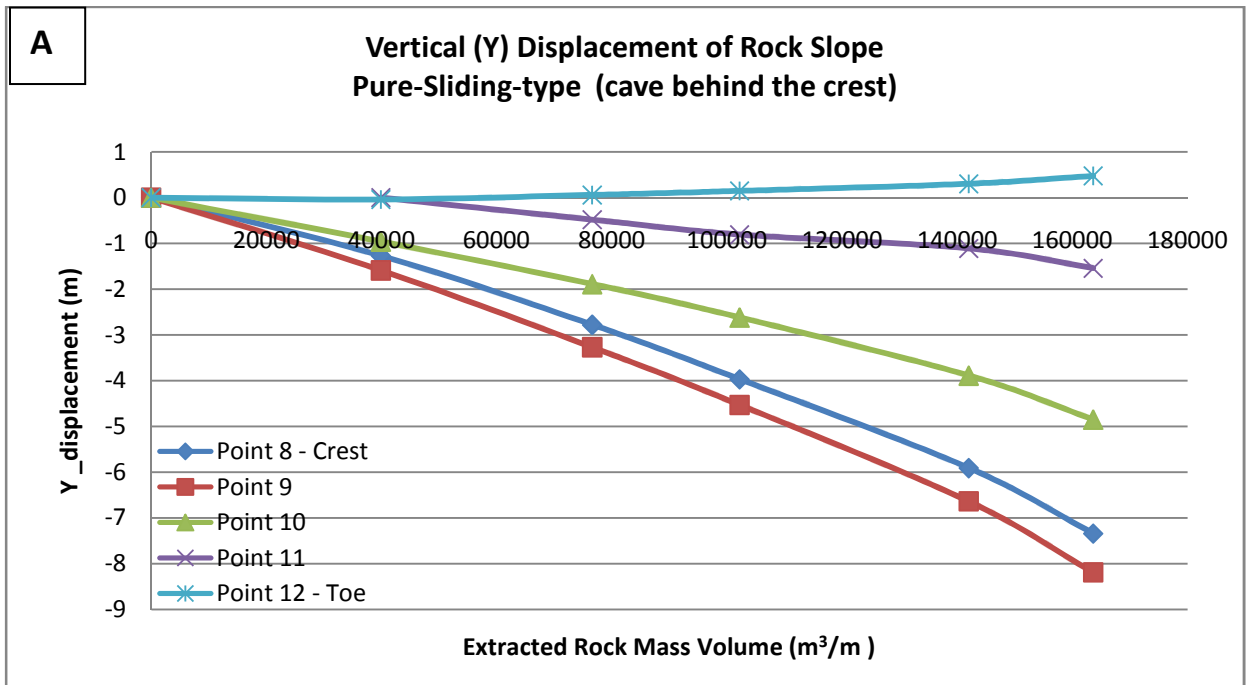


Figure 4.3: Vertical rock slope displacements for **A:** the model of pure-sliding-type (cave behind the crest); and **B:** the model of sliding-type with cross-joints (cave behind the crest).

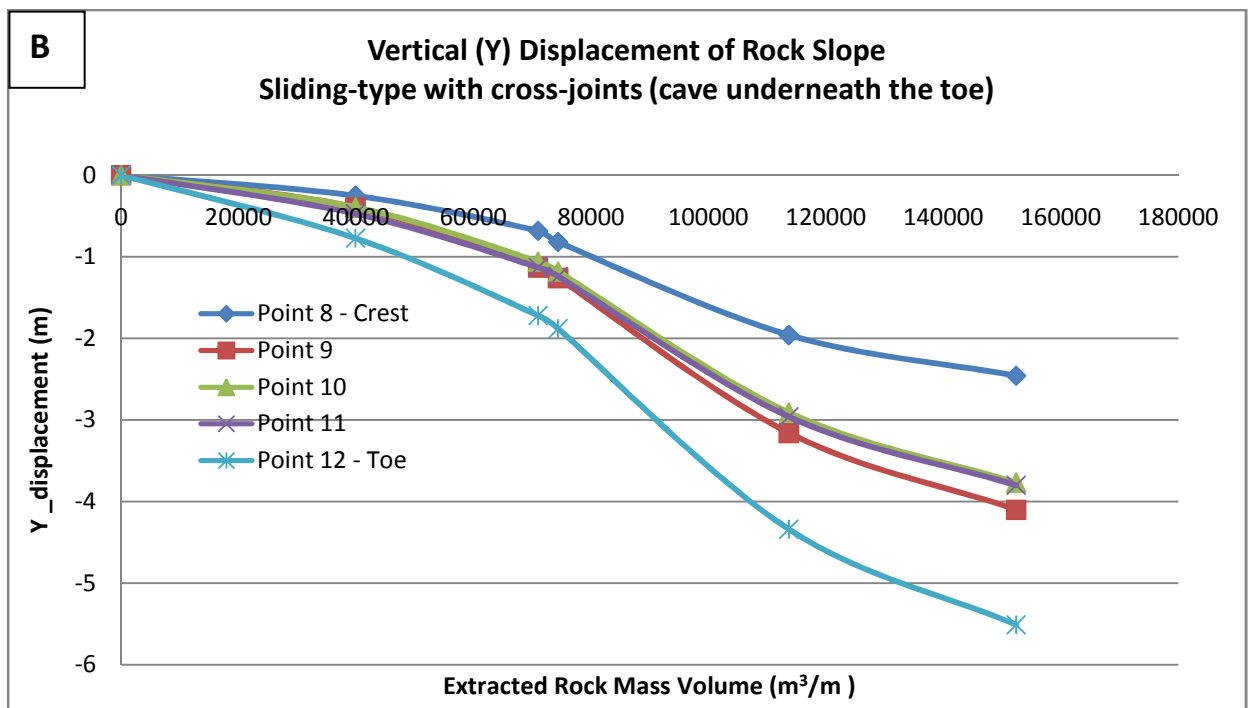
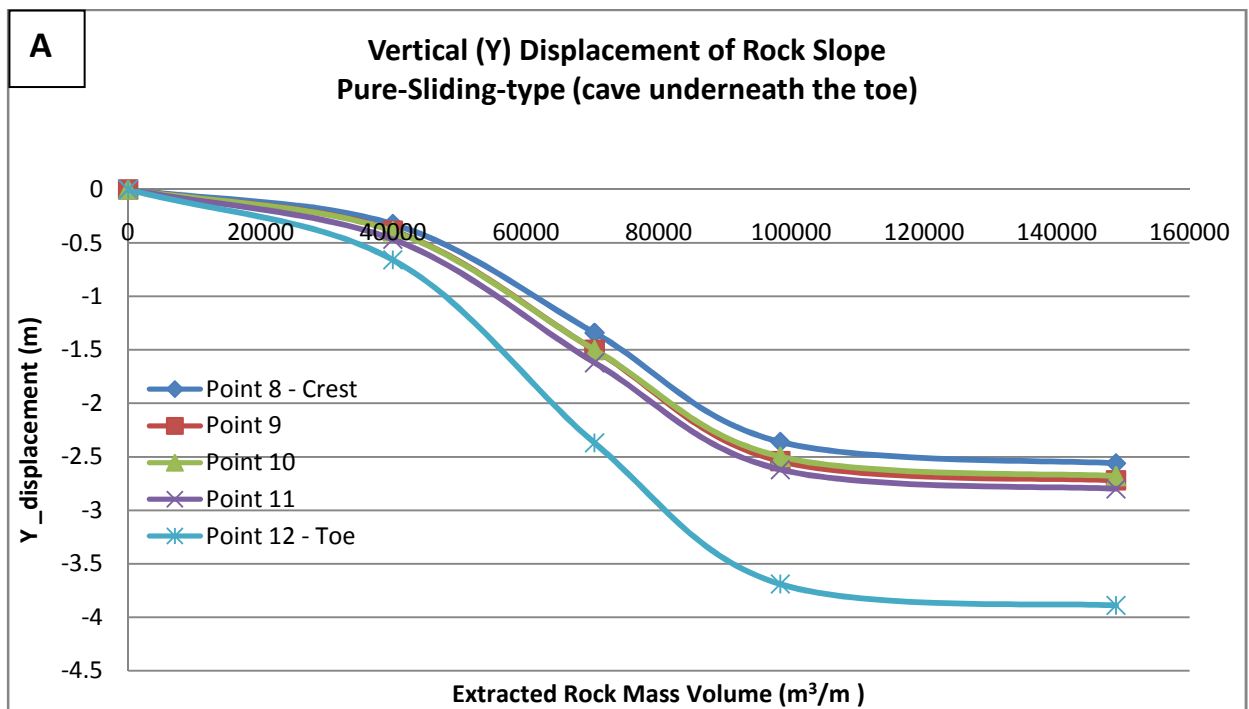


Figure 4.4: Vertical rock slope displacements for **A:** the model of pure-sliding-type (cave underneath the toe); and **B:** the model of sliding-type with cross-joints and (cave underneath the toe).

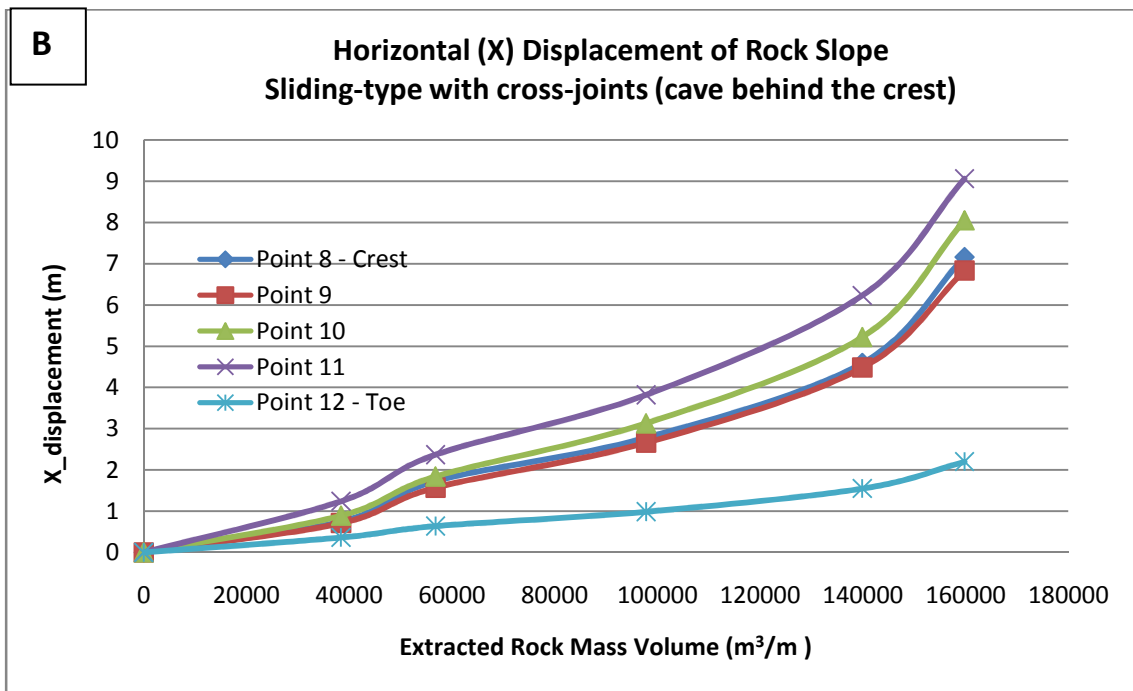
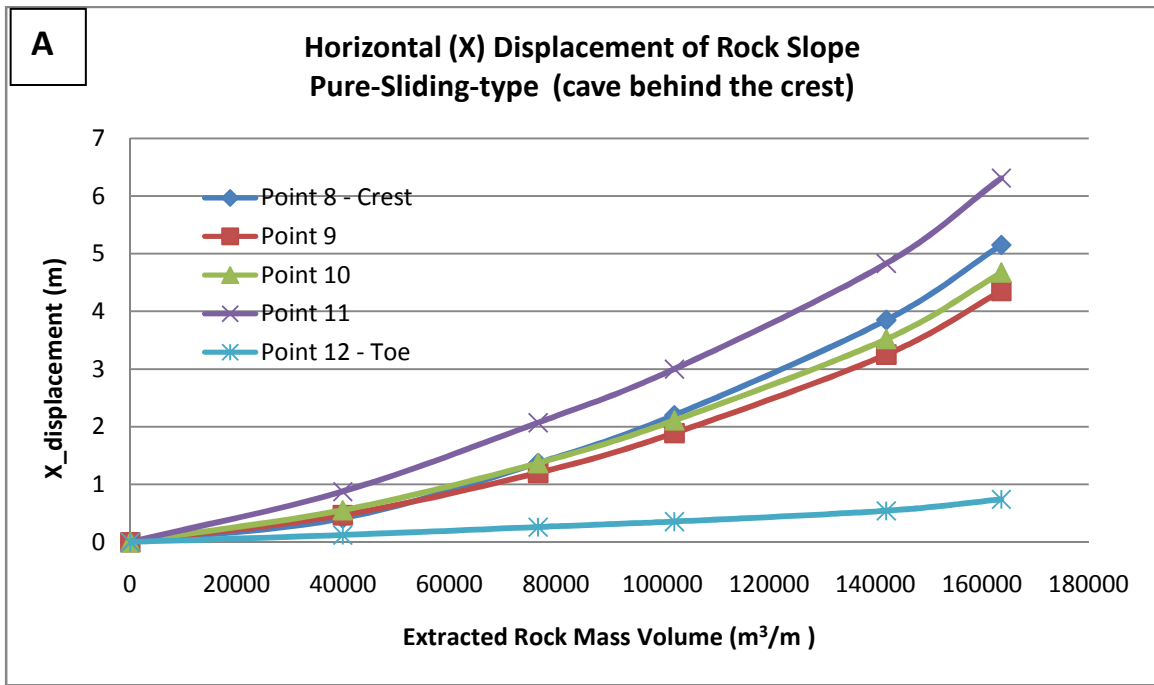


Figure 4.5: Horizontal rock slope displacements for **A:** the model of pure-sliding-type (cave behind the crest); and **B:** the model of sliding-type with cross-joints (cave behind the crest).

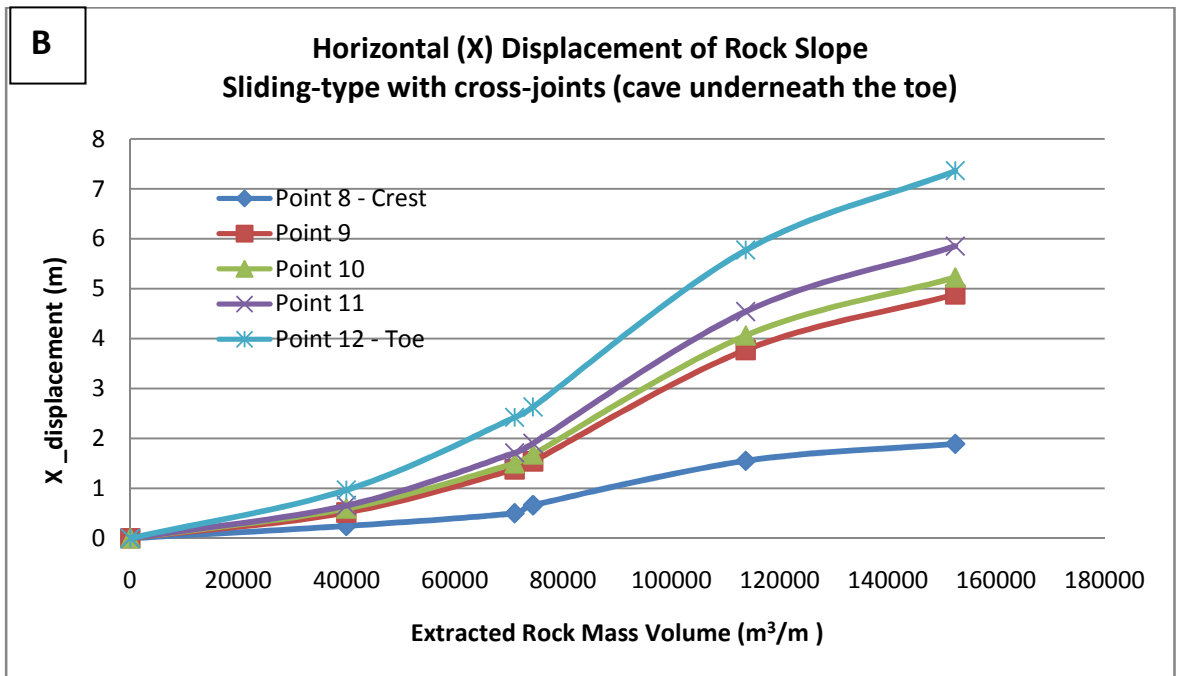
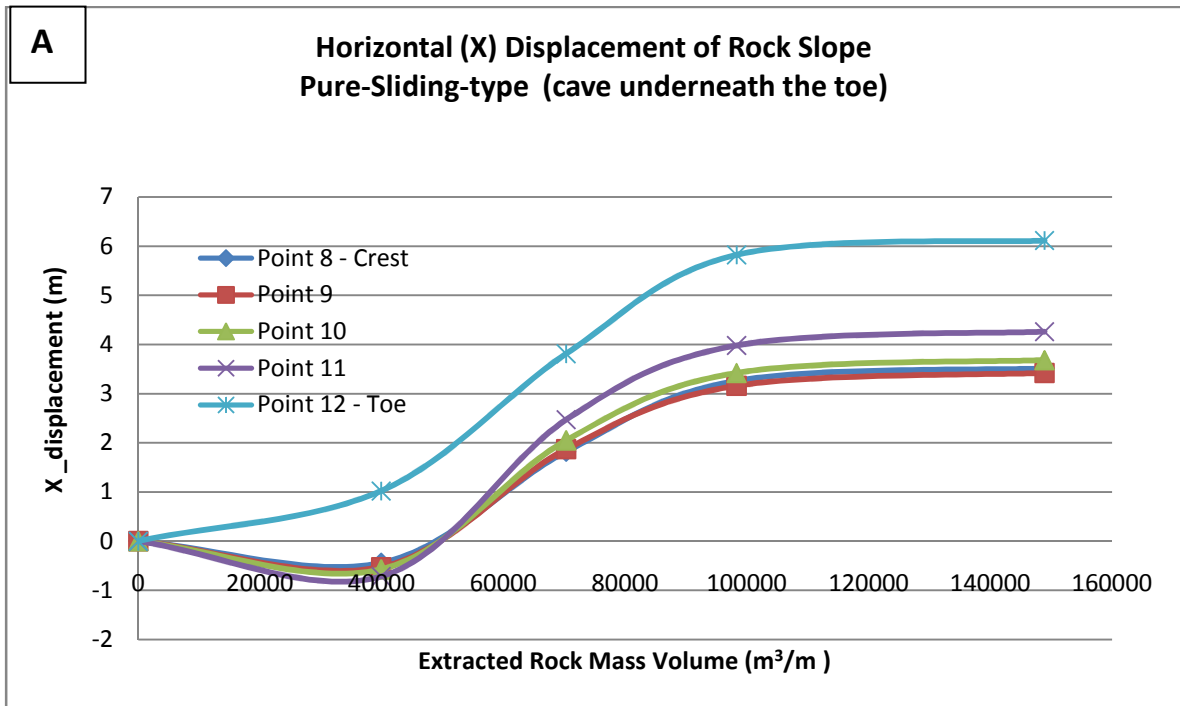


Figure 4.6: Horizontal rock slope displacements for **A:** the model of pure-sliding-type (cave underneath the toe); and **B:** the model of sliding-type with cross-joints (cave underneath the toe).

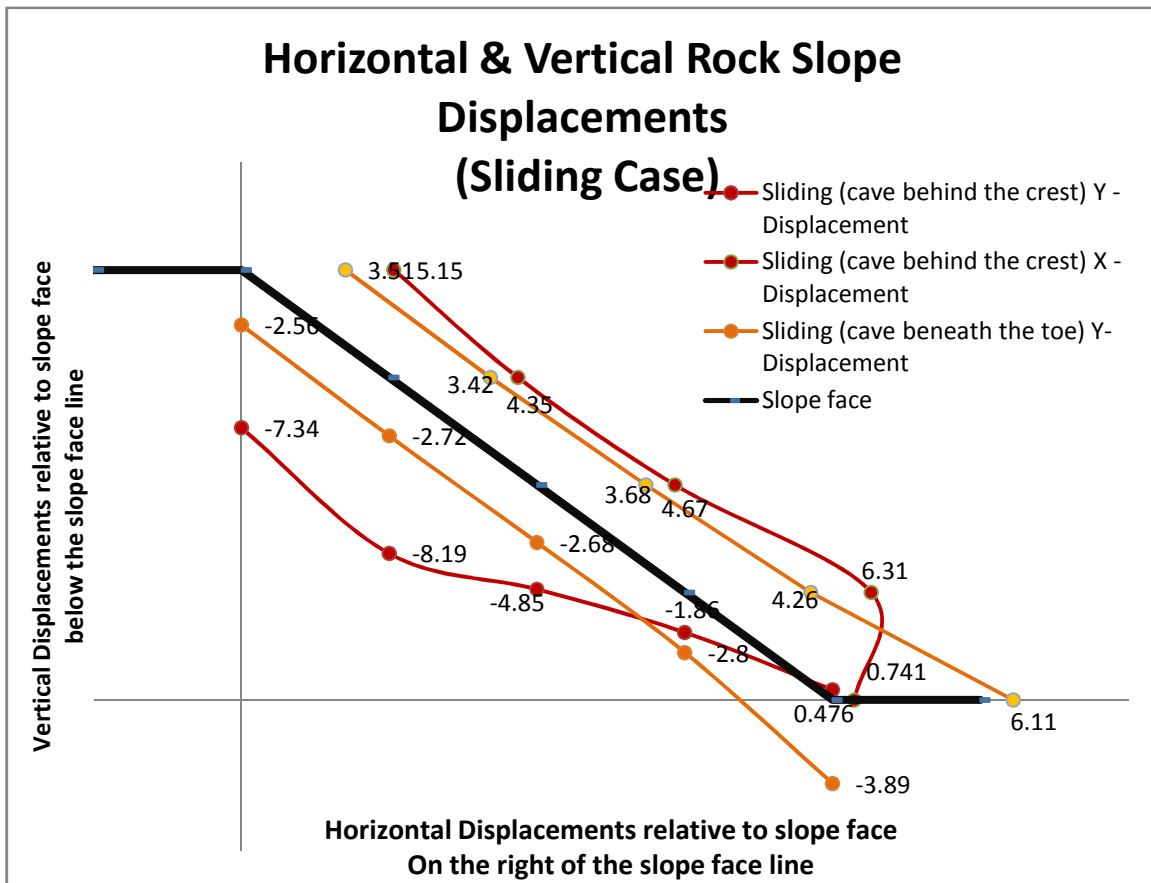


Figure 4.7: Horizontal and vertical components of displacements for the sliding-type rock slope cases. Figures 4.7 and 4.8 illustrate the horizontal and vertical displacements of the rock slope relative to the slope itself for the sliding type models (without and with cross joints, respectively). All values are in meters and are not to scale relative to the height of the slope depicted. The total displacements are plotted in Figure 4.9. Together, these figures give a greater insight into how each scenario responds to block caving. The lateral movements of blocks above and around the cave towards it, reduces confinement and opens up the volume so as to allow the blocks within the slope to either subside into the space created, as is observed in the upper half of the slope, or slide out of the face as is seen in the lower part of the slope (Fig. 4.10). On the other hand, when the cave is beneath the toe, the reduced confinement and space created forces the blocks to progressively move toward the cave in a constant translational manner as shown in Figures 4.8 and 4.9.

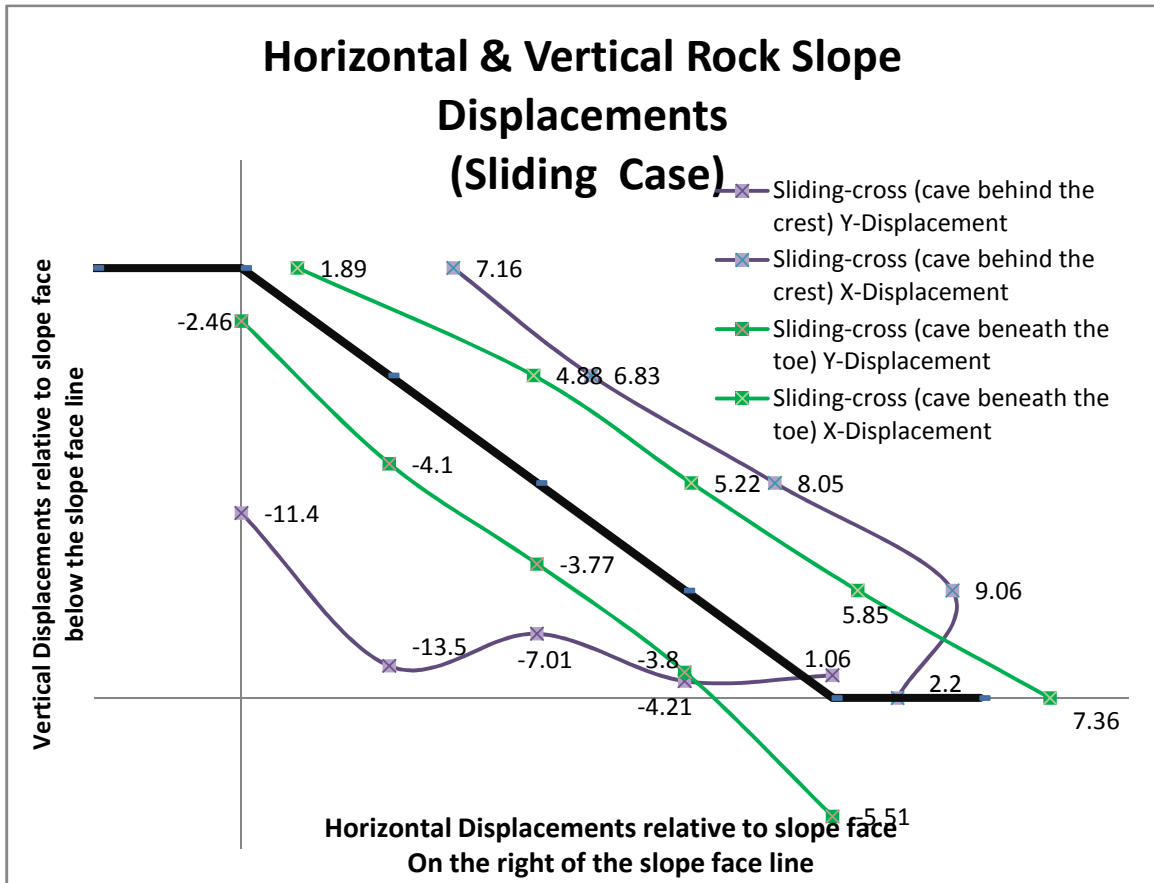


Figure 4.8: Horizontal and vertical components of displacements for the sliding-type with cross-joints models.

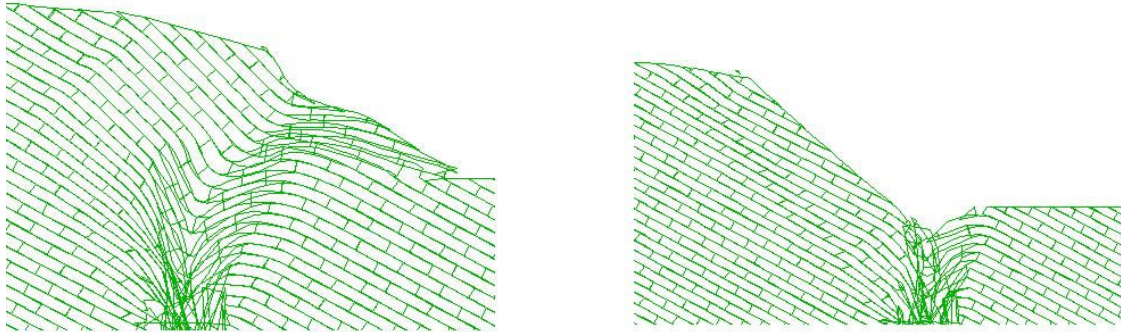


Figure 4.9: Displacements for the sliding-type with cross-joints models magnified 20 times for **Left:** cave behind the crest ; and **Right:** Cave beneath the toe (Slope height is 800 meters)

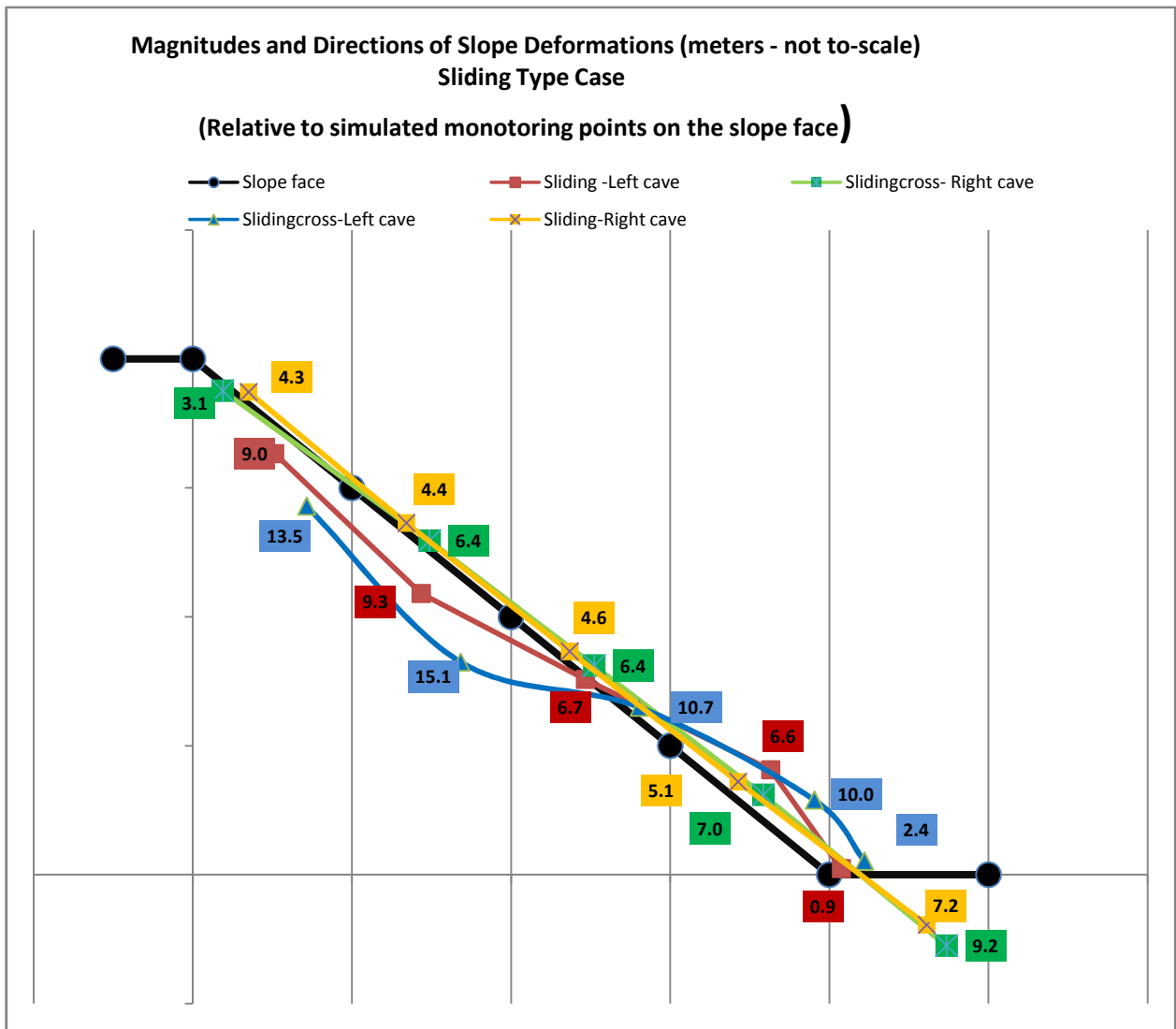


Figure 4.10: Modeled magnitudes and directions of slope deformations (sliding type). Related to the deformation patterns seen in the sliding type models, are the induced stresses solved for by UDEC, which are based on the initial in situ stresses, model geometry and rock mass properties assigned to the deformable blocks before caving is simulated. The ratio between the initial horizontal and vertical stress can vary greatly between different regions and tectonic settings, and for these results it is assumed to be approximately 0.33 ($k = 0.33$) as discussed in Chapter 3. Thus, the maximum principal stress is generally vertical where it is not overly influenced by the topography (i.e. away from the slope). Near the slope, the maximum principal stress orientates itself parallel to the slope surface (Fig. 4.11).

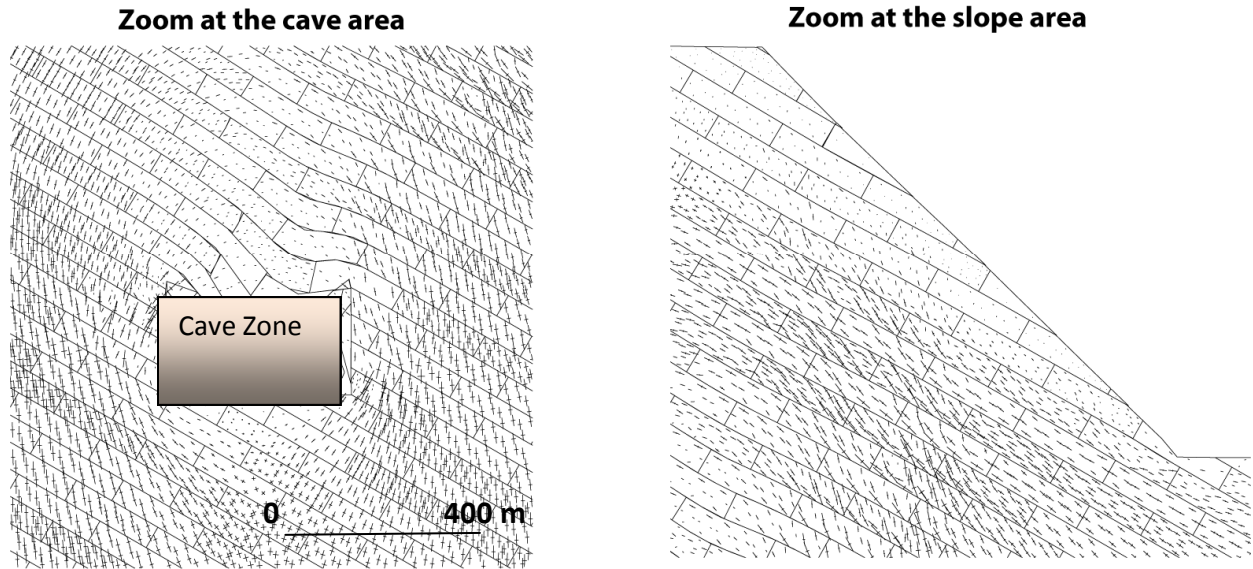


Figure 4.11: The direction of principal stress after caving starts. (Slope height is 800 meters) Similar to the influence of the slope geometry, the block caving process further disturbs the in-situ stress field in the sliding-type models. The stress field is redistributed as a result of the extracted volume from the excavation. The vertical orientation of the in situ major principal stress results in a configuration where the induced stresses around the cave concentrate in the sides of the cave parallel to the direction of the maximum initial principal stress as shown in Figure 4.11. A relaxation zone is developed in the roof of the cave that helps to promote caving of the strata upwards to the surface.

The induced stress field contributes to the constitutive failure mechanism of the rock mass based on the Mohr-Coulomb criteria. The horizontal stress (σ_{xx}), shown in Figure 4.12-A, is decreased just above the cave. Vertical and in-plane stresses around the left-positioned cave drop dramatically just above the cave and remain constant at less than 10 MPa toward the crest. Both sides of the cave encounter high zones of concentrated (σ_{yy}) stress. Figure 4.12-B illustrates the contour line of the vertical stress (σ_{yy}) field. It should be stated that, although it is a 2-D plane-strain problem, there are out-of-plane stresses or (σ_{zz}). The magnitude of the in-plane stress is produced by both types of normal stress: (σ_{yy}) and (σ_{xx}). The general relaxation schemes shown in Figure 4.12 represent two models, one with cross-joints and another without cross-joints. It is represented to only show the general stress relaxation, not intended to account for magnitudes. The reason for that is due to the complex rock behavior, the horizontal stress contour could not be visually analyzed.

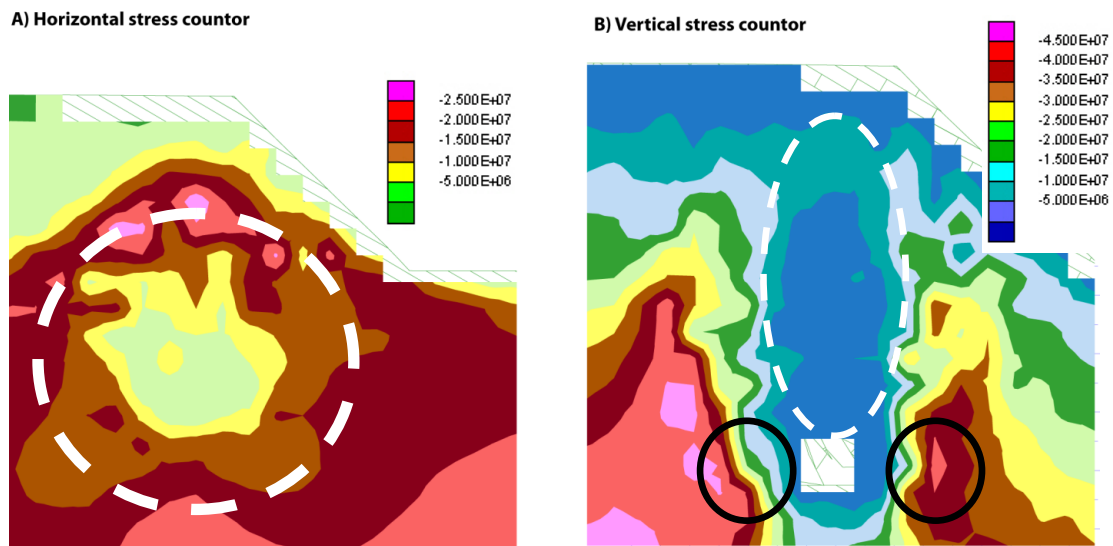


Figure 4.12: The contours distribution of the horizontal and vertical stress around the cave zone. Relaxation zone (dotted white) and confinement zone (black). (Slope height is 800m)

The rock mass strength of the deformable blocks is based on the failure criteria of Mohr-Coulomb (M-C). The plasticity model is used for material such as rocks that yield when subjected to shear loading, with a tensile cutoff used for failure in tension. It should be noticed that the plastic model criteria is based on the major, intermediate and minor principal stresses. The key parameters of the rock mass strength for the M-C failure criteria are the friction angle, cohesion and the tensile strength. The rock mass strength and the strength of structural discontinuities control the overall strength of rock slope.

The plasticity measure indicates that structural discontinuities and position of the cave play significant role in the way the rock mass behaves. Figures 4.13 and 4.14 illustrate the failure mechanism of the two different positions of the cave, behind the crest and underneath the toe. The cave positioned behind the crest forces the slender columns of rock to collapse and fall into the cave. As a result, the rock mass failure trend above the cave increases by 60-70 degrees in the direction to the slope as shown in Figure 4.13. Both models where the cave is located behind the crest, pure-sliding-type and sliding-type with cross joints, experience the same failure mechanism, and the shapes of the two plastic zones are alike. The movements of blocks open the interlayer between the blocks allowing the free edge blocks on the slope to slide along the surface of the discontinuities. An indication of tension cracks is simulated showing that there are incidences of sliding movements at the upper surface of the slope.

On the other hand, the influence of the cave beneath the slope toe has a different effect on the slope failure mechanism. Ultimately, the major joint set controls the behavior of the failure. At the top of the pure-sliding-type slope model, a major sliding surface localizes at an angle sub parallel to the slope but slightly steeper than the dip of the major joint set as illustrated in Figure 4.14. It is an indication of a

mostly translational kinematic sliding failure mechanism. The model also illustrates the stepped path failure at the bottom of the slope near the cave. The combination of translational sliding, stepped-path configuration, and rock mass shear is generated in the sliding-type model with cross-cross joints. This case incorporates more step-path and block shear than translational sliding along the joints relative to the previous case (compare left and right diagrams in Fig. 4.14).

The movement of rock slope affects the stresses that develop within the rock mass. The destressing and movement of the rock blocks, either from the toe toward and parallel to the cave underneath the toe, or from the middle of the slope that is perpendicular to the cave located behind the crest, allow the blocks to redistribute in all sliding-type models. Subsequently, the stress level is also redistributed based on the weight, orientation, and rotation of blocks with respect to the direction of the entire rock slope. In fact, different failure mechanisms are well simulated for both cave positions relative to the sliding type configuration.

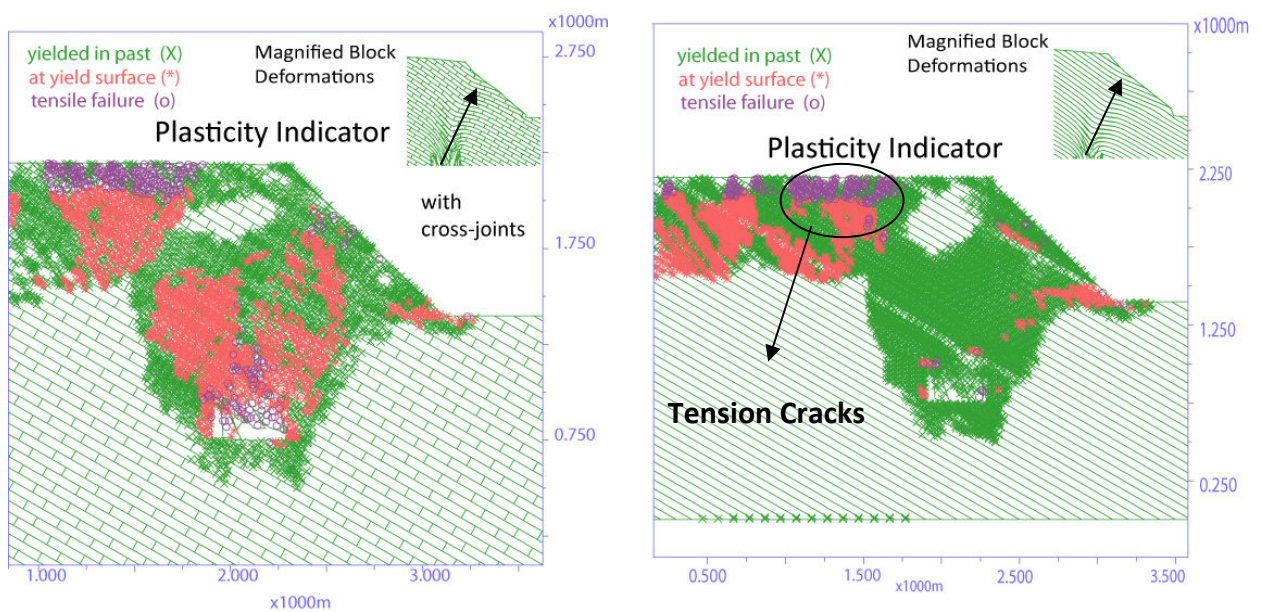


Figure 4.13: Plasticity induced by cave behind the crest models Left: Sliding-type with cross-joints. Right: Pure sliding-type model. (Slope height is 800 meters)

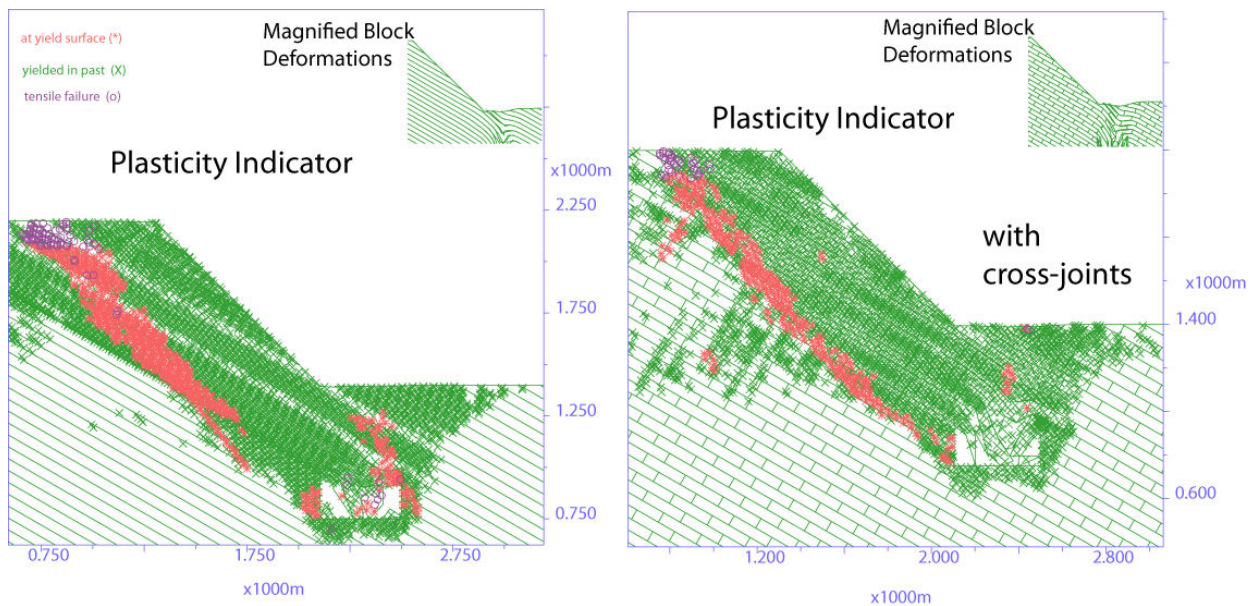


Figure 4.14: Plasticity induced by the cave beneath the toe models Left: Pure sliding-type model. Right: Sliding-type with cross-joints. (Slope height is 800 meters)

4.2 Toppling-type model results

The same monitoring points located along the rock slope are defined in the toppling type simulations as were used for the sliding-type models (from point 8 at the crest to point 12 at the toe). Figures 4.15 to 4.18 show the deformations of each individual point for the different undercuts (lifts) of ore extraction. As already stated, simulated horizontal and vertical displacements of the rock slope are functions of the volume of ore extracted from each lift; the final deformations are the accumulated movements for all extraction steps.

Since the primary joint configuration of the toppling-type dips 75 degrees into the slope and therefore dips towards the cave when it is positioned behind the crest of the slope, the upper part of the slope experiences the highest vertical movements for this scenario. The orientation of the structural discontinuities has a significant impact on the vertical deformations, with the crest (point 8) moving directly towards the cave for both pure-toppling-type and toppling type with cross joints models (Fig. 4.15). In particular, the pure-toppling-model causes the blocks to slide along the toppling joints toward the cave zone. A 10 m vertical movement occurs at point 8; however, the next point lower down the slope face, point 9, only moves 2 m vertically, as shown in Figure 4.15A. The rest of the points show no movements at all in pure-toppling-type model as the dipping structures lower in the slope dip below the disturbed strain field above the undercut/cave. The toppling-type with cross-joints model shows the same response, except with higher vertical deformations for point 9, and slightly higher deformations for the rest of the slope to point 12, as shown in Figure 4.15B. Here, the cross-joints

separate the long, slender blocks, permitting more movement in the middle part of the slope. As demonstrated in contour plots in Figure 4.19, the lower parts of the slope show no significant vertical deformations.

Destressing of the toe creates well-known toppling conditions, which lead to associated slope deformations. The flexural toppling behavior of the pure-toppling-type model directly forces the slope to nearly uniform vertical and horizontal movements as shown in Figures 4.17 and 4.18. In this model, about 7 and 10 m of vertical and horizontal movements are predicted at the crest. The vertical and horizontal deformations of the toe attain 6 m. The slender blocks buckle and deform entirely toward the toe as shown in Figure 4.20.

Additionally, the toppling-type with cross-joints has limited the slope deformations as an effect of the orthogonal cross-joints. The pure flexural toppling is not expected because of the typical presence of orthogonal cross-joints which separate the persistent sub vertical major joint set. The combination between block toppling and flexural toppling moderate the deformations to approximately one third to half of the pure-toppling type as shown in Figures 4.15 and 4.16.

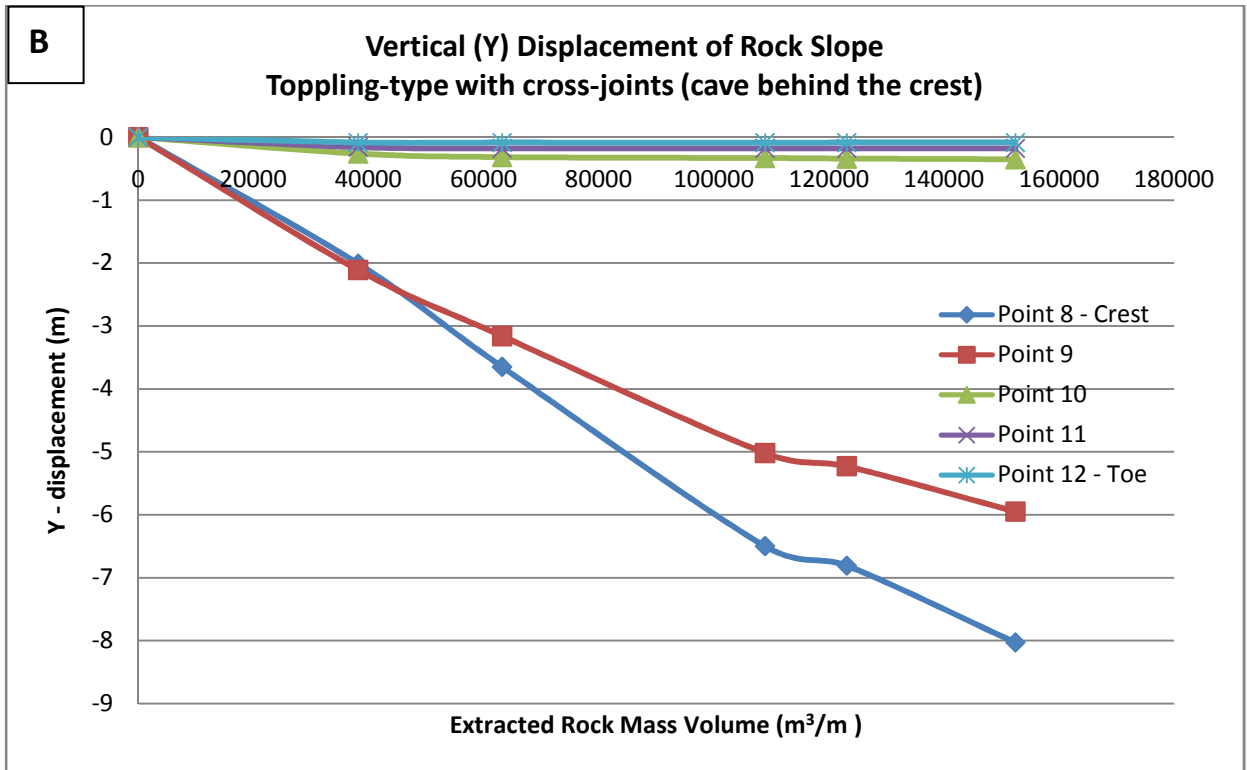
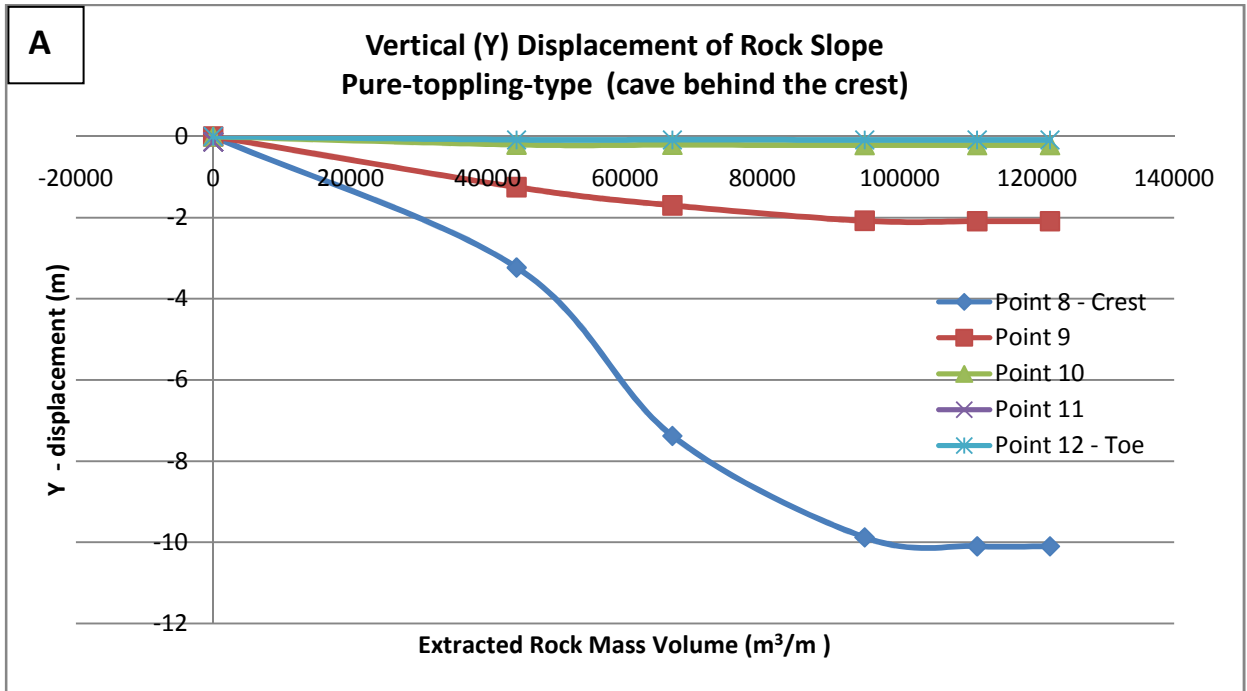


Figure 4.15: Vertical displacements of rock slope **A:** the model of pure-toppling-type (cave behind the crest) **B:** The model of toppling-type with cross-joints (cave behind the crest).

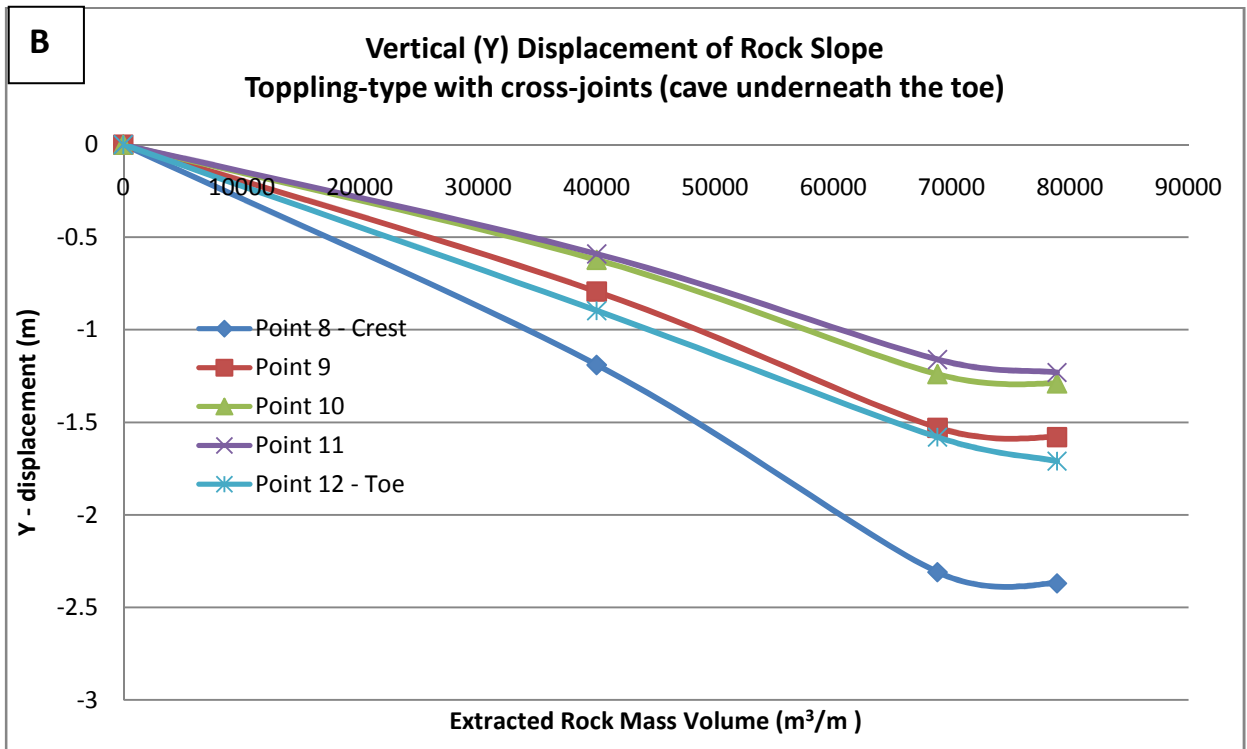
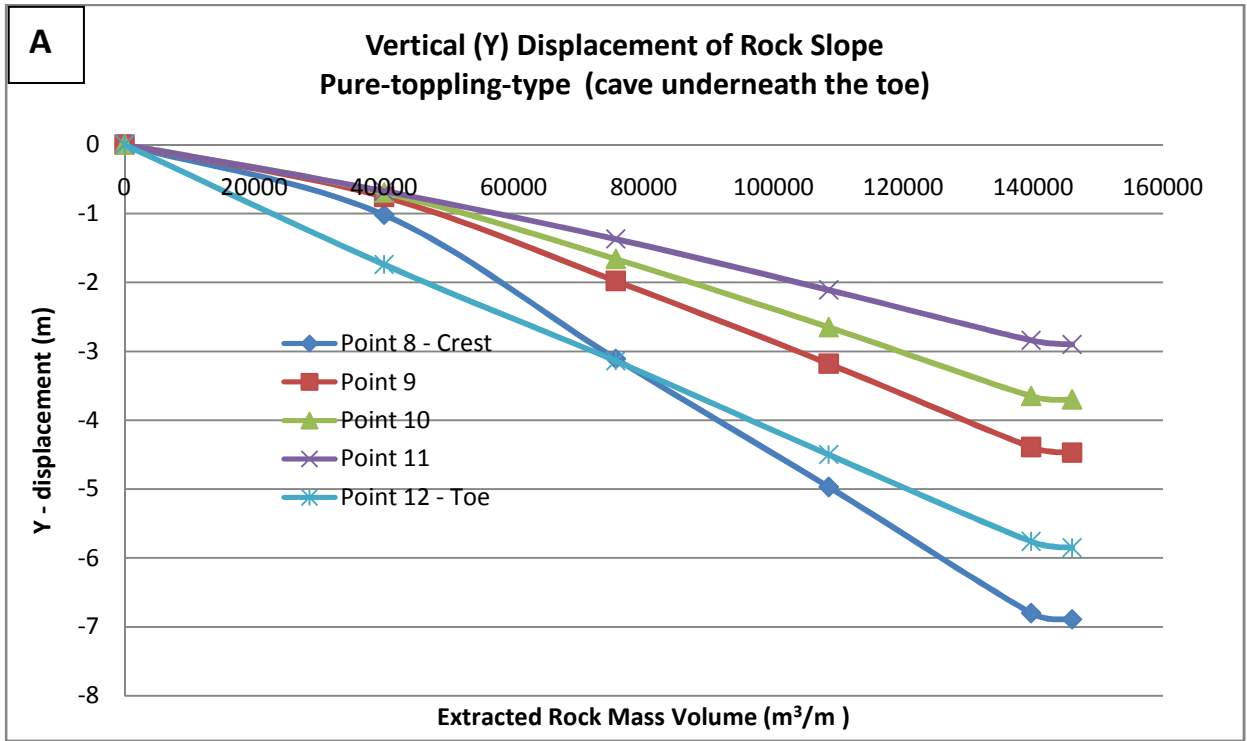


Figure 4.16: The Vertical displacements of rock slope **A:** the model of pure-toppling-type (cave underneath the toe) **B:** The model of toppling-type with cross-joints (cave underneath the toe).

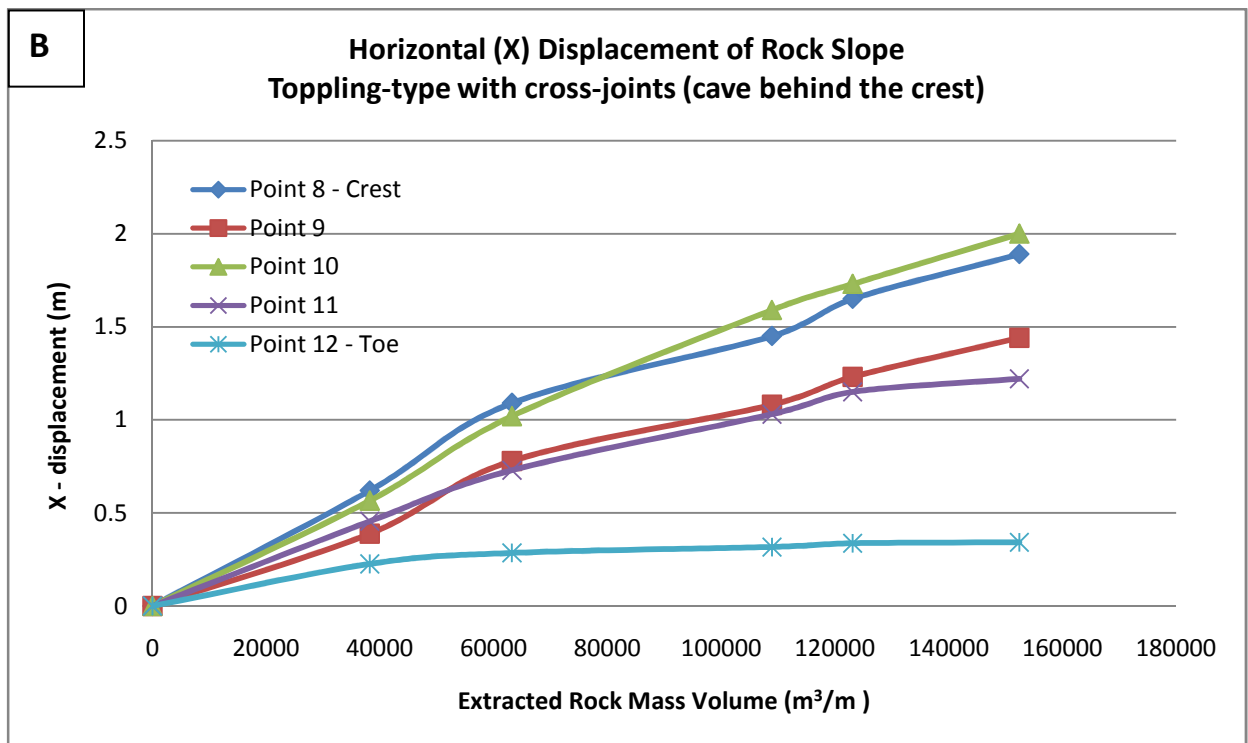
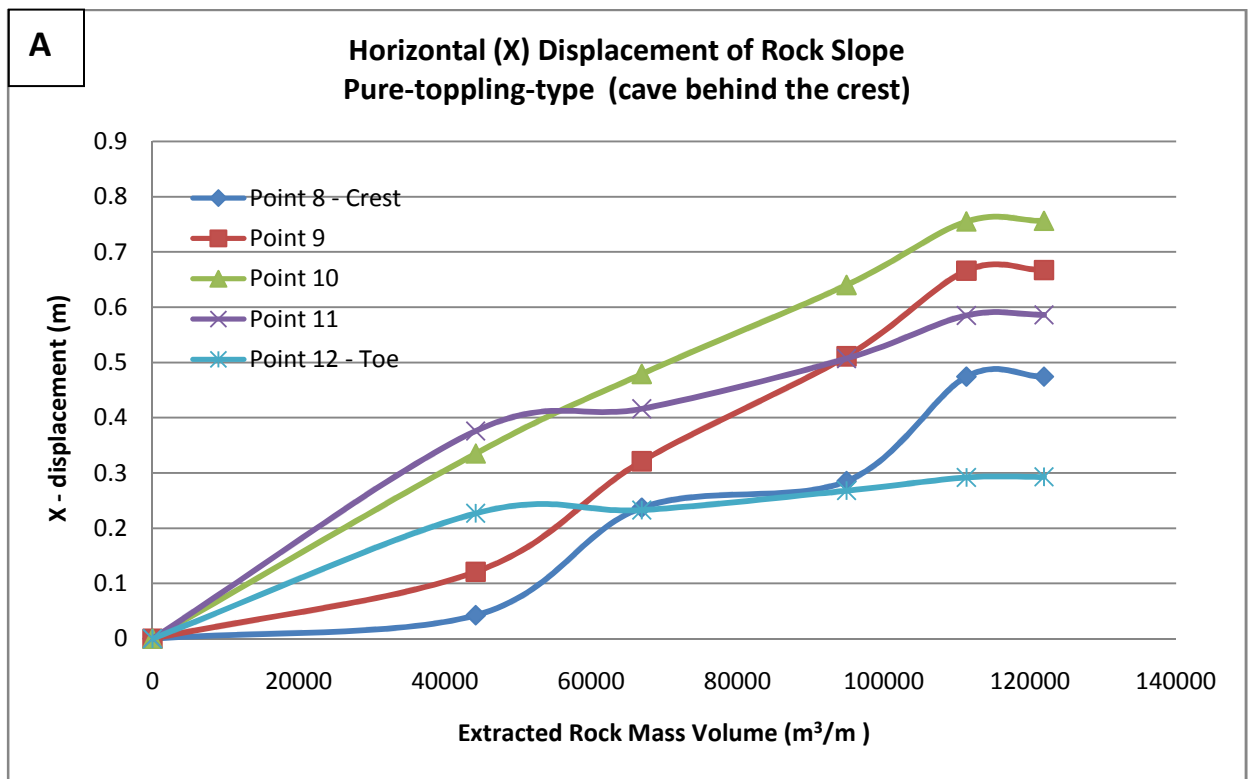


Figure 4.17: Horizontal displacements of rock slope **A:** the model of pure-toppling-type (cave behind the crest). **B:** The model of toppling-type with cross-joints (cave behind the crest).

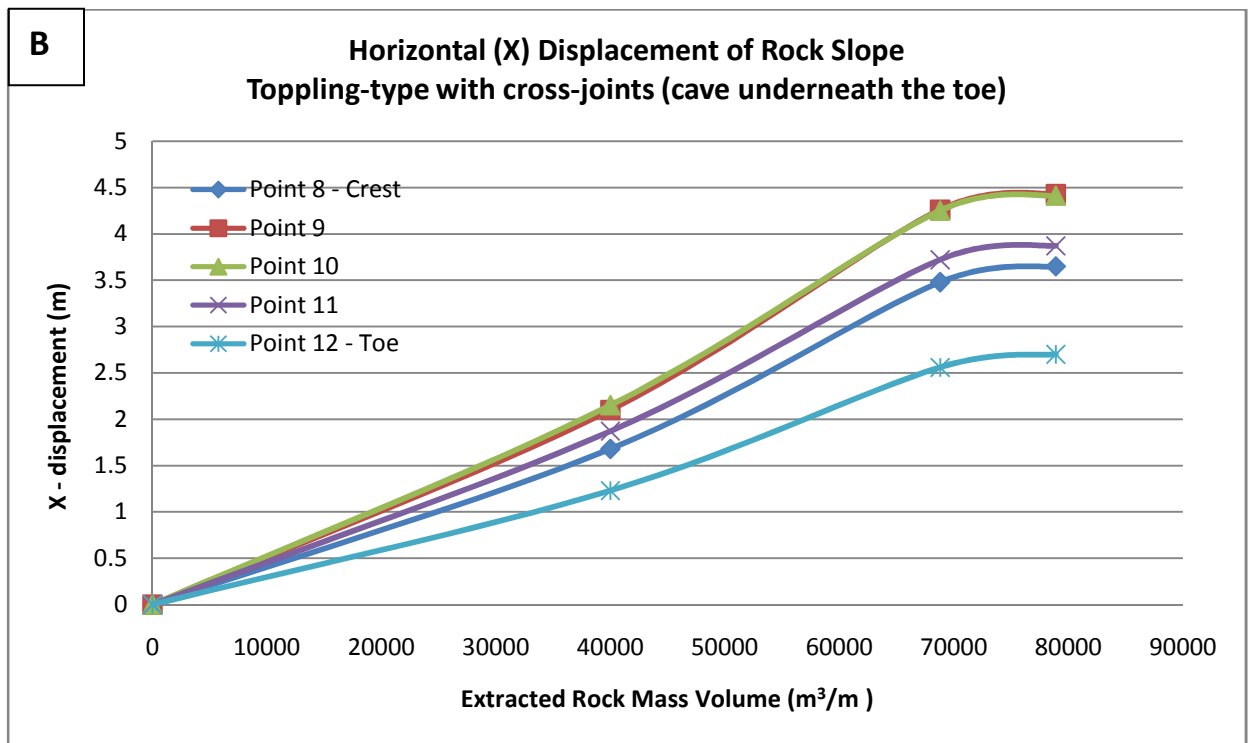
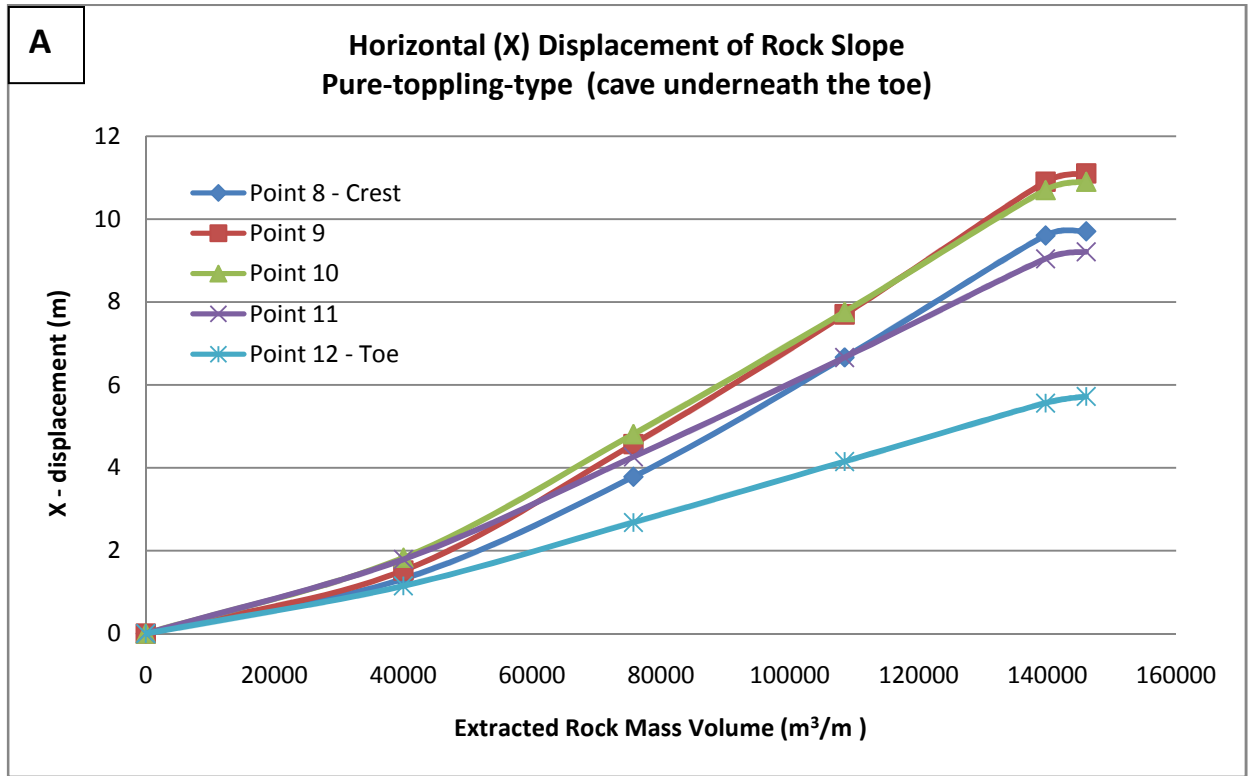


Figure 4.18: The Horizontal displacements of rock slope **A:** the model of pure-toppling-type (cave underneath the toe). **B:** The model of toppling-type with cross-joints (cave underneath the toe).

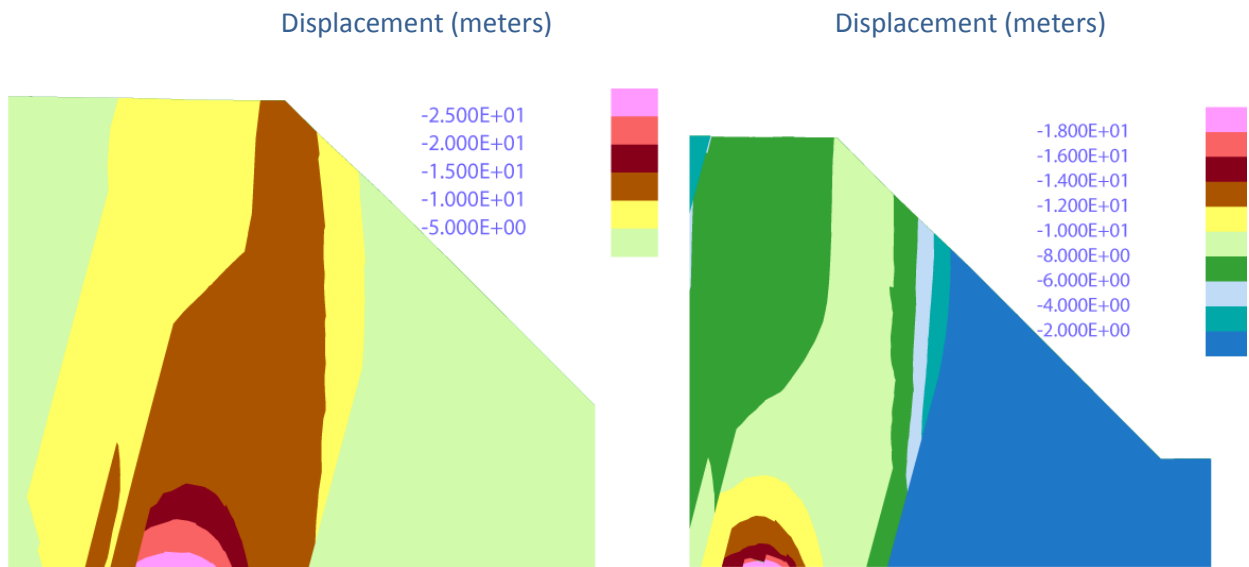


Figure 4.19: The contours distribution of the vertical rock slope displacements (cave behind the crest). **Left:** toppling – type model. **Right:** toppling-type with cross joints. (Slope height is 800 meters, units in meters)

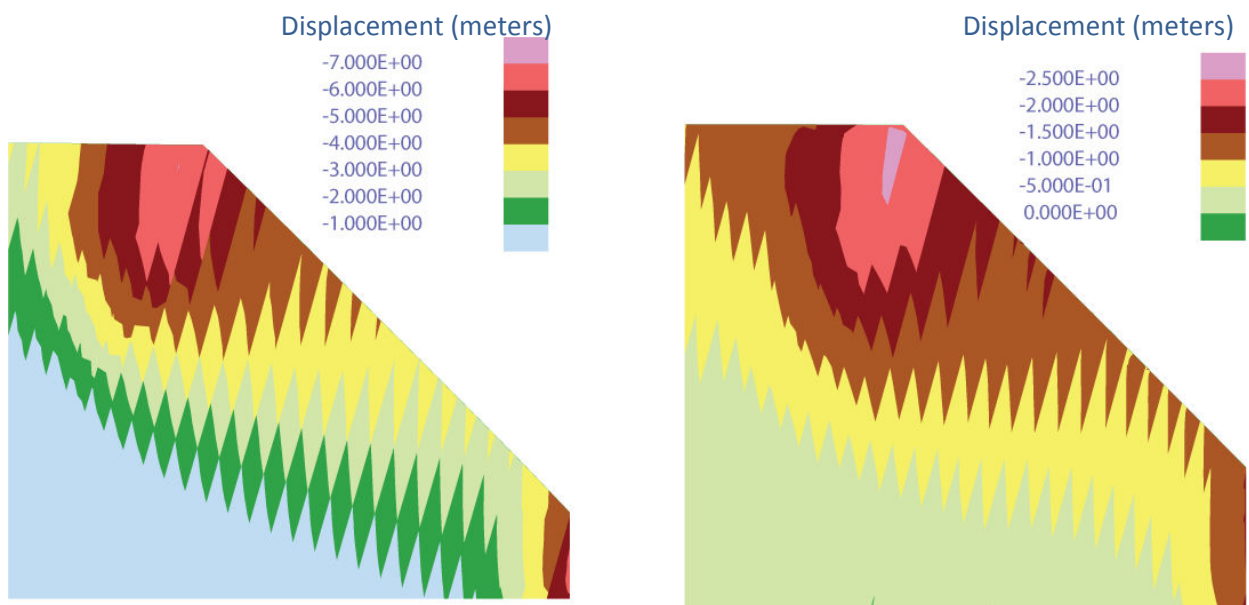


Figure 4.20: The contours distribution of the vertical rock slope displacements (cave beneath the toe). **Left:** toppling – type model. **Right:** toppling-type with cross joints (Slope height is 800 meters, units in meters)

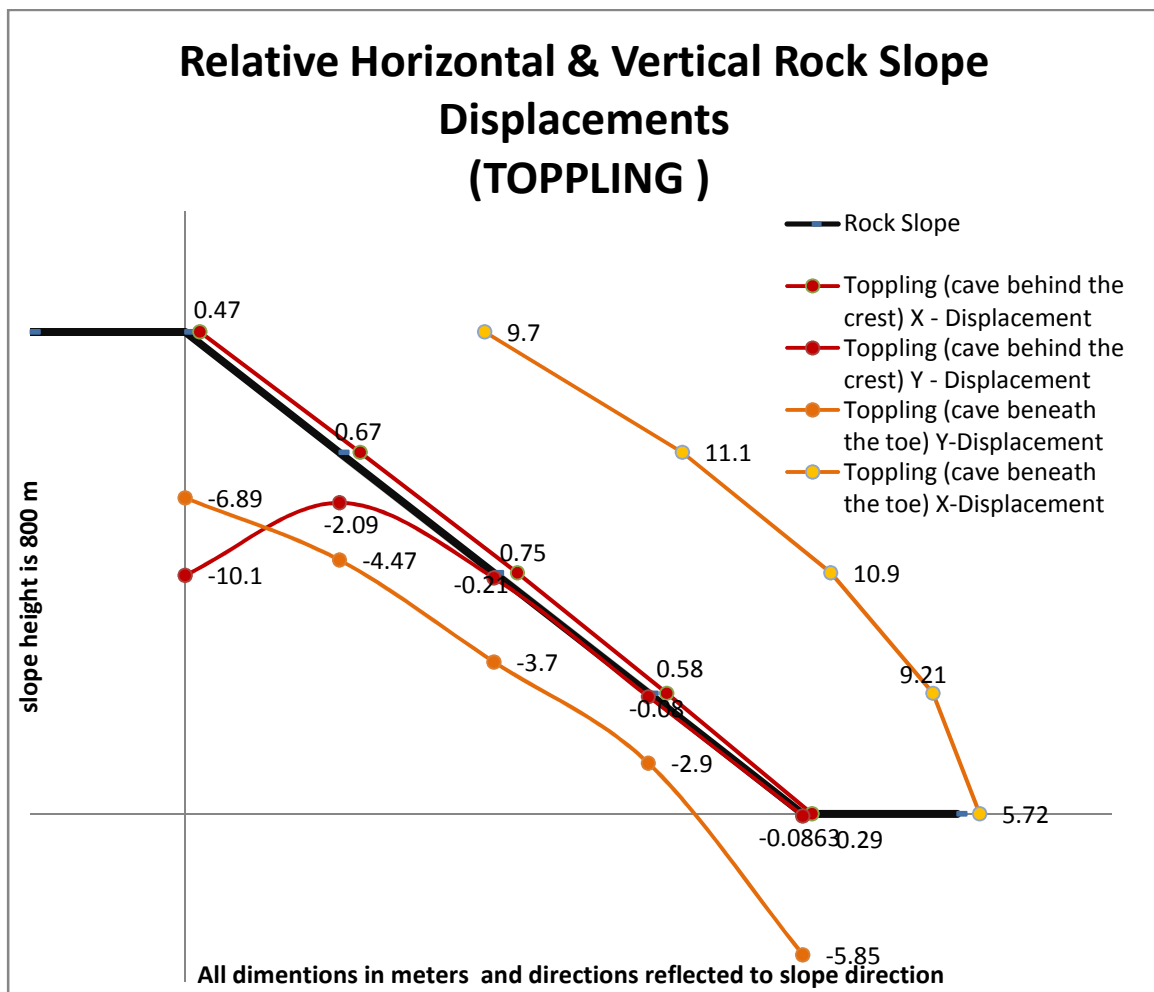


Figure 4.21: Horizontal and vertical components of displacements of rock slope (Generated by UDEC in Toppling type cases)

Summary graphs are presented in Figures 4.21 to 4.24, the displacements of the rock slope and each component of the slope displacements are influenced by the position of the cave and structural discontinuity configuration. A high potential for flexural toppling failure is expected due to the effect of the cave beneath the toe. The reason for this is the de-stressing of the pillar under the bottom of the pit enabling the rock mass to freely rotate and topple. However, the cross-joints in the toppling type case limit the slope's susceptibility to pure toppling, leading to less than half of the total displacements when compared to the models without cross-joints. Ultimately, the effect of the cave position is noteworthy on rock slope horizontal and vertical deformations. The influence of structural discontinuities that promote toppling in this case is considerable in terms of the mechanics of the rock mass reaction to block caving. Although, the orthogonal joint set influences the magnitude of the deformations, in most cases limiting them, it has only a minor effect in terms of the differences between the pure-toppling-type and toppling-type with cross-joints models.

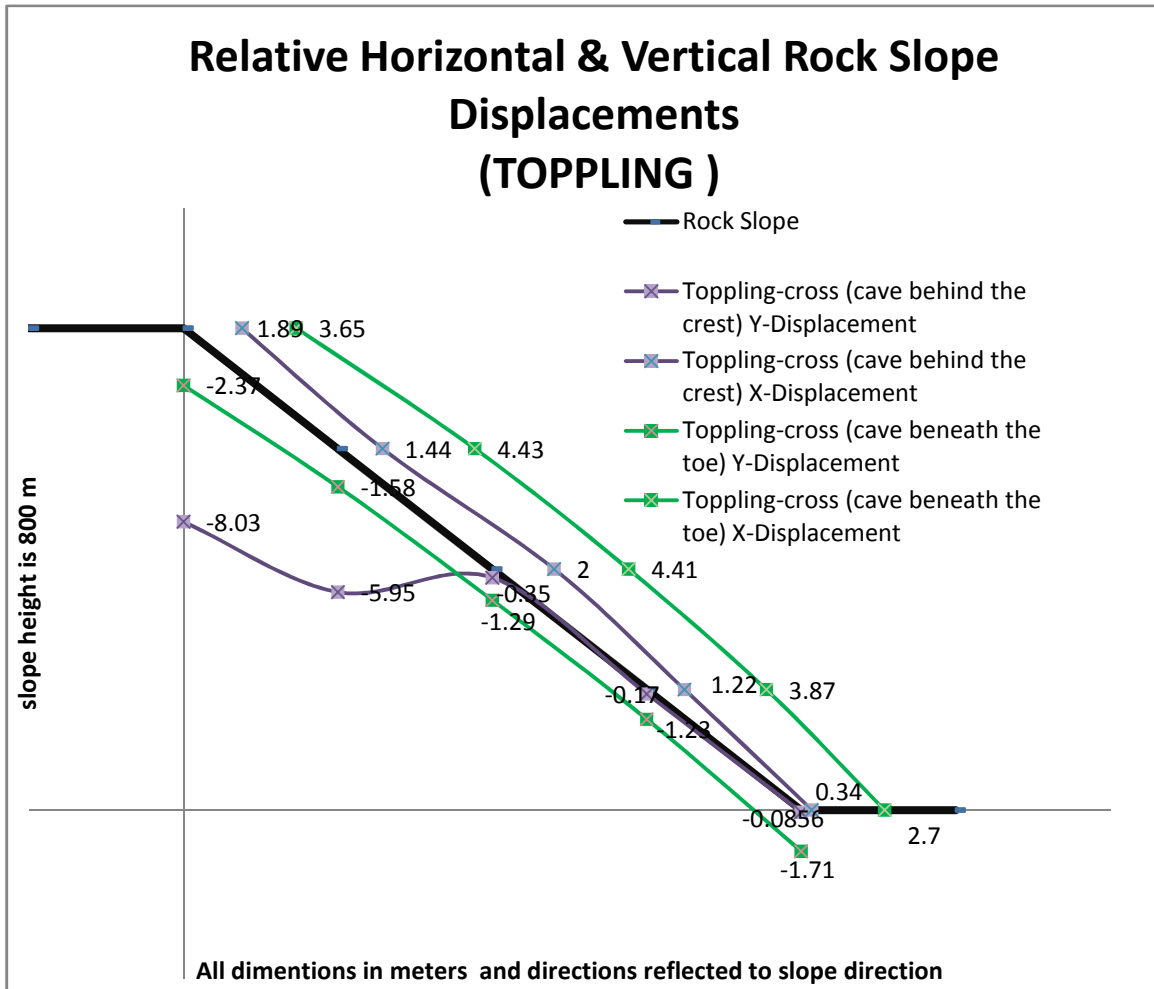


Figure 4.22: Horizontal and vertical components of displacements of rock slope (Generated by UDEC in Toppling type cases)

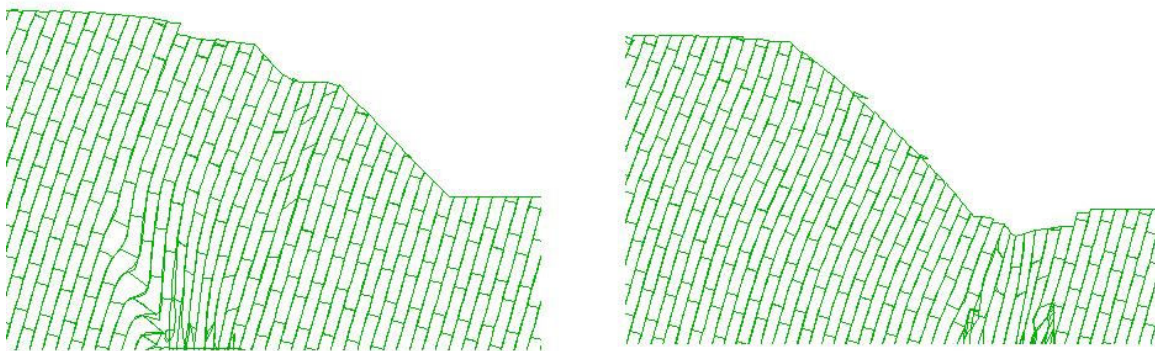


Figure 4.23: Displacements for the toppling-type with cross-joints models magnified 20 times for **Left:** cave behind the crest ; and **Right:** Cave beneath the toe (Slope height is 800 meters)

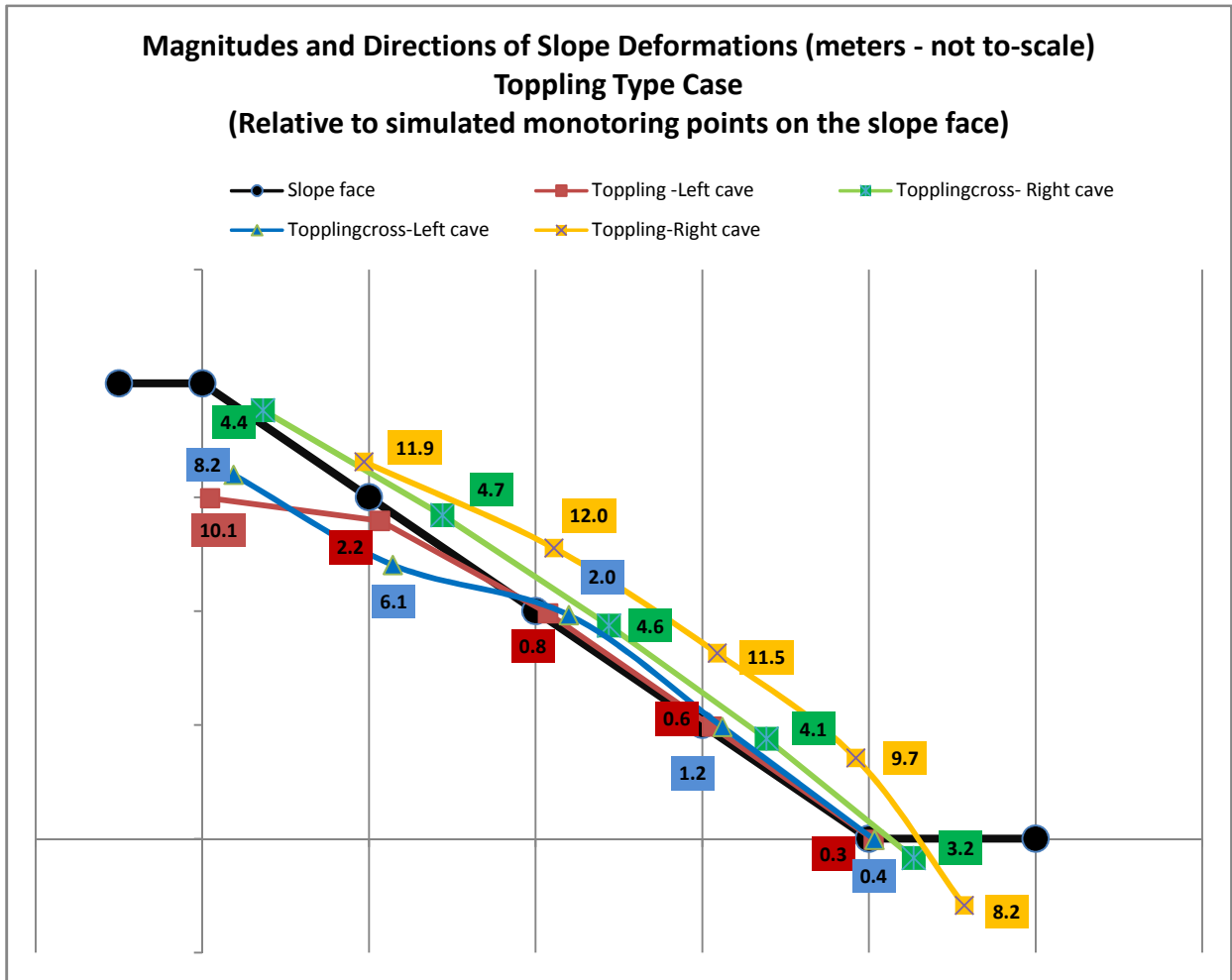


Figure 4.24: Magnitudes and Directions of Slope Deformations (Toppling Type Case)

The disturbed stress conditions observed in the models show that in the pure-toppling-type, the slender columns of rocks tend to move sub-vertically along the dipping angle at 75 degrees toward the cave. Since these slender blocks are continuous up to the surface, large changes in stress occur just above the cave. As shows in Figures 4.25 and 4.26, relaxation of stress takes place in the area above the cave zone all the way to the surface as these columns move into the cave. Similarly, in the toppling-type with cross-joints model, the blocks are permitted to move downward along the steep subvertical joints along their long sides. Thus, the same scenario of stress relaxation takes place.

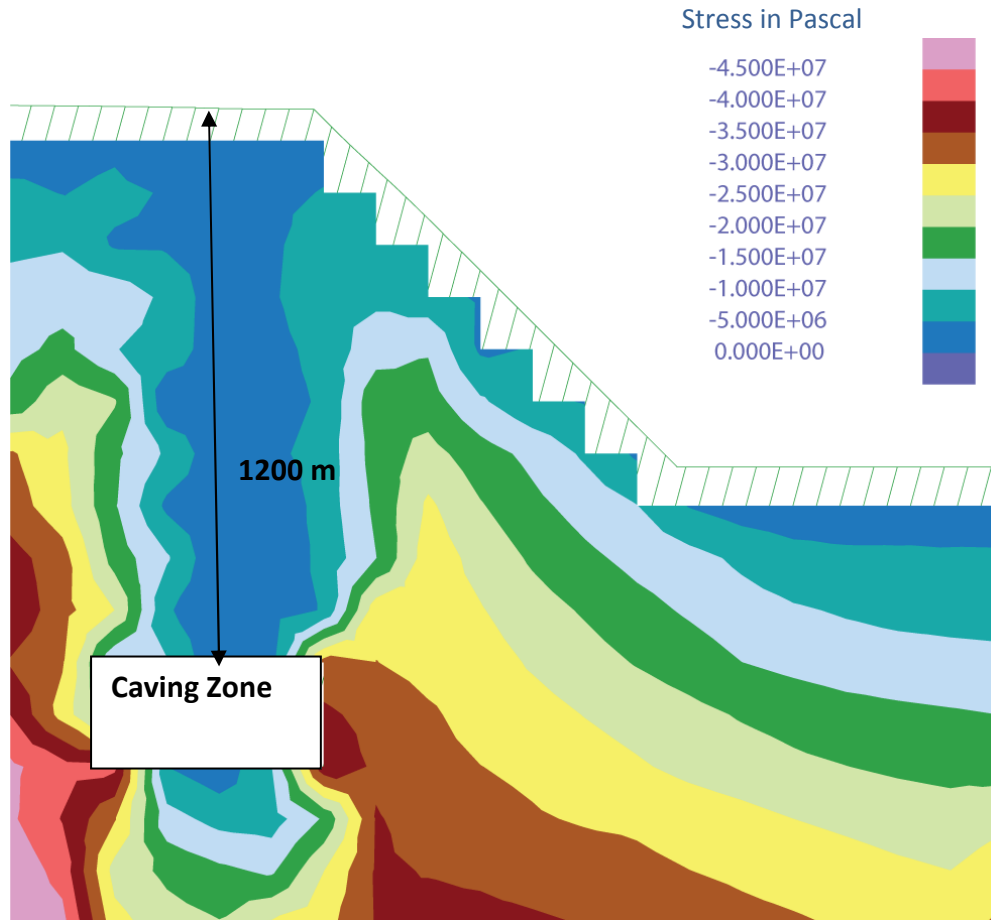


Figure 4.25: The contours of the vertical stress state induced by the cave behind the crest (Pure-toppling-type model). (Slope height is 800 meters, stress units in Pascal)

In terms of stress redistribution, the effect of the position of the cave is similar for all toppling-type models. Above the cave zone when the cave is behind the crest, the vertical stress (σ_{yy}) drops from 30 to 5 MPa (Fig. 4.25). When it is located under the toe, the vertical stress (σ_{yy}) drops from 10 to 5 MPa as shown in Figure 4.26. The slender blocks tend to buckle and topple in the direction of the slope as a result of the destressing of the toe. Therefore, the major principal stress is parallel to the slope (Fig. 4.25). The disturbance of the stress field is minor with respect to the strata farther away from the cave.

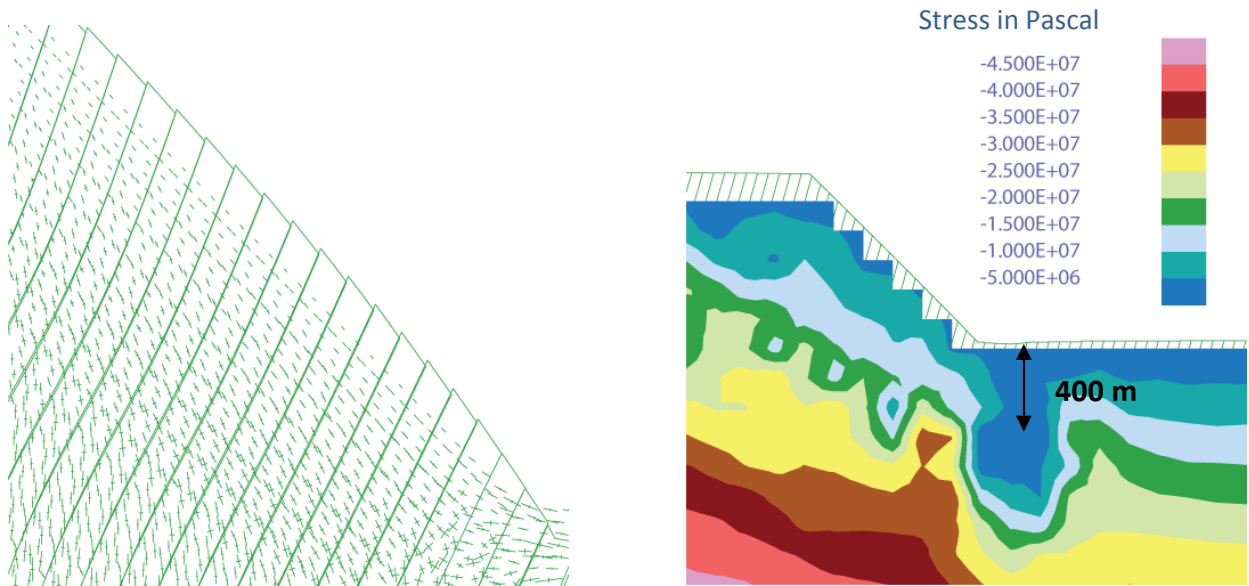


Figure 4.26: **Left:** the major principal stress is parallel to the slope face. **Right:** The vertical stress state induced by right cave (Pure-toppling-type model). (Slope height is 800 meters, stress units in Pascal) As previously discussed, the Mohr-Coulomb failure mode is utilized to identify the rock mass elasto-plastic behavior. Values of rock mass and structural discontinuity parameters are tabulated in the methodology section.

Toppling as a movement mechanism is simulated in four different generic cases as mentioned and leads to large-scale slope deformations, as discussed previously. The ductile and brittle toppling mechanisms are the two ideal modes of failure associated with rock slope deformations. The ductile mechanism (flexural toppling) is simulated in both pure-toppling-type scenarios where the cave is positioned behind the crest and underneath the toe. The flexural toppling normally occurs when there is only one dominant joint set steeply dipping into the face which is the case in the pure-toppling-type model, as shown in Figure 4.27. The transition between flexural toppling and block toppling is accommodated by cross-joints, as exhibited in real rock slopes. Toppling-type with cross-joints model caused the slope to perform this block-flexural toppling mode. The cave under the toe, in particular, clearly shows that the slope is induced to behave in this mode.

The position of the cave exclusively controls the behavior of rock slope in terms of plastic yielding of the rock mass in the toppling type models. As shown in Figure 4.27, the slender columns of rocks dipping steeply into the rock slope tend to slide towards and into the cave zone when it is positioned under the crest (left cave), forcing the adjacent columns to yield and topple. Along the slope surface, the slender columns buckle as a result of destressing of the slope and topple toward the face. Alternatively, destressing of the toe induced by the cave below the slopes toe (right cave) forces the rock slope to

deform in the direction of the cave. This release causes the slope to self-stabilize as it deforms. Yielding of the rock mass is most active at the toe but also involves shear localization along a roughly rotational rupture surface as shown in Figures 4.28 and 4.29.

The impact of block caving on rock slope and surface deformations are considerable in terms of plasticity. The large movements of the rock slope forces the deformable blocks to undergo significant plastic yielding. Similar to the kinematic description of toppling failures provided by Goodman and Bray (1979), the rock slope for all toppling-type models self-stabilize after the volume of rock mass above the cave reaches an equilibrium. However, the probability of a potential rock slope failure either through flexural toppling or block-flexural toppling is high.

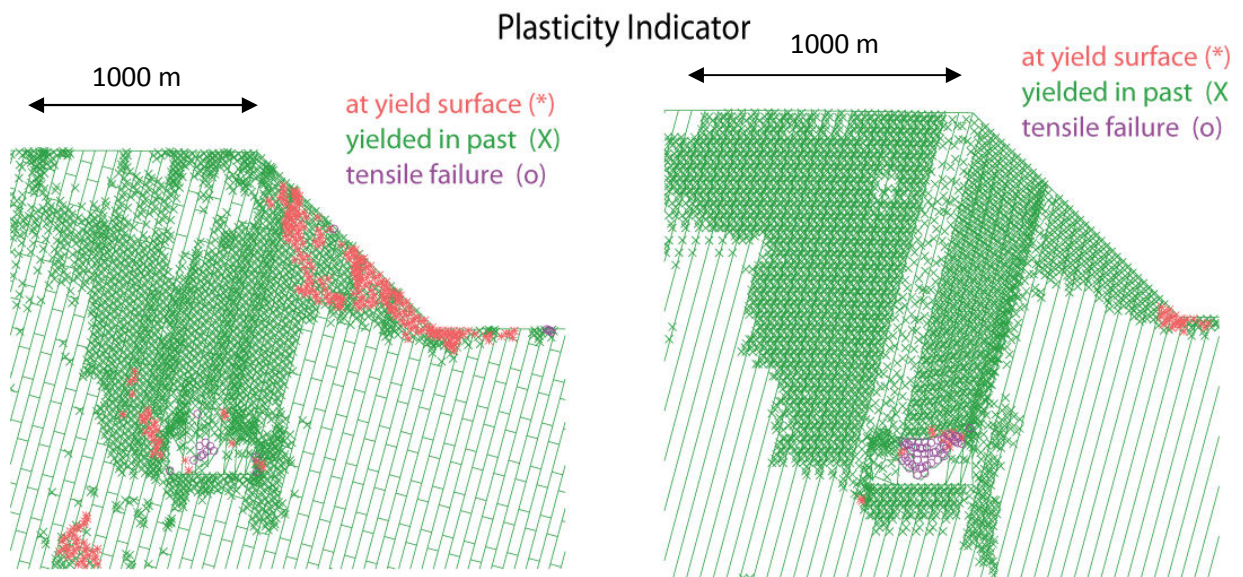


Figure 4.27: Plasticity induced by cave behind the crest models: **Left:** Toppling-type with cross-joints. **Right:** Pure-Toppling-type model.

Plasticity Indicator

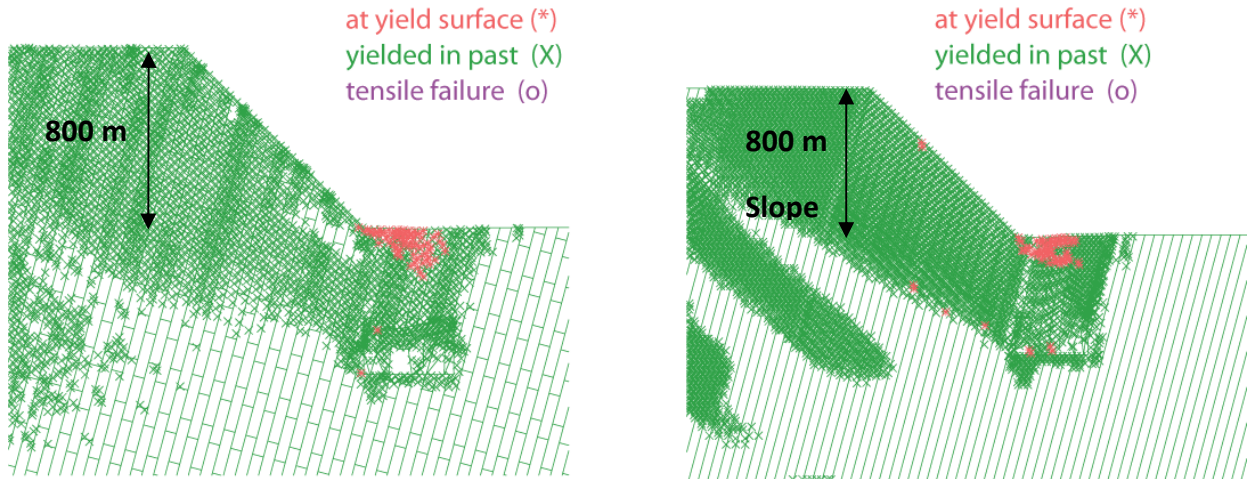


Figure 4.28: Plasticity induced by Right cave models; **Left:** Toppling-type with cross-joints. **Right:** Pure-Toppling-type model.

Magnified Block Deformation



Figure 4.29: Self-stabilizing of rock blocks and potential catastrophic rock mass failure. (Magnified deformation - 10 times, Slope height – 800 meters)

4.3 Buckling- and bi-Planar- type model results

Unlike the sliding-type model with cross joints influenced by the cave positioned behind the crest, the bi-planar model shows overall lower vertical and horizontal deformations, as demonstrated in Figure 4.30. Since the free edge at the crest permits the blocks to displace and rotate, the upper part of the slope encounters most of the deformations. On the other hand, the lower part shows no significant movements. The lower surface pins the toe and the surrounding blocks limit any further movements; however, strains are accumulated as the caving progresses. Yielding and bulging of the toe is the main concern here.

As a result of the cave located behind the crest in the buckling type model, the middle part of the slope is affected by the fact that the toe is fixed. Blocks are deformed along the major joint set toward the cave. Therefore, the exposed blocks to the slope are opened and this leads to more horizontal deformations in the middle of the slope as shown in Figure 4.30A. Between the cave and the middle of the slope, a portion of zero deformation separates the positive horizontal movement of the slope from the negative movements of the blocks near to cave zone as shown in Figure 4.30A.

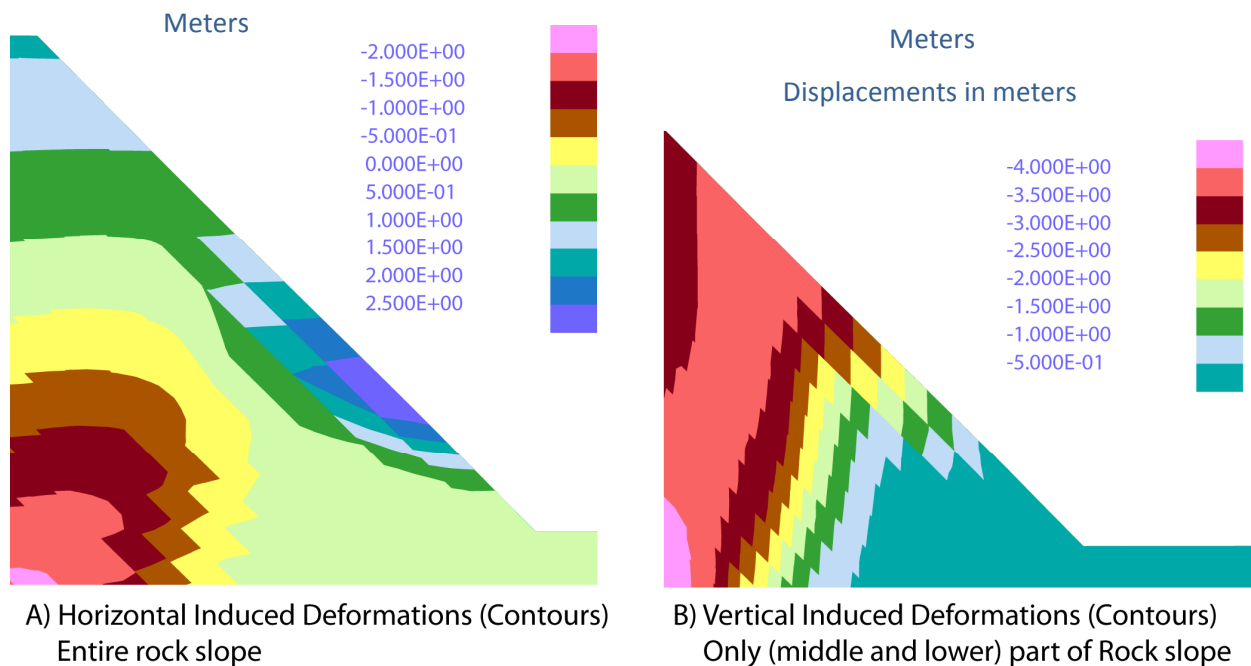


Figure 4.30: Simulated **A:** horizontal, and **B:** vertical deformations in for the Bi-planar and Buckling-type models. (Slope height is 800 meters, Deformation units in meters)

The movements of the buckling-type model induced by the cave below the toe of the slope are similar to the pure-sliding-type model. The cave zone is located 400 m below the lower surface of the slope and therefore allows the slender blocks to slide relative to one another into the caving area. As previously stated, the toe is confined laterally by the location of the pit floor that directly forces the long slender blocks to slide toward the cave. Figure 4.31 illustrates the relatively consistent and translational sliding mechanism.

Different behavior of rock slope occurs due to the effect of the left cave under the slope crest. The direction of the deformation is perpendicular to the direction of the slender blocks, thus, the fixed support at the toe resists the action of the slender blocks and causes them to bulge out of the slope. As a result, only the upper part of the slope experiences significantly larger movements. Because of the bulging and opening of the exposed layer of rocks, horizontal deformation at just 50 m distance above the toe is 2.5 m, as presented in Figure 4.32.

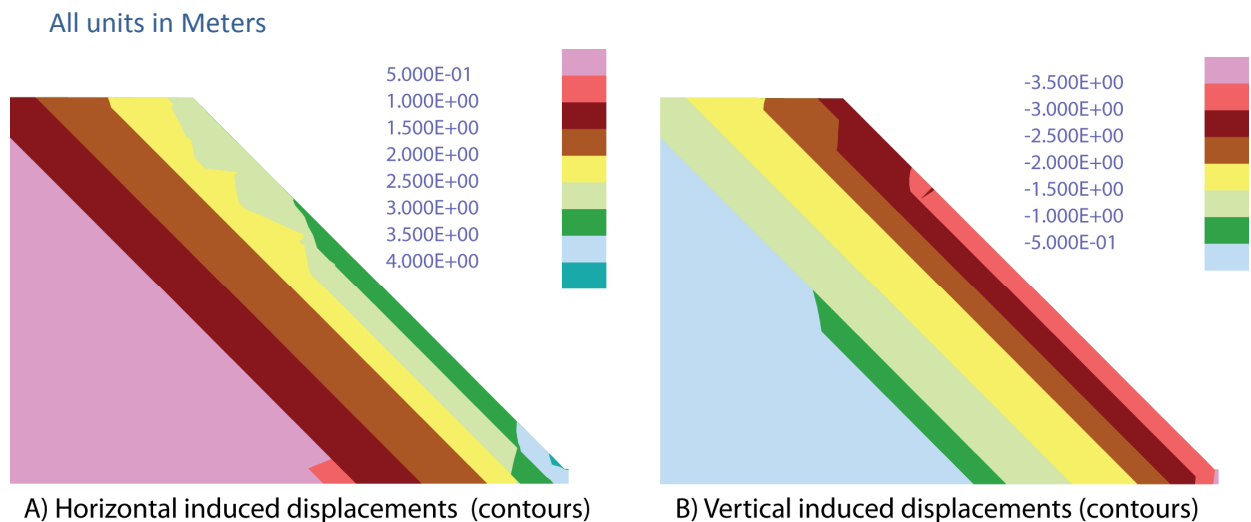


Figure 4.31: Displacement contour induced by the cave beneath the toe “buckling-type model”. A: Horizontal displacements. B: Vertical displacement. . (Slope height is 800 meters)

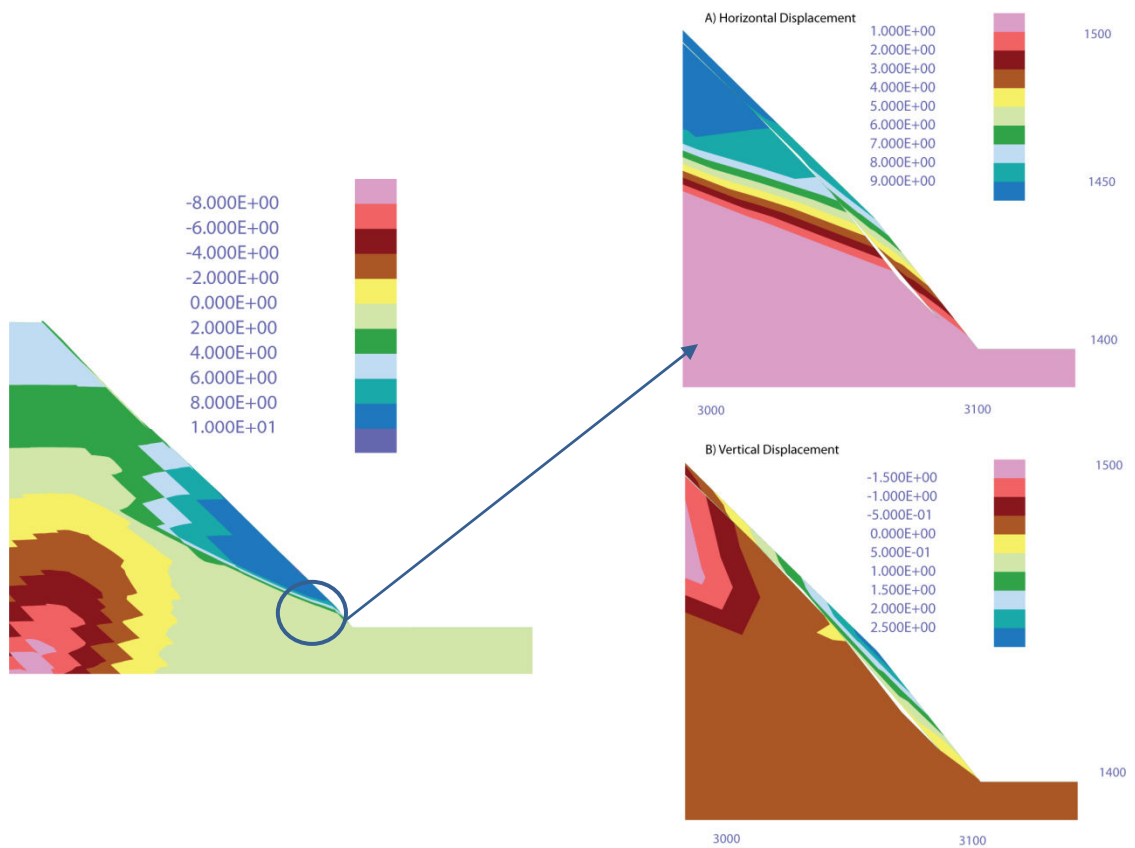


Figure 4.32: Displacement contour induced by the cave behind the toe “buckling-type model”. Left: Horizontal displacements. (Slope height is 800 m)

Both bucking-type and bi-planar-type simulations display similar plastic behavior of the deformable blocks. As an effect of the cave sited behind the crest, the blocks yield predominantly in shear for both models. Similar to the sliding-type mechanism, the plastic zone increases about 60 to 70 from the top of the cave to the slope and upper surface. However, the effect of the cave sited underneath the toe is similar to that in the pure-sliding-type model. The blocks tend to slide in a translational manner towards the cave with little deformation of the blocks themselves. Figures 4.33 and 4.34 illustrate the plasticity indicators for the two buckling-type models induced by the cave positioned behind the crest and beneath the toe, respectively. Overall the continuous major joint set controls the behavior of the rock mass as influenced by the cave positioned behind the crest, which is in contrast with the cave positioned beneath the toe where the rock mass properties controls the rock mass behavior.

Plasticity Indicator

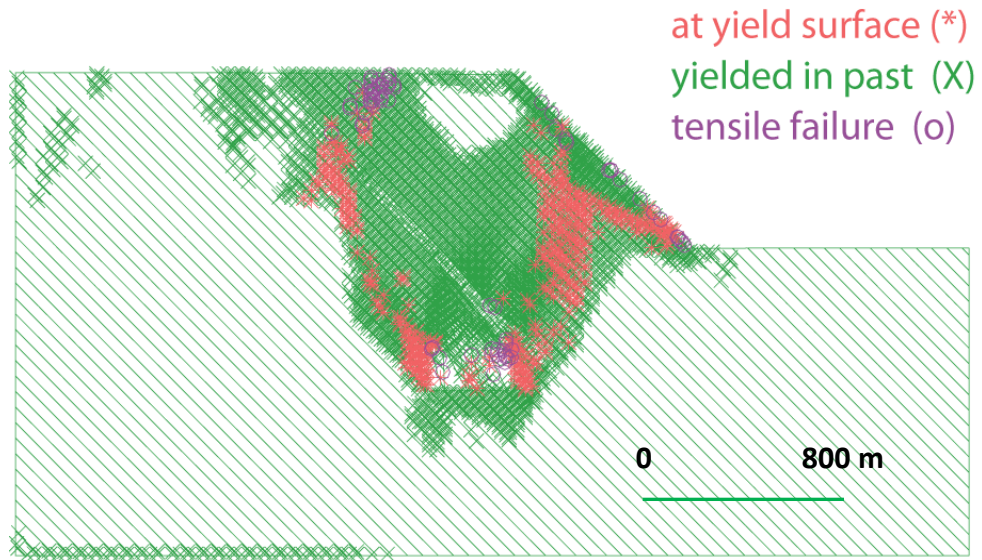


Figure 4.33: Plasticity induced by cave behind the crest models in “Buckling-type model”. (Slope is 800 meters)

Plasticity Indicator

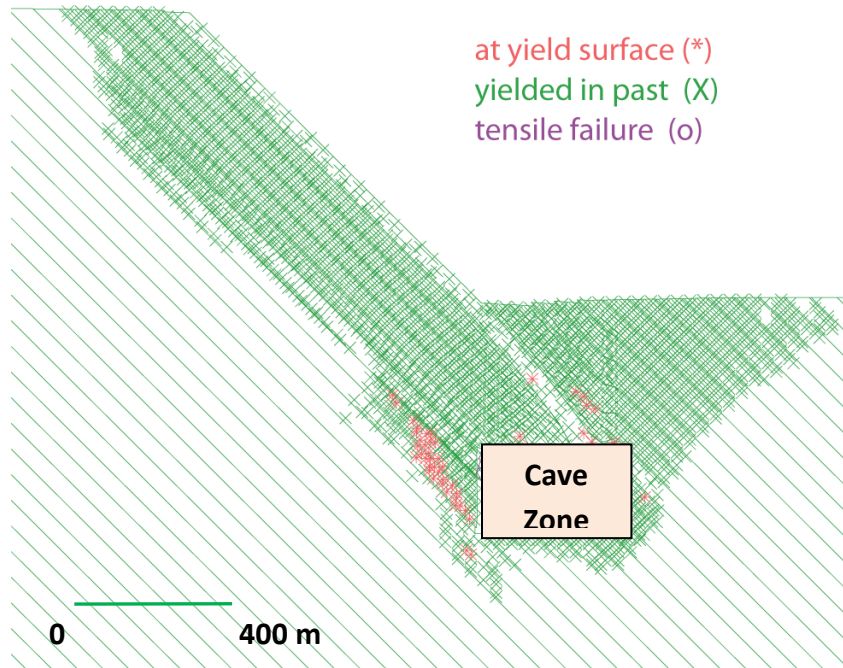


Figure 4.34: Plasticity induced by right cave in “Buckling-type model”. (Slope is 800 meters)

5 DISCUSSION ON SURFACE SUBSIDENCE

Surface subsidence is created by destressing the rock mass as a result of the dynamic nature of the block caving process. Figure 5.1 illustrates the general contour distribution of the vertical deformations associated with the two different cave positions in sliding-type models. As shown in Figure 5.1(left), the highest movement trend is perpendicular to the dip direction of the continuous joint set towards the middle of the cave behind the crest. In other words, the largest amount of vertical movement connects the cave to the surface along a sub-vertical trend that deviates from vertical due to the influence of the slope topography and dipping continuous joint set. Therefore, the zone around the crest is expected to achieve the highest amount of subsidence. This is in contrast when the cave positioned beneath the toe, where the vertical displacements are greatest at the toe above the cave, but also develop to promote significant downward movement of the slope itself, which reaches about 2 meters of movement.

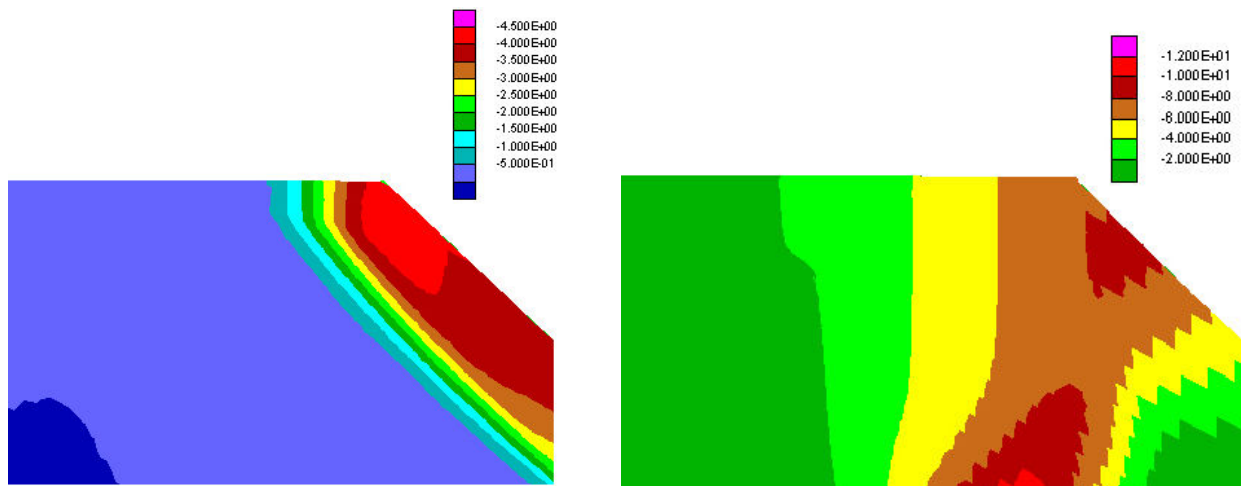


Figure 5.1: The general scheme of the contour line of the vertical displacement for both the pure-sliding-type and sliding-type with cross cuts; **Left:** cave underneath the toe. **Right:** Cave behind the crest. (Slope height is 800 meters)

Likewise, the highest generated surface subsidence among the four simulated models is the sliding-type with cross-cuts influenced by the left cave position (cave behind the crest). Figure 5.2 shows that a displacement of 11 meters is achieved at 100 meters away from the crest. The effective subsidence zone is approximately 1 km away from the crest in the two left cave models. In the right cave models, it reaches about half of that reached by the left cave models.

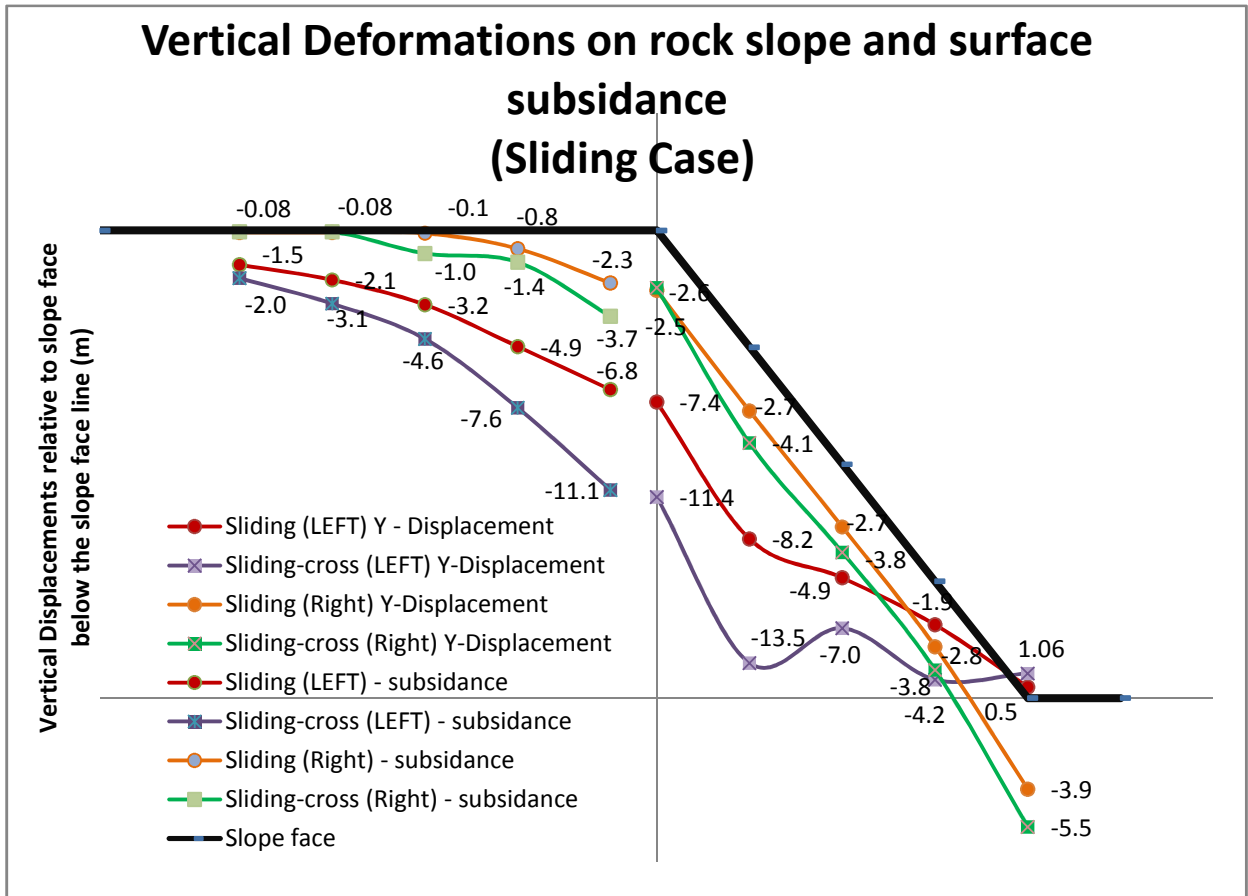


Figure 5.2: The induced surface and rock slope subsidence (vertical deformations) at selected monitoring points (Sliding Type simulations)
 Based on the study of Van As et al. (2003), surface subsidence characteristics can be characterized based on the different ways the subsidence manifests itself (Figure 2.12). The extent of the different subsidence zones, and associated angles, projected in the UDEC models is shown in Figures 5.3 and 5.4 for the pure-sliding-type model with the cave beneath the crest and sliding-type with cross joints model with cave beneath the toe, respectively.

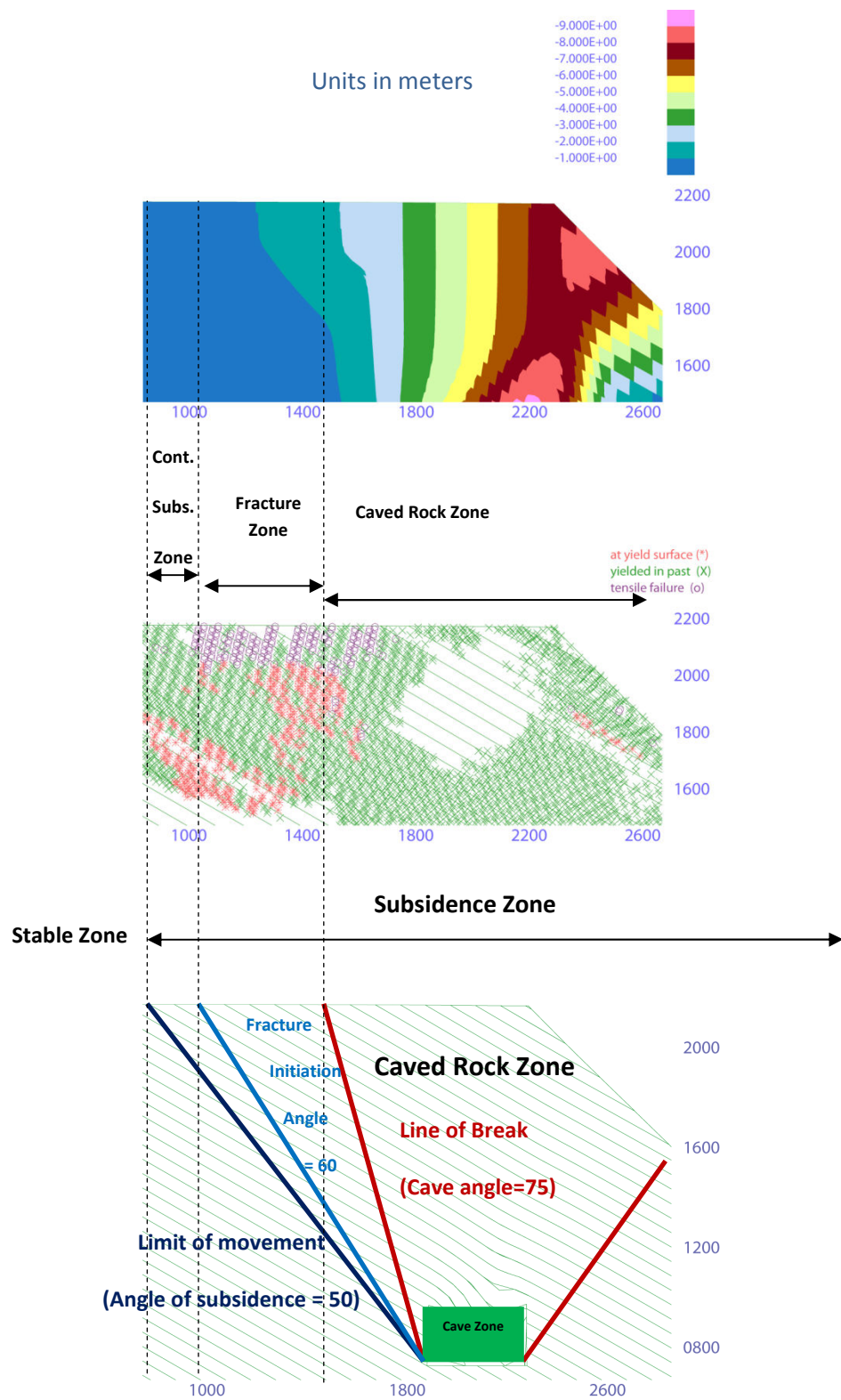


Figure 5.3: Subsidence zones for pure-sliding-type simulation induced by the left cave.

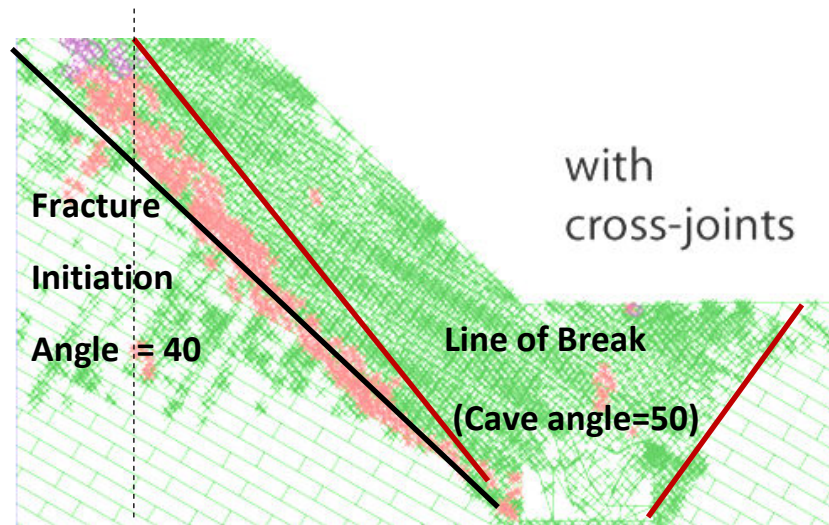


Figure 5.4: Subsidence zones for sliding-type with cross joints simulation induced by the cave beneath the toe.

As noted in the sliding mechanism section, surface subsidence is defined as the surface disturbance associated with the simulated caving and progressive failure of the rock mass into the cave. The toppling type simulations likewise predict the magnitude and extent of subsidence as a function of many factors, e.g. rock mass strength characteristics. As a result, each type of examined generic model shows different values of vertical deformations.

The position of the cave significantly affects the magnitude of subsidence; however, the subsidence zones, as defined by Van As et al. (2003) in the methodology section, are approximately similar in all models. The highest magnitudes of subsidence are near the crest for all simulations in which the cave is positioned beneath the crest. The pure-toppling-type model in particular imposes the maximum value of subsidence compared to all other models. A value of about 10 m is predicted just 100 m behind the crest, as shown in Figure 5.5. The orthogonal cross-joints in the toppling-type with cross-joint model allow the rotation of blocks to occur and resists the entire rock mass moments toward the cave; therefore, about only 75% of the pure-toppling –type subsidence is predicted, a value of 7.5 m of vertical deformation. On the other hand, the cave positioned beneath the toe induced smoother translational and gradual deformations over the upper area of the slope. A maximum of 2 meters is predicted just around the crest. Figure 5.5 summarizes the subsidence of all toppling type models for all generated monitoring points along the surface.

The extent of the caving zone encompasses several other zones. The active cave zone which is comprised of the failed caved rocks, which move downwards as they are drawn from below, is approximately equal for the four toppling type models. The extent of the subsidence along the upper surface behind the crest of the slope is from 1000 m to 1100 m. However, as shown in Figures 5.6 and

4.39, the caved rock zone extends further for pure-toppling-type models. The dimensions of the continuous subsidence zone, which is the area that exhibits elastic deformation or continuous non-elastic strains (movements about 2 mm or greater) are 100 m and 200 m, in both the pure-toppling type and toppling-type with cross-joints models, respectively.

The induced subsidence deformations, as a result of the cave positioned behind the crest, and the plasticity indicators defining the cave zones and its associated cave angles, are shown in Figures 5.6 and 4.38. The angle of subsidence is 65° for both induced subsidence by cave positioned behind the crest for both toppling type models. The cave boundary angles (angle of break) are 70° and 75° for both pure-toppling-type and toppling-type with cross cuts respectively.

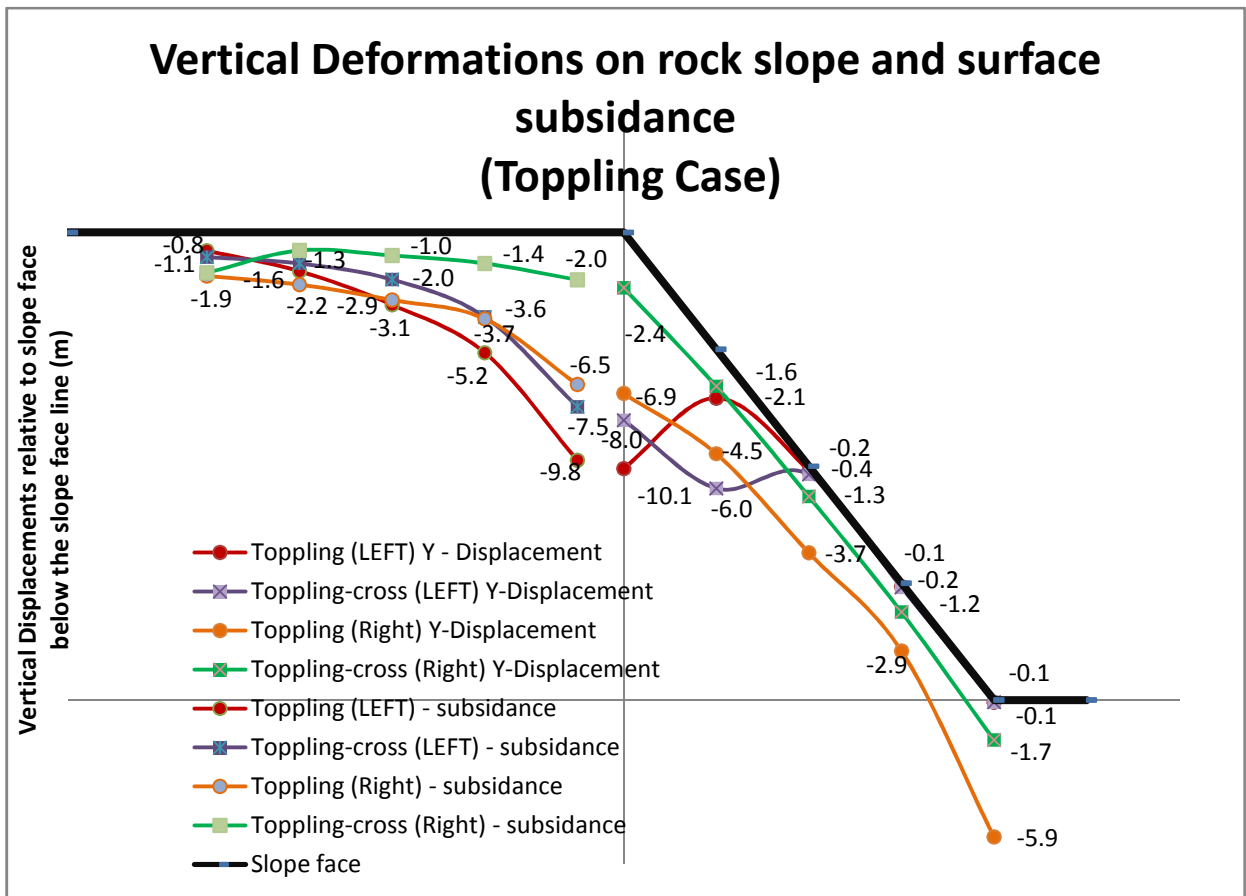


Figure 5.5: The induced surface and rock slope subsidence (vertical deformations) at selected monitoring points (Toppling Type simulations)

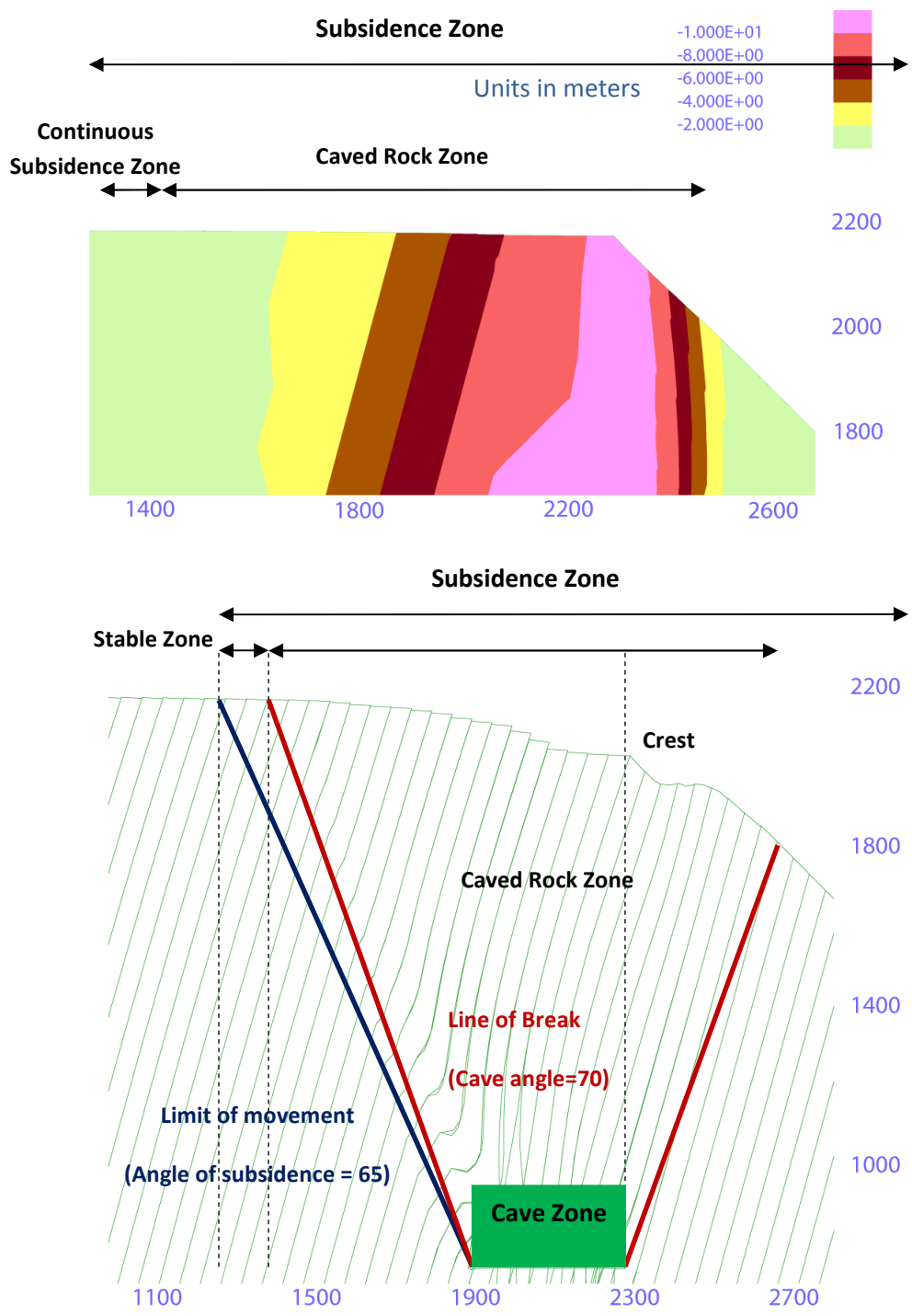


Figure 5.6: Subsidence zones for pure-toppling-type simulation induced by the cave behind the crest

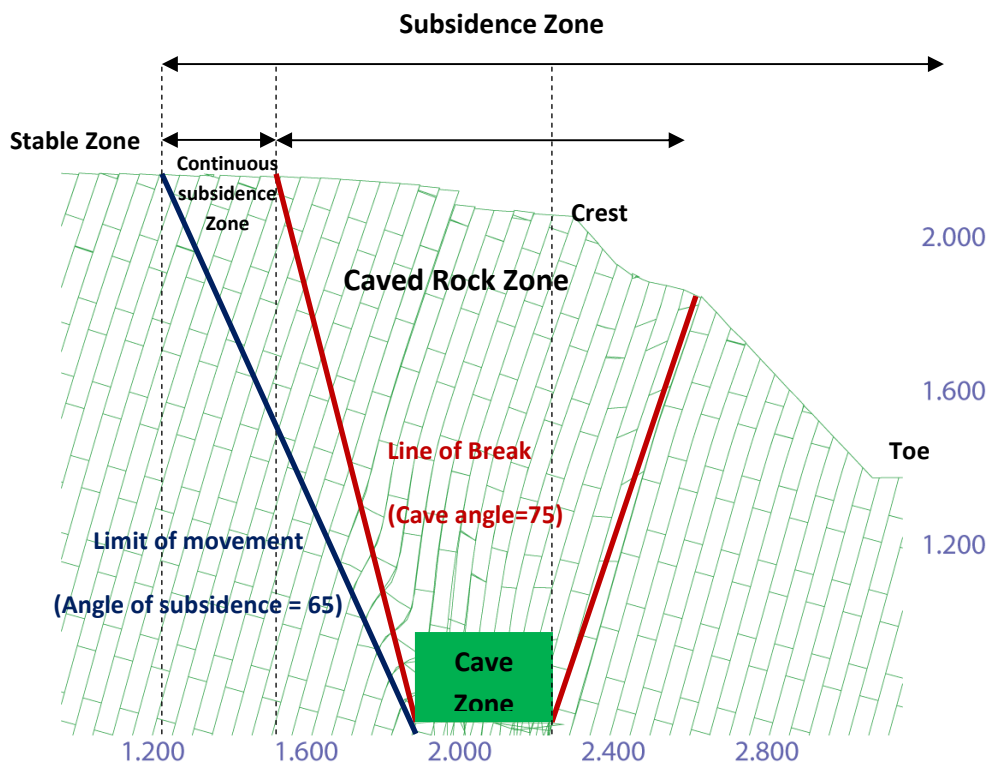
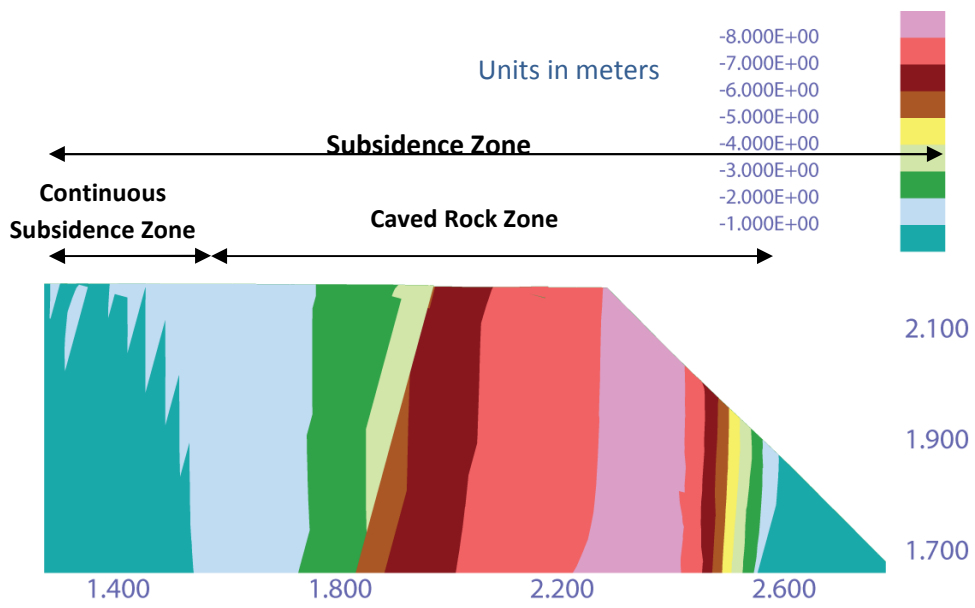


Figure 5.7: Subsidence zones for toppling-type with cross-joints simulation induced by the cave behind the crest

6 CONCLUSION

Based on the conducted literature review and the results obtained from the UDEC modeling study, the following findings were obtained:

- For the different modeling variables employed in the numerical simulations and the simplified assumptions representing the rock mass properties and properties of the discontinuities, accurate modeling of the dynamic block caving process was achieved using the discrete element method. In cases where the development of the cave zone is to be modeled, the explicit modeling of brittle fracture would be beneficial, however, the formulation adopted sufficiently enabled the impact of block caving on a generic rock slope and surrounding strata to be investigated. The direct block deletion method successfully creating the destressing configuration within the rock mass worked towards capturing the potential movements of the rock slope and upper ground surface.
- Despite the fact that the geological structure has significant influence on the magnitude of deformations, the position of the cave plays an equally major role in how the slope behaves and displaces. The potential of the toppling failure mechanism, flexural toppling of slender blocks or flexural block toppling of rocks with cross-joints, is characterized by inward movements of the rock mass toward the cave beneath the toe. However, huge vertical displacements on the upper part of the slope are distinguished as an influence of the cave behind the crest. Moreover, a consistent horizontal and vertical slope displacement toward the cave beneath the toe associated with sliding movements gives evidence that the cave zone influences the overall slope to move toward the toe.
- The extent of subsidence behind the slope crest ranges from between five hundred to one thousand meters for almost all simulations. Subsidence diminishes traveling away from the crest, from about ten to twelve meters at the crest (for both the toppling and sliding type models with the cave positioned behind the crest) to about half to around one meter at 1000 meters away from the crest, in some cases where the cave is left-positioned, higher cutoff distance at the same range of extent is used to eliminate the effect of boundary condition. The associate range of the caved rock zones varies from 500 m to 600 m away from the crest.

- The outcomes using the “Direct Block Deletion Method” show better results than the “Displacement Boundary Condition, in terms of capturing the physical behavior of the rock mass strata. It should be stressed that only for this specific geometry, cave-to-slope related dimensions, and generic models, DBD was successful in creating caving characteristics and rock slope mechanism of deformations.
- Since the dip slope models, bi-planar-type and buckling-type, are sensitive to slope movements, the stability of bi-planar-type was critical to only three sequential undercut stages. A numerical error occurred and precluded those models to continue progressing. Therefore, a complete comparison between Sliding-type and Toppling-type became the main focus. A study of the toe-breakout was presented.
- Simulations show that the cave behind the crest produces higher values of vertical and horizontal slope deformations than the cave beneath the toe in toppling-type and sliding-type simulations. Moreover, the effect of cross-joints is obvious in view of the fact that the blocks tend to move and rotate more freely than when represented as long slender blocks. Thus, the vertical deformations of slope and upper surface of simulations utilizing the geological structure with cross-joints were higher than those simulations without cross-joints. Table 5.1 presents a relative qualitative ranking from the highest to the lowest magnitude of vertical and horizontal slope deformation.

Table 6.1: Ranking of the magnitude and the extent of deformations along the surface and slope face.

| Cases | | Ranking | | | |
|----------------------------------------|-----------------------|------------------------------------------|--------------------------------------------|--------------------------------------------|-----------------------------------------|
| | | Magnitude of Vertical Slope Deformations | Magnitude of Horizontal Slope Deformations | Magnitude of Subsidence Behind Slope Crest | Extent of Subsidence Behind Slope Crest |
| Pure-sliding-type | Cave behind the crest | Medium | Medium | Medium | Medium |
| | Cave beneath the toe | Low | Medium | Low | Low |
| Sliding-type with cross-joints | Cave behind the crest | High | High | High | High |
| | Cave beneath the toe | Low | Medium | Medium | Low |
| Pure-toppling-type | Cave behind the crest | High | Low | High | Medium |
| | Cave beneath the toe | Medium | High | Medium | High |
| Toppling-type with cross joints | Cave behind the crest | Medium | Low | Medium | Medium |
| | Cave beneath the toe | Low | Medium | Low | Medium |

- All sliding-type models show consistent vertical deformation in terms of upper surface movements. The sliding discontinuities daylight in the slope and as a result the magnitude of subsidence correlates with the maximum magnitude of subsidence just below the crest.
- On the other hand, in the toppling-models, the peak of the subsidence occurs just behind the crest and diminishes rapidly to very low movements. The dipping of the persistent joint set is related to cave position and the slender blocks daylighting in the crest zone move toward the cave creating a bulging feature.

According to the plasticity illustrations and shape of potential failure and displacements, ranking between all models in terms of likely potential failure is presented in Table 5.2.

Table 6.2: Ranking of potential failure mechanism resulting from block caving.

| Cases | Cave position | Ranking of Potential failure mechanism (High) indicated the highest potential – (Low) the least potential |
|---------------------------------|-----------------------|--------------------------------------------------------------------------------------------------------------|
| Pure-sliding-type | Cave behind the crest | Medium |
| | Cave beneath the toe | Low |
| Sliding-type with cross-joints | Cave behind the crest | High |
| | Cave beneath the toe | Medium |
| Pure-toppling-type | Cave behind the crest | Low |
| | Cave beneath the toe | High |
| Toppling-type with cross-joints | Cave behind the crest | Low |
| | Cave beneath the toe | Medium |
| Bi-planar-type | Cave behind the crest | High |
| | Cave beneath the toe | Low |
| Buckling-type | Cave behind the crest | Medium |
| | Cave beneath the toe | Low |

(High - indicated the highest, Low - indicates the least)

6.1 Recommendations

The following recommendation and future work are based on the results obtained from the simulation using the distinct element code UDEC (Itasca, 2004).

- The study has shown that UDEC is very suitable to model the rock slope stability associated with different trends of geological structures. The different failure mechanisms commonly observed in open pit mines and/or natural rock slopes can be modeled using the distinct element approach. However, uncertainty in the model inputs and the sensitivity of the results to the assumed individual parameters limit the use of the models for outright prediction. The sensitivity to rock mass strength, structural geology, in-situ stress properties call for further

work in better understanding these parameters and their effect on the accuracy of the modeling. Site-specific details are required and mandatory to precisely predict the subsidence and slope deformations coupled to block cave mining.

- Safety and environmental concerns are nowadays important issues in any large-scale and long-term projects. Also, economically, it is important to address the risk and impact of block caving related to these factors. Subsidence is one major issue that arises where block caving is implemented. In some cases where surface infrastructure is sensitive to any differential settlements, a set back distance is required to satisfy the design needs. Specifically in this study, all UDEC models show that a scale of one kilometer is the effective zone of large-strain deformations.
- The study shows the need to focus on a comprehensive and very detailed study integrating site investigation and data collection with analytical, empirical and numerical analyses. The complexity and uncertainty of rock mass properties and geology are the key challenges to better capturing the physical response of the rock mass strata to block caving. Factors such as water pressure and drainage, height and width of the cave, etc., have to be included to minimize the uncertainties and to increase the level of confidence in the engineering decision making process related to the execution of block caving as a primary mining method or transition from open pit mining.

7 REFERENCES

- Abel J.F. and Lee F.T., 1980. *Subsidence Potential in Shale and Crystalline Rocks*. USGS OF 80-1072, 52, U. S. Geological Survey, Reston, VA.
- AMEC, 2005. Earth observation market development program land subsidence pre-commercial trial Palabora mine, South Africa. AMEC Report VM00344, 82 pp
- Barton, N.R., 1971. *A model study of behavior of excavated slopes*, Ph.D. Thesis, University of London, Imperial College of Science and Technology.
- Brummer, R.K., Li, H., and Moss, A., 2006. The transition from open pit to underground mining: an unusual slope failure mechanism at Palabora. In *Stability of Rock Slopes in Open Pit Mining and Civil Engineering Situations*, Johannesburg, S.A., SAIMM, pp 411-420.
- Clarke, G. 1981. *The Palabora Complex*. Industrial Minerals (London), no. 169: 45-62.
- Wyllie, D. C. and Mah, C. W., 2004. *Rock Slope Engineering: Civil and Mining*, 4th edition. Taylor and Francis, London.
- Du Plessis, Louis, and Dennis C. Martin. 1991, *Numerical Modeling Studies for Design of High Rock Slopes at Palabora Copper Mine*. Proceedings; Seventh International Congress on Rock Mechanics." Proceedings of the Congress of the International Society for Rock Mechanics 7 799-804.
- Elmo D., Vyazmensky A, Stead D., Rance J. R. ,2007. A hybrid FEM/DEM approach to model the interaction between open-pit and underground block-caving mining. In *First CANADA-USA Rock Mechanics Symposium*, Vancouver, Canada, p. 1287
- Evert Hoek & John Bray, 1981. *Rock slope engineering*. Routledge, UK.
- Fisher, B.R. and Eberhardt E., 2007. Dip slope analysis and parameter uncertainty – Case history and practical recommendations. In *First CANADA-USA Rock Mechanics Symposium*, Vancouver, Canada, p. 871
- Goodman, R.E. and Bray, J.W., 1976. *Toppling of rock slopes*. In *Rock Engineering*. American Society of Civil Engineers, Geotechnical Engineering Division Conference, Boulder, Colorado, Vol. II, pp. 201–234.
- Hanekom, H.J, van Staden C.M.v.H , Smit P. J., and Pike D.R., 1965. *Geology of Palabora Igneous Complex*. South Africa Geological Survey -- Memoir, no. 54:179.
- Itasca, 2004. UDEC4.0: Command Reference (Version 4.0). Itasca Consulting Group, Minneapolis.
- Julin, D.E, 1992. Block caving. Chapter 20.3, *Mining Engineering Handbook*, 2nd edition, Howard L. Hartman, ed., Society for Mining Metallurgy & Exploration.
- Laubscher D.H., 1981. Planning Mass Mining Operations, In *Design and Operation of Caving and Sublevel Stopping Mines*, R.D. Stewart, ed., AIME, New York. 843 p.

Lupo, John F., 1996. *Evaluation of deformations resulting from mass mining of an inclined orebody*. Ph.D., Colorado School of Mines

Martin, D.C, Steenkamp N.S.L , and Lill J.W, 1986. Application of a Statistical Analysis Technique for Design of High Rock Slopes at Palabora Mine, South Africa. In *Mining Latin America*, IMM Conference, Santiago, Chile, pp. 241-255.

Moss, A., Diachenko S, and Townsend P. ,2006. Interaction between the Block Cave and the Pit Slopes at Palabora Mine. *Journal of the South African Institute of Mining and Metallurgy* 106, no. 7: 479-484.

Nichol, S.L., Hungr, O., Evans, S.G., 2002. Large scale brittle and ductile toppling of rock slopes. *Canadian. Geotechnical Journal* 39(4): 773– 788.

Olavarría. S., Adriasola, P., Karzulovic, A.,2006. Transition from Open Pit To Underground Mining at Chuquicamata, Antofagasta, Chile. In *International Symposium on Stability of Rock Slopes in Open Pit Mining and Civil Engineering*, The South African Institute of Mining and Metallurgy pp. 421-434.

Rance, J. R., Van As, A., Owen, D. R. J., Feng, Y. T. and Pine, R. J., 2007. Computational modeling of multiple fragmentations in rock masses with application to block caving. In *First CANADA-USA Rock Mechanics Symposium*, Vancouver, Canada, p. 477

Resolution Copper Mining, 2006. Sustainable Development Report. Available at www.resolutioncopper.com/res/ourapproach/10.html (accessed April 1, 2008)

Manske, S. L. and Paul, A. H., 2002. Geology of a Major New Porphyry Copper Center in the Superior (Pioneer) District, Arizona. *Economic Geology*, 97(2): 197-220.

Palabora Mining Company Limited, Mine Geological and Mineralogical Staff, 1976. The Geology and the Economic Deposits of Copper, Iron, and Vermiculite in the Palabora Igneous Complex; a Brief Review. *Economic Geology* 71(1): 177-192.

Stead, D., Coggan, J. S. and Eberhardt, E., 2004. Realistic Simulation of Rock Slope Failure Mechanisms: The Need to Incorporate Principles of Fracture Mechanics. *International Journal of Rock Mechanics and Mining Sciences* 41: 2-17.

Stead, D., Eberhardt, E. and Coggan, J. S. 2006. Developments in the Characterization of Complex Rock Slope Deformation and Failure using Numerical Modeling Techniques. *Engineering Geology* 83(1-3): 217-235.

Van As, A., Davison, J., Moss A., 2003. *Subsidence Definitions for Block Caving Mines*. Technical Report prepared for Rio Tinto Technical Services, Project Code GBC097.

Vyazmensky, A., Elmo, D., Stead, D., Rance, J. R., 2007. Combined finite-discrete element modeling of surface subsidence associated with block caving mining. In *First CANADA-USA Rock Mechanics Symposium*, Vancouver, Canada.

8 APPENDICES

Appendix 1 – sample of - UDEC input file (.dat) - sliding-type with cross joints, right-positioned cave

```
new
; Model Generation-----
round 1
block 0,0 0,2200 1300,2200 2100,1400 4400,1400 4400,0
jregion id=1 0,1000 0,2200 4400,2200 4400,1000
jset -30,0 1200,0 0,0 50,0 0,0 range jregion 1
jset 60,0 50,0 50,0 200,0 0,0 range jregion 1
jset 60,0 60,0 40,0 200,0 100,0 range jregion 1
jregion id=2 0,0 0,1000 2100,1000 2100,0
jset -30,0 1200,0 0,0 50,0 0,0 range jregion 2
jset 60,0 50,0 50,0 200,0 0,0 range jregion 2
jset 60,0 60,0 40,0 200,0 100,0 range jregion 2
jregion id=3 2500,0 2500,1000 4400,1000 4400,0
jset -30,0 1200,0 0,0 50,0 0,0 range jregion 3
jset 60,0 50,0 50,0 200,0 0,0 range jregion 3
jset 60,0 60,0 40,0 200,0 100,0 range jregion 3
jregion id=4 2100,0 2100,750 2500,750 2500,0
jset -30,0 1200,0 0,0 50,0 0,0 range jregion 4
jset 60,0 50,0 50,0 200,0 0,0 range jregion 4
jset 60,0 60,0 40,0 200,0 100,0 range jregion 4
jregion id=5 2100,750 2100,1000 2500,1000 2500,750
jset -30,0 1200,0 0,0 50,0 0,0 range jregion 5
jset 60,0 50,0 50,0 200,0 0,0 range jregion 5
jset 60,0 60,0 40,0 200,0 100,0 range jregion 5
crack 2100,1000 2100,750
crack 2500,1000 2500,750
crack 2100,1000 2500,1000
crack 2100,950 2500,950
```

```

crack 2100,900 2500,900

crack 2100,850 2500,850

crack 2100,800 2500,800

crack 2100,750 2500,750

gen quad 50

gen edge 100

;----- material properties-----

; (E=20 GPa v=0.25)

; run as elastic (cons=1)

; so that initial conditions are elastic

change mat=1 cons=1

prop mat=1 dens=2600 k=13.3e9 g=8e9 c=10e6 f=40 di=10

prop jmat=1 jkn=5e9 jks=5e8 jfric=40 jcoh=1e5 jten=0

;-----boundary condition

bound xvel=0 range -1 1 -1 2201

bound xvel=0 range 4399 4401 -1 2201

bound yvel=0 range -1 4401 -1 1

;-----in situ stress (horz/vert 1.3)

insitu stress -84.2e6 0 -56.1e6 ygrad 3.82e4 0 2.55e4 &

szz -56.1e6 zgrad 0 2.55e4

grav 0 -9.81

hist unbal

solve

step 5000

save slidingcrossbig-elastic-d30-k1.5-cut-right.sav

; call slidingcrossbig-elastic-d30-k1.5-cut-right.dat

new

restore slidingcrossbig-elastic-d30-cut-right.sav

reset displ jdispl jndisp vel rot

change mat=1 cons=3

change mat=2 cons=3 range 2090 2510 740 1010

change jmat=2 range 2090 2510 740 1010

```

```

prop mat=1 dens=2600 k=13.3e9 g=8e9 c=1e6 f=40 t=5e5 di=10

prop jmat=1 jkn=5e9 jks=5e8 jfric=35 jcoh=0 jten=0

prop mat=2 dens=2600 k=13.3e9 g=8e9 c=1e6 f=40 t=5e5 di=10

prop jmat=2 jkn=10e9 jks=5e8 jfric=40 jcoh=1e5 jten=0

;-----change properties for elasto-plastic case

;prop mat=1 dens=2600 k=13.3e9 g=8e9 c=1.25e6 f=40 t=1.25e5 di=10

;prop mat=1 dens=2600 k=13.3e9 g=8e9 c=2.5e6 f=40 t=2.5e5 di=10

;prop mat=1 dens=2600 k=13.3e9 g=8e9 c=2e6 f=40 t=2e5 di=10

;prop mat=1 dens=2600 k=13.3e9 g=8e9 c=1.5e6 f=40 t=1.5e5 di=10

hist unbal

solve

step 5000

save slidingcrossbig-plastic-d30-cut-f35-right.sav

; call slidingcrossbig-plastic-d30-cut-f35-right.dat

new

restore slidingcrossbig-plastic-d30-cut-f35-right.sav

reset displ jdispl jndisp vel rot

; y displacements

hist ydis 400,2200 ; history 3 upper

hist ydis 600,2200 ; history 4 upper

hist ydis 800,2200 ; history 5 upper

hist ydis 1000,2200 ; history 6 upper

hist ydis 1200,2200 ; history 7 upper

hist ydis 1300,2200 ; history 8 Slope (crest Y-disp)

hist ydis 1500,2000 ; history 9 Slope

hist ydis 1700,1800 ; history 10 Slope

hist ydis 1900,1600 ; history 11 Slope

```

```
hist ydis 2100,1400 ; history 12 Slope (toe Y-disp)

hist ydis 2200,1400 ; history 13 lower

hist ydis 2400,1400 ; history 14 lower

hist ydis 2600,1400 ; history 15 lower

hist ydis 2800,1400 ; history 16 lower

hist ydis 3000,1400 ; history 17 lower

; X displacements

hist xdis 400,2200 ; history 18 upper

hist xdis 600,2200 ; history 19 upper

hist xdis 800,2200 ; history 20 upper

hist xdis 1000,2200 ; history 21 upper

hist xdis 1200,2200 ; history 22 upper

hist xdis 1300,2200 ; history 23 Slope (crest X-disp)

hist xdis 1500,2000 ; history 24 Slope

hist xdis 1700,1800 ; history 25 Slope

hist xdis 1900,1600 ; history 26 Slope

hist xdis 2100,1400 ; history 27 Slope (toe X-disp)

hist xdis 2200,1400 ; history 28 lower

hist xdis 2400,1400 ; history 29 lower

hist xdis 2600,1400 ; history 30 lower

hist xdis 2800,1400 ; history 31 lower

hist xdis 3000,1400 ; history 32 lower

;history 1, 2 (unbalanced forces from elastic & plastic models)

;-----

;

; delete the bottom to top blocks - 50 m block

set log on
```

```
set log slcr6-vol.dat

delete range 2100 2500 750 850

solve

step 5000

save slidingcrossbig-cavingone-d30-cut1-f35-right-250m.sav

delete range 2100 2500 750 850

delete range 2348 2385 915 935

; this way to prevent the overlap problem (delete this block)

solve

step 5000

save slidingcrossbig-cavingone-d30-cut2-f35-right-250m.sav

delete range 2100 2500 750 800

solve

step 5000

save slidingcrossbig-cavingone-d30-cut3-f35-right-250m.sav

delete range 2100 2500 750 870

solve

step 5000

save slidingcrossbig-cavingone-d30-cut4-f35-right-250m.sav

delete range 2100 2500 750 875

solve

step 5000

save slidingcrossbig-cavingone-d30-cut5-f35-right-250m.sav

; call slidingcrossbig-cavingone-d30-cut-f35-right-250m.dat
```

Appendix 2 – sample of volume tracker (.xlsx) sliding-types with cross joints, left-positioned cave.

| (1) Sliding-cross (LEFT) | | | | |
|---------------------------------|--------------|---------------|---------------|---------------|
| ok | ok | ok | ok | ok |
| Cut 1 75m | Cut 2 75m | Cut 3 150m | Cut 4 100m | Cut 5 100m |
| 4.76E+03 | 7.56E+03 | 7.63E+03 | 1.69E+04 | 4.45E+03 |
| 4.11E+03 | 9.22E+03 | 2.28E+02 | 1.42E+04 | 3.91E+03 |
| 4.08E+03 | 1.60E+03 | 7.24E+03 | 1.09E+04 | 1.16E+04 |
| 2.87E+03 | | 1.21E+01 | 7.54E+01 | |
| 9.66E+02 | | 1.16E+01 | | |
| 2.79E+02 | | 3.20E+02 | | |
| 2.79E+02 | | 7.66E+03 | | |
| 4.93E+03 | | 2.84E+02 | | |
| 5.95E+01 | | 7.35E+03 | | |
| 8.88E+02 | | 3.87E+03 | | |
| 2.38E+02 | | 5.34E+02 | | |
| 8.88E+02 | | 2.44E+01 | | |
| 1.88E+03 | | 9.82E+02 | | |
| 2.38E+02 | | 3.85E+03 | | |
| 4.72E+03 | | 1.03E+03 | | |
| 2.52E+03 | | | | |
| 4.72E+03 | | | | |
| 3.84E+04 | 1.84E+04 | 4.10E+04 | 4.21E+04 | 1.99E+04 |
| Total | up to cut 3 | 9.78E+04 | up to cut 5 | 1.60E+05 |